



Print ISSN: 2152-4157
Online ISSN: 2152-4165

SPRING/SUMMER 2010
VOLUME 2, NUMBER 1

WWW.IJERI.ORG

International Journal of Engineering Research & Innovation

Editor-in-Chief: Mark Rajai, Ph.D.
California State University Northridge



Published by the
International Association of Journals & Conferences



TIME TO CHANGE THE WAY ACADEMICS WORK? TRY ACAMEDICS!

If you are not using the Internet, please skip this ad and enjoy the rest of the journal. The average burden of reading this ad is two minutes, which may add two months of productivity to your academic life. Seriously!

Whether you organize a conference, publish a journal, or serve on a committee to collect and review applications, you can use the Internet to make your life easier. We are not talking about emails. We are talking about state-of-the-art online systems to collect submissions, assign them to reviewers, and finally make a decision about each submission. We are talking about value-added services, such as payment and registration systems to collect registration fees online. We are talking about digital document services, such as proceedings CD/DVD development and duplication, or creating professional looking digital documents.

Finally, we are talking about AFFORDABLE PRICE, QUALITY, and CUSTOMIZATION. And we are talking about each of them at the same time.

By the way, you don't have to be a computer geek to use our systems. We have a couple them, and they will do all the technical mumbo jumbo for you. We also have a few select people from academics like you, and they know what you do. You just relax and enjoy our systems.

If you are still reading this ad, chances are you are interested in our systems or services. So, visit us at www.acamedics.com. While you are there, check the names of our clients as well. Most of them are quite familiar, and the list is quite long to put here.



INTERNATIONAL JOURNAL OF ENGINEERING RESEARCH AND INNOVATION

The INTERNATIONAL JOURNAL OF ENGINEERING RESEARCH AND INNOVATION (IJERI) is an independent and nonprofit publication which aims to provide the engineering community with a resource and forum for scholarly expression and reflection.

IJERI is published twice annually (Fall and Spring issues) and includes peer-reviewed research articles, editorials, and commentary that contribute to our understanding of the issues, problems, research associated with the engineering and related fields. The journal encourages the submission of manuscripts from private, public, and academic sectors. The views expressed are those of the authors, and do not necessarily reflect the opinions of the IJERI or its editors.

EDITORIAL OFFICE:

Mark Rajai, Ph.D.
Editor-In-Chief
Office: (818) 677-5003
Email: mrajai@csun.edu
College of Engineering and
Computer Science
California State University
Northridge, CA 91330-8332

THE INTERNATIONAL JOURNAL OF ENGINEERING RESEARCH AND INNOVATION EDITORS

Editor-In-Chief:

Mark Rajai

California State University-Northridge

Associate Editor:

Ravindra Thamma

Central Connecticut State University

Production Editor:

Julie Mengert

Virginia Tech.

Subscription Editor:

Morteza Sadat-Hossieny

Northern Kentucky University

Financial Editor:

Li Tan

Purdue University North Central

Associate Editor- in- chief:

Sohail Anwar

Penn State University

Manuscript Editor:

Philip D. Weinsier

Bowling Green State University -Firelands

Copy Editors:

Li Tan

Purdue University North Central

Ahmad Sarfarz

California State University-Northridge

Publishers:

Hisham Alnajjar

University of Hartford

Saeid Moslepour

University of Hartford

Web Administrator:

Saeed Namyar

Namyar Computer Solutions

TABLE OF CONTENTS

<i>Editor's Note: IJERI Welcomes A New Sister Journal</i>	3
<i>Philip Weinsier, IJERI Manuscript Editor</i>	
<i>An Innovative Application of 3D CAD for Human Wrist Ligamentous Injury Diagnosis</i>	5
<i>Haoyu Wang, Central Connecticut State University; Frederick W. Werner, SUNY Upstate Medical University; Ravindra Thamma, Central Connecticut State University</i>	
<i>Utilizing Advanced Software Tools in Engineering and Industrial Technology Curriculum</i>	12
<i>Faruk Yildiz, Sam Houston State University; Recayi "Reg" Pecan, University of Northern Iowa; Ayhan Zora, University of Northern Iowa</i>	
<i>Securing Virtualized Datacenters</i>	23
<i>Timur Mirzoev, Georgia Southern University; Baijian Yang, Ball State University</i>	
<i>Practical Soft-Switching High-Voltage Dc-Dc Converter for Magnetron Power Supplies</i>	30
<i>Byeong-Mun Song, Baylor University; Shiyong Lee, The Pennsylvania State University Berks Campus; Moon-Ho Kye, Power Plaza, Inc.</i>	
<i>A New Method For A Non-Invasive Glucose-Sensing Polarimetry System</i>	36
<i>Sunghoon Jang, New York City College of Technology of CUNY; Hong Li, New York City College of Technology of CUNY</i>	
<i>A Service-Learning Approach in a Basic Electronic Circuits Class</i>	43
<i>Fei Wang, California State University-Long Beach</i>	
<i>Tool Condition Monitoring System in Turning Operation Utilizing Wavelet Signal Processing</i>	49
<i>and Multi-Learning ANNs Algorithm Methodology Samson S. Lee, Central Michigan University</i>	
<i>A Process for Synthesizing Bandlimited Chaotic Waveforms for Digital Signal Transmission</i>	56
<i>Chance M. Glenn, Sr., Rochester Institute of Technology</i>	
<i>Evaluating the Accuracy, Time, and Cost Trade-offs Among Alternative Structural Fitness Assessment Methods</i>	62
<i>Michael D. Johnson, Texas A&M University; Akshay Parthasarathy, Texas A&M University</i>	
<i>A Reduced-Code Linearity Test for DAC Using Wavelet Analysis</i>	69
<i>Emad Awada, Prairie View A&M University; Cajetan M. Akujuobi, Prairie View A&M University; Matthew N. O. Sadiku, Prairie View A&M University</i>	
<i>Investigation of the Factors Affecting Surface-Plasmon Efficiency</i>	77
<i>Padmarekha Vemuri, University of North Texas; Vijay Vaidyanathan, University of North Texas; Arup Neogi, University of North Texas</i>	
<i>Instructions for Authors</i>	86

EDITOR'S NOTE: IJERI WELCOMES A NEW SISTER JOURNAL



Philip Weinsier, IJERI Manuscript Editor

IAJC Journals

As noted in the previous issue, the inception of IJERI was in response to the overwhelming success over the last ten years of the International Association of Journals and Conferences' flagship journal—IJME. But while some articles in IJERI will be on par with papers on engineering research appearing in IJME, its design is for a broader readership and includes studies in new, emerging and innovative fields of research.

IAJC, the parent organization of IJERI and IJME, is a first-of-its-kind, pioneering organization acting as a global, multilayered umbrella consortium of academic journals, conferences, organizations, and individuals committed to advancing excellence in all aspects of education related to engineering and technology. IAJC is fast becoming the association of choice for many researchers and faculty, due to its high standards, personal attention, fast-track publishing, biennial IAJC conferences, and its diversity of journals—IJERI, IJME and about 10 other partner journals.

Only weeks before we went to print, IAJC took over the editorship of a third journal: the Technology Interface Journal, stewarded since 1996 by its founding editor, Dr. Jeff Beasley. Everyone at IAJC would like to thank Dr. Beasley for all that he has done for the field of engineering technology. The journal will continue its dedication to the field of engineering technology, but readers can expect a few changes, not the least of which will be a minor name change to the Technology Interface International Journal (TIIJ); visit us at www.tiij.org. Also, the journal will now be published both online and in print, and use the same publishing standards as required by IJME and IJERI.

Current Issue

The acceptance rate for this issue was roughly 40%. And, due to the hard work of the IJERI editorial review board, I am confident that you will appreciate the articles published here. Both IJERI and IJME are available online (www.ijeri.org & www.ijme.us) and in print.

2011 IAJC-ASEE Joint International Conference

The editors and staff at IAJC would like to thank you, our readers, for your continued support and look forward to seeing you at the next IAJC conference. Look for details on the IAJC web site and for email updates. Please also look through our extensive web site (www.iajc.org) for information on chapters, membership and benefits, and journals.

The third biennial IAJC conference will be a partnership with the American Society for Engineering Education (ASEE) and will be held at the University of Hartford, CT, April 15-16, 2011. The IAJC-ASEE Conference Committee is pleased to invite faculty, students, researchers, engineers, and practitioners to present their latest accomplishments and innovations in all areas of engineering, engineering technology, math, science and related technologies.

Presentation papers selected from the conference will be considered for publication in one of the three IAJC journals or other member journals. Oftentimes, these papers, along with manuscripts submitted at-large, are reviewed and published in less than half the time of other journals. Please refer to the publishing details at the back of this journal, or visit any of our web sites.

International Review Board

IJERI is steered by IAJC's distinguished board of directors and is supported by an international review board consisting of prominent individuals representing many well-known universities, colleges, and corporations in the United States and abroad. To maintain this high-quality journal, manuscripts that appear in the *Articles* section have been subjected to a rigorous review process. This includes blind reviews by three or more members of the international editorial review board—with expertise in a directly related field—followed by a detailed review by the journal editors.

Acknowledgment

Listed here are the members of the editorial board, who devoted countless hours to the review of the many manuscripts that were submitted for publication. Manuscript reviews require insight into the content, technical expertise related to the subject matter, and a professional background in statistical tools and measures. Furthermore, revised manuscripts typically are returned to the same reviewers for a second review, as they already have an intimate knowledge of the work. So I would like to take this opportunity to thank all of the members of the review board.

Editorial Review Board Members

If you are interested in becoming a member of the IJERI editorial review board, go to the IJERI web site (Submissions page) and send me—Philip Weinsier, Manuscript Editor—an email. Please also contact me also if you are interested in joining the conference committee.

Mohammad Badar	Indiana State University (IN)	Dave Hunter	Western Illinois University (IL)
Rendong Bai	Eastern Illinois University (IL)	Ghassan Ibrahim	Bloomsburg University (PA)
Kevin Berisso	Ohio University (OH)	John Irwin	Michigan Tech University (MI)
Kaninika Bhatnagar	Eastern Illinois University (IL)	Sudershan Jetley	Bowling Green State University (OH)
Elinor Blackwell	North Carolina Ag&Tech State (NC)	Rex Kanu	Ball State University (IN)
Boris Blyukher	Indiana State University (IN)	Petros Katsioloudis	Berea College (KY)
Walter Buchanan	Texas A&M University (TX)	Khurram Kazi	Acadiaoptronics (MD)
Jessica Buck	Jackson State University (MS)	Satish Ketkar	Wayne State University (MI)
John Burningham	Clayton State University (GA)	Daphene Cyr Koch	Purdue University (IN)
Vigyan Chandra	Eastern Kentucky University (KY)	John Kugler	Youth Technology Corps
Isaac Chang	Cal Poly State University SLO (CA)	Ognjen Kuljaca	Alcorn State University (MS)
Hans Chapman	Morehead State University (KY)	Ronald Land	Penn State University (PA)
Rigoberto Chinchilla	Eastern Illinois University (IL)	Jane LeClair	Excelsior College (NY)
Raj Chowdhury	Kent State University (OH)	Jay Lee	Purdue University Calumet (IN)
Michael Coffman	Southern Illinois University (IL)	Margaret Lee	Appalachian State University (NC)
Kanchan Das	East Carolina University (NC)	Shiyoung Lee	Penn State University Berks (PA)
Paul Deering	Ohio University (OH)	Soo-Yen Lee	Central Michigan University (MI)
Brad Deken	Southeast Missouri State U. (MO)	Stanley Lightner	Western Kentucky University (KY)
Z.T. Deng	Alabama A&M University (AL)	Jimmy Linn	Eastern Carolina University (NC)
Raj Desai	Univ of Texas Permian Basin (TX)	Daniel Lybrook	Purdue University (IN)
Dave Dillon	North Carolina A&T State U. (NC)	G.H. Massiha	University of Louisiana (LA)
Marilyn Dyrud	Oregon Institute of Technology (OR)	Jim Mayrose	Buffalo State College (NY)
David Edward	Ivy tech C.C. of S. Indiana (IN)	Thomas McDonald	Eastern Illinois University (IL)
Joseph Ekstrom	Brigham Young University (ID)	David Melton	Eastern Illinois University (IL)
Mehran Elahi	Elizabeth City State University (NC)	Richard Meznarich	University of Nebraska-Kearney (NE)
Ahmed Elsayy	Tennessee Tech University (TN)	Sam Mryyan	Excelsior College (NY)
Bob English	Indiana State University (IN)	Arun Nambiar	California State U.—Fresno (CA)
Rasoul Esfahani	DeVry University, USA	Ramesh Narang	Indiana Univ - Purdue U. (IN)
Clara Fang	University of Hartford (CT)	Argie Nichols	Univ Arkansas Fort Smith (AR)
Fereshteh Fatehi	North Carolina A&T State U. (NC)	Troy Ollison	University of Central Missouri (MO)
Dominic Fazzaro	Sam Houston State University (TX)	Basile Panoutsopoulos	United States Navy
Verna Fitzsimmons	Kent State University (OH)	Jose Pena	Purdue University Calumet (MI)
Vladimir Genis	Drexel University (PA)	Karl Perusich	Purdue University (IN)
Liping Guo	Northern Illinois University (IL)	Patty Polastri	Indiana State University (IN)
Earl Hansen	Northern Illinois University (IL)	Mike Powers	III Technical Institute (OH)
Bernd Haupt	Penn State University (PA)	Huyu Qu	Honeywell International, Inc.
Rita Hawkins	Missouri State University (MO)	John Rajadas	Arizona State University (AZ)
Shelton Houston	Univ of Louisiana at Lafayette (LA)	Desire Rasolomampionona	Warsaw U. of Technology (POLAND)
Luke Huang	University of North Dakota (ND)	Mulchand Rathod	Wayne State University (MI)
Charles Hunt	Norfolk State University (VA)	Sangram Redkar	Arizona State University-Poly (AZ)
		Michael Reynolds	Univ Arkansas Fort Smith (AR)
		Marla Rogers	Wireless Systems Engineer
		Anca Sala	Baker College (MI)
		Darrel Sandall	Purdue University (IN)
		Balaji Sethuramasamyraja	Cal State U.—Fresno (CA)
		Ajay K Sharma	Ambedkar Institute of Technology (INDIA)
		J.Y. Shen	North Carolina Ag&Tech State (NC)
		Ehsan Sheybani	Virginia State University (VA)
		Musibau Shofoluwe	North Carolina A&T State U. (NC)
		Carl Spezia	Southern Illinois University (IL)
		Randy Stein	Ferris State University (MI)
		Li Tan	Purdue University North Central (IN)
		Ravindra Thamma	Central Connecticut State U. (CT)
		Li-Shiang Tsay	North Carolina Ag&Tech State (NC)
		Jeffrey Ulmer	University of Central Missouri (MO)
		Philip Waldrop	Georgia Southern University (GA)
		Abram Walton	Purdue University (IN)
		Haoyu Wang	Central Connecticut State U. (CT)
		Jyhwen Wang	Texas A&M University (TX)
		Baijian (Justin) Yang	Ball State University (IN)
		Faruk Yildiz	Sam Houston State University (TX)
		Emin Yilmaz	U. of Maryland Eastern Shore (MD)
		Yuqiu You	Morehead State University (KY)
		Pao-Chiang Yuan	Jackson State University (MS)
		Biao Zhang	US Corp. Research Center ABB Inc.
		Chongming Zhang	Shanghai Normal U., P.R. (CHINA)
		Jinwen Zhu	Missouri Western State U. (MO)

AN INNOVATIVE APPLICATION OF 3D CAD FOR HUMAN WRIST LIGAMENTOUS INJURY DIAGNOSIS

Haoyu Wang, Central Connecticut State University; Frederick W. Werner, SUNY Upstate Medical University;
Ravindra Thamma, Central Connecticut State University

Abstract

Instability of the scapholunate joint is frequently manifested by wrist pain and is sometimes visualized by a 2-4 mm gap between the scaphoid and lunate. Surgical repairs have had limited success, due in part to the surgeon being unsure which ligament or ligaments have been torn until the time of surgery. Various methods have been used to describe this gap between the bones, and various levels of instability have been described. Ideally, a surgeon would have an imaging technique such as x-ray, CT scan or MRI that would help in determining which ligaments have been damaged by visualizing the gap between the bones. In this study, the authors proposed and implemented three measurements: a 1D (one-dimensional) minimum gap between the bones, a 2D (two-dimensional) area descriptor of the gap, and a 3D (three-dimensional) volume descriptor of the gap. Cadaver wrists were moved through cyclic flexion-extension (FE) and radioulnar deviation (RU) motions under computer control.

Three-dimensional scaphoid and lunate motion data were collected in the intact specimens and after sequentially sectioning three ligaments, in two sequences. Data were again collected after 1000 cycles of motion to mimic continued use after injury. CT-scan images of each wrist were contoured and stacked with imaging software after which the surface models (dxf) were converted to solid objects (IGES). Finally, a DLL (Dynamic Link Library) was created in C++ to interface with SolidWorks®. The experimentally collected kinematic data of the carpal bones were used to move the virtual bone models through the DLL in SolidWorks®. The articulating surface on each bone is a 3D surface with 3D curves as boundary. The 1D, 2D, and 3D gaps were automatically created and calculated by the DLL in SolidWorks®, while the scaphoid and lunate were in motion. These methods can help the surgeon in better visualizing the injury.

Introduction

Damage to the ligaments of the wrist is a common injury, but one that is not well publicized. In 1999, traumatic wrist injuries were reported by 88,000 workers in private industry and by 580,000 people whose ligamentous injuries were related to consumer products (Bureau of Labor Statistics, National Electronic Injury Surveillance System (NEISS)). In

particular, injuries due to recreational activities such as snowboarding, skateboarding, and riding scooters has increased at a rate of 15% per year.

One region of the wrist that is commonly injured after falling on an outstretched hand is the scapholunate (SL) joint; see Figure 1. An impact to the wrist may produce carpal instability, where the stabilizing ligaments of the wrist are compromised, as indicated in Figure 2. The instability pattern between the scaphoid and lunate may cause pain and the inability to grasp tools or lift objects. As noted by Garcia-Elias et al. [1], the adverse effects of the ligament tears are underestimated and the injury is frequently untreated or poorly managed. Numerous surgical treatments have been developed with varying success [2].



Figure 1. Scapholunate joint

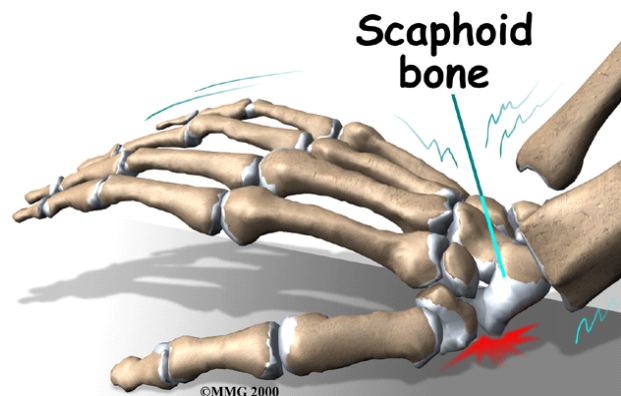


Figure 2. Stabilizing ligaments injury due to impact

The purpose of this study was to develop a methodology to determine if various joint-gap measurements between the scaphoid and lunate could be related to specific ligament injuries through 3D computer models of the scapholunate joint. Three-dimensional models are useful tools for the study of complex joint motions. In-vitro 3D animations and models have been based on motion of the forearm at various static positions [3], dynamic vertebral motion [4], passive motion of extremities [5], and passive motion of carpal bones [6]. In-vivo motions have been modeled using biplanar radiographs at static joint angles [7], high-speed biplanar radiographs in a canine [8], and 3D model fitting of fluoroscopic videos [9]. Multiple in-vivo 3D CT data sets, taken at various static joint positions, have been animated by Crisco et al. [10] and Snel et al. [11]. These different techniques have quantified and illustrated rotation angles, motion axes, contact areas, and ranges of motion.

Although each method has its inherent benefits, no single technique animates dynamic human joint motion with commercial software. Static and passive motion studies may not account for kinematic changes due to dynamic tendon loads, and the need for custom software development can be overwhelming. The goals of this study were to present a technique to (a) develop methodology to characterize separation of scaphoid and lunate with ligamentous sectioning and (b) determine which wrist positions might best differentiate these effects. These interbone gaps help describe bone motions and kinematic changes due to ligamentous injury.

Methods and Materials

A servo-hydraulic simulator was used to move cadaver hands through repeatable wrist motions [12]. Fastrak motion sensors (Polhemus, Colchester, VT) collected kinematic data at 27 Hz for the scaphoid, lunate, and radius, and at 82 Hz for the 3rd metacarpal. A wrist flexion-extension motion representing 50° of third metacarpal flexion to 30° of extension, and a radial-ulnar deviation of 10° radial to 20° ulnar were also performed. After testing, each arm was removed from the simulator and rigidly fixed within a styrofoam box using expanding urethane foam. Fastrak kinematic data were collected and a CT scan was performed on the arm. The post-test kinematic data were used to establish a spatial relationship between the sensor data and the location and orientation of the bones in the CT slices, as indicated in Figure 3.

The CT images were segmented with SliceOmatic imaging software (Tomovision, Montreal, Canada) to produce surface shells, or polygonal models, of the bones. This software uses a proprietary algorithm to automatically contour regions of high gray-level contrast. The user traces an area by using a mouse and cursor to place points around the structure to be contoured. The algorithm then uses the origi-

nal gray-level gradient of the image to place a contour near the user-selected points, based on the highest contrast in that immediate area.

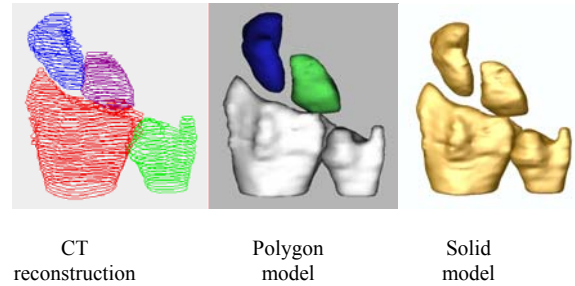


Figure 3. CT slice model, polygon model, and solid model

The user-selected points are replaced with software-generated points along the gradient that are spaced at two pixels apart. The user can limit the amount of curvature allowed in the contour. For this study, the carpal bones were contoured at the subchondral bone/cartilage interface and at the outer edges of the magnetic coils for the sensors. In order to calculate interbone gaps, the polygonal bone models were exported from 3DStudio-MAX and converted to NURBS (Non-Uniform Rational B-Spline) surface models using Geomagic Studio [13]. NURBS (.igs) are smooth, continuous surfaces defined over a quadrilateral region, based upon vertex points and allow the models to be analyzed with three-dimensional CAD software. The polygons were decimated, refined and replaced with a grid pattern to fit a closed surface. The surface consisted of 1000 patches per bone.

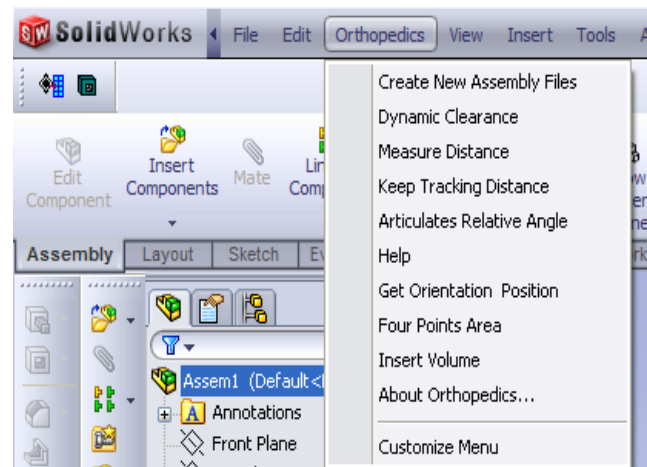


Figure 4. Orthopedics Add-in in SolidWorks

Animations of the bones' solid models and interbone-gap calculations for each frame of an animation were implemented in Solidworks 3D CAD software [14]. In this study, the author developed in-house software, ORTHOPEDICS, in C++, using the SolidWorks API (Application Programming Interface) on a Windows platform; refer to Figures 4

and 5. The software has the form of DLL (Dynamic Link Library), which is easily loaded and unloaded in SolidWorks just like any other standard add-ins.

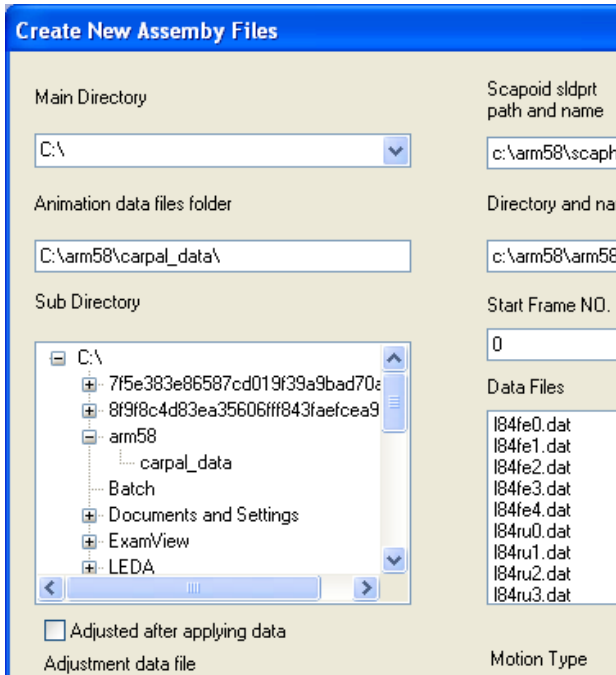


Figure 5. Orthopedics Dialog Box

ORTHOPEDECS automatically created separate CAD assemblies, based on the Fastrak carpal data, to replicate each animation frame produced in 3DStudioMAX. Instead of the conventional rotation matrix, Quaternions were used in calculating motions of the scaphoid and lunate carpal bones as they are more efficient and more numerically stable. For each assembly, the software computed 1D, 2D, and 3D interbone gaps between scaphoid and lunate.

1. 1D gap calculation

A 1D gap is defined as the minimum distance between the carpal bones. The minimum distance is calculated by what can be called a “pingpong” algorithm. The top image in Figure 6 illustrates this method. If the bones are opened and separated like a book, the articulating surfaces can be seen, as in the lower image in Figure 6. The SolidWorks API is capable of locating a point on a face that is closest to a point in the space. Starting from a point that is in between the scaphoid and lunate, a point on one of the articulating faces of scaphoid can be found. This point can now be used as the starting point for finding the closest point on the face of the lunate. For each patch-to-patch comparison, points were compared based on a user-defined spacing—or tolerance—of 1 mm. The algorithm searched for an individual point in one patch that was closest to a second point on the other

bone. Thus, it ‘ping-ponged’ between points on these two patches until the newest point on one patch was within 1 mm of the previous point. In order to increase the efficiency of the algorithm, the authors selected the patches to be examined for distance computation. A line was drawn between the bones to represent the minimum distance, and the CAD assembly saved. The algorithm created the next assembly in the motion, calculated the minimum distance, and saved the distances to a text file. Methods of validation of the minimum distance can be found in [15].

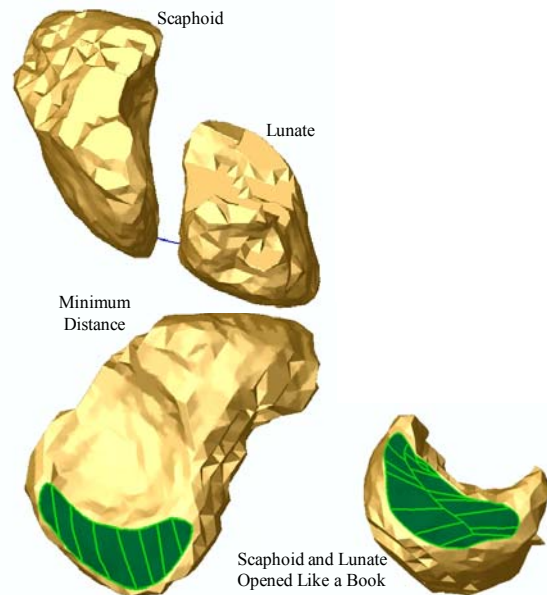


Figure 6. Ping-pong algorithm for 1D gap

2. Calculation of a 2D gap

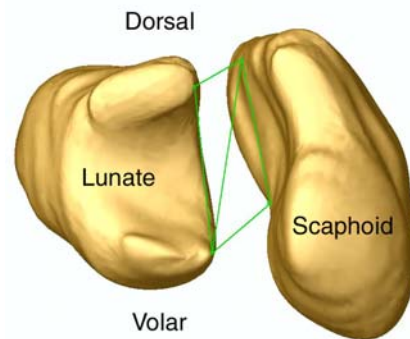


Figure 7. 2D gaps (dorsal and volar gaps)

A 2D gap is defined as a quadratic area between the carpal bones. This was inspired by the regular practices of hand surgeons as they diagnosed these kinds of injuries. Figure

7 shows two dorsal points and two volar points chosen by the authors to represent a selection by a hand surgeon. The dorsal separation and volar separation were then calculated. Three of the four points were used to define a plane, while the fourth point was projected onto the plane. Then, the quadratic area was calculated.

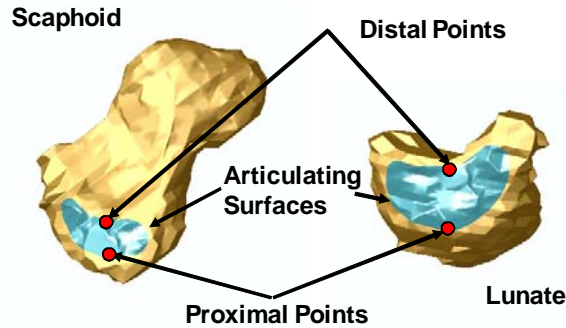


Figure 8. 2D gaps (distal and proximal gaps)

The user can otherwise pick four points that detect the distal and proximal separations, as indicated in Figure 8. In this figure, one can also see the articulating surfaces. These were used to generate the volume between the scaphoid and lunate.

3. Calculation of a 3D gap

A 3D gap is defined as the lofted volume between the articulating surfaces of the carpal bones; refer to Figure 9. Since CAD software can only calculate the volume and surface area of a complex shape when the model is a solid, it was necessary to first describe a contained volume between the scaphoid and lunate. As the articulating surface on each bone is a 3D surface with a 3D curve as a boundary, the idea of lofting was chosen to generate the volume between the two articulating surfaces. Lofting creates a feature by making transitions between profiles. Using the lofting method to generate the volume has two advantages. First, the 3D boundary curves and 3D surfaces of both articulating surfaces are used directly instead of being approximated when generating the volume. Second, it offers the flexibility of changing the definition of the volume by changing the guide curves of the loft. For any frame of motion of the carpal bones, the volume between the articulating surfaces is generated physically by using the Solid Lofting feature provided in SolidWorks.

There are five ligaments that are thought to stabilize the scaphoid and lunate. The scapholunate interosseous ligament, seen in Figure 10, known as SLIL, connects the scaphoid and lunate. On the dorsal side of the wrist, is the dorsal intercarpal ligament known as DIC, and the dorsal radio

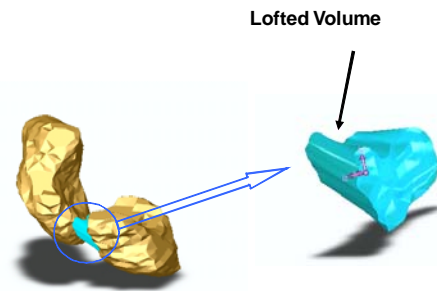


Figure 9. 3D gaps (lofted volume)

carpal ligament known as DRC. On the volar aspect of the wrist is the radioscapo-capitate ligament known as RSC, and the scapho-trapezium ligament known as ST.

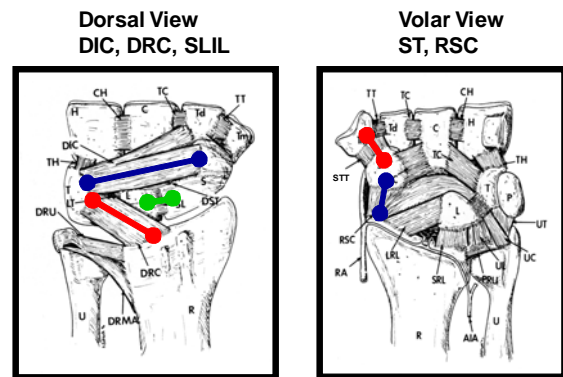


Figure 10. Ligamentous stabilizers

In each of 19 freshly frozen cadaver forearms that were tested for this study, Fastrak electromagnetic motion sensors were mounted onto the scaphoid, lunate, third metacarpal, and distal radius in order to measure their 3D motion with electromagnetic sources mounted onto a platform and attached to the ulna. Four groups of arms were studied. For each group of arms, three ligaments were sequentially sectioned in the sequences shown below, each of which saw 1000 cycles of motion.

- Group 1: SLIL, RSC, ST, - 5 arms
- Group 2: ST, SLIL, RSC, - 4 arms
- Group 3: DRC, DIC, SLIL, - 5 arms
- Group 4: DIC, SLIL, DRC, - 5 arms

The motion of the scaphoid and lunate was measured with the wrist intact, after each ligament was sectioned for each of the 3 sequences shown here, and after 1000 cycles of motion.

Results

Figure 11 shows the minimum distances computed for each level of sectioning during wrist flexion/extension. An increase of the minimum distance was observed only when SLIL was sectioned. This was accentuated with sectioning of the RSC ligament and even more so with the addition of 1000 cycles of repetitive motion. It is important to note that the maximum gap always occurred during wrist flexion. Figure 12 shows another average minimum distance plot during wrist flexion/extension but with a different sectioning sequence. An increase of the minimum distance occurred only after the SLIL was sectioned. A further increase was observed after 1000 cycles of motion. Again the maximum gap measured by the minimum distance appeared during wrist flexion.

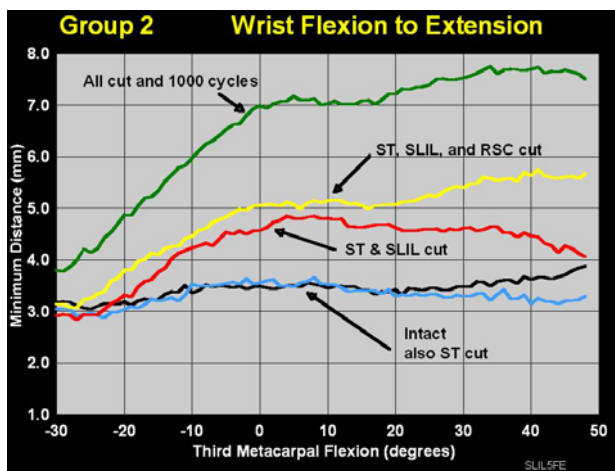


Figure 11. 1D gap after section of ST, SLIL, and RSC

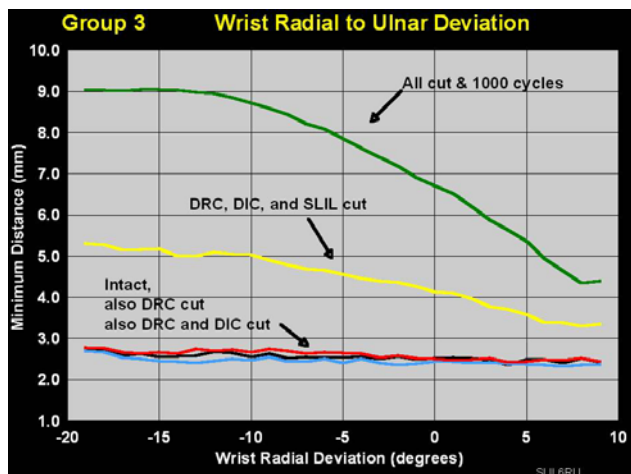


Figure 12. 1D gap after section of DRC, DIC, and SLIL

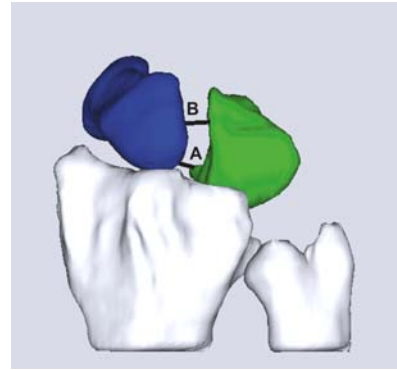


Figure 13. 1D gap as on an X-Ray

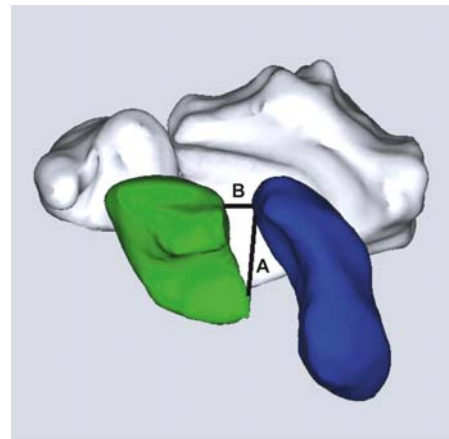


Figure 14. Actual 1D gap between carpal bones deviation

During radial/ulnar deviation, an increase in the minimum distance was observed only after SLIL was sectioned. In addition, the maximum value of the minimum distance was detected in ulnar deviation. Figure 13 shows the dorsal view of the wrist joint as if measurements were being made on an x-ray machine. Looking at Figure 14, distances A and B appear to be similar in length, when in fact they have very different lengths. It is better illustrated from this view. This is why the minimum distance in this study, based on the 3D model, is a much better descriptor than the distance measured in 2D on an X-ray.

Measurement of the dorsal and volar gaps between the scaphoid and lunate showed an increase in the distance between the scaphoid with ligamentous sectioning (Figure. 15). This graph shows the percentage increase in the gap after all ligaments had been cut and after 1000 cycles. As shown in this series of arms, the dorsal and volar distances increased the most in wrist flexion after all of the ligaments were sectioned. Also, the dorsal gap increased more than the volar gap and the bones did not separate evenly.

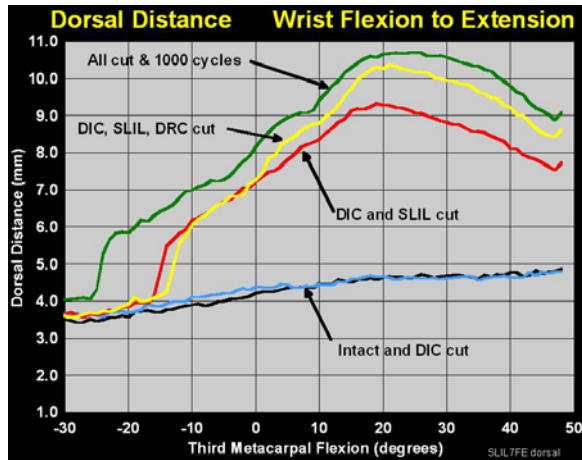


Figure 15. 2D dorsal gap

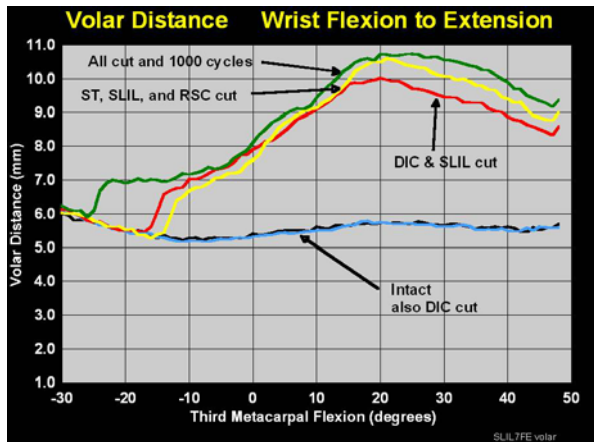


Figure 16. 2D volar gap

Looking at the graph in Figure 16, it can be seen that the distances between the proximal and distal points on the articulating surfaces also increased with ligamentous sectioning. Additionally, the increase was greater in flexion than in extension and the dorsal distance increased more than the proximal distance during only a small part of the motion.

Volume changes in the gap during the wrist flexion/extension motion can be seen in Figure 17. The volume of the gap was greater in flexion and correlates well with the 1D minimum distance changes for both when the ligaments are intact and after all have been sectioned. Intuitively, one can consider volume as a better gap descriptor as it is 3D in nature and more informative. How it could help in describing the gap between the scaphoid and lunate, is still under study.

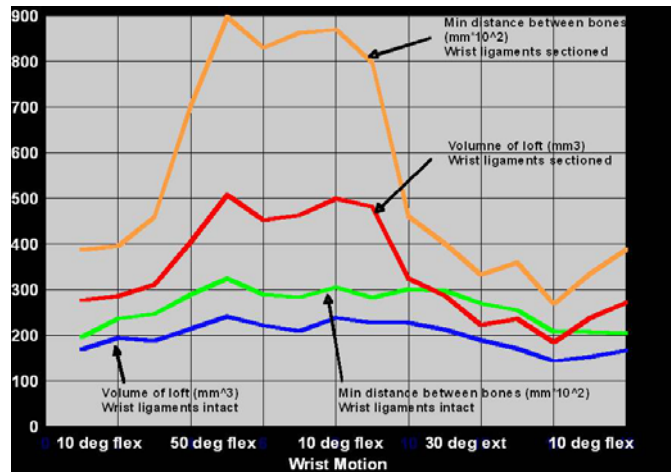


Figure 17. Correlation between 3D gap and 1D gap

Conclusions

This study showed that changes in carpal bone position are better detected using 3D visualization techniques. The nature of an x-ray is a projection of a 3D object onto a 2D screen. Thus, the actual scapholunate gap could be foreshortened, making the results misleading. Therefore, accuracy of measuring a gap on a 2D x-ray with the wrist positioned in neutral was questioned. In this study, three methodologies were developed to characterize the scapholunate gap. First, a ping-pong algorithm was developed and implemented to calculate the minimum distance between the carpal bones, scaphoid and lunate. Second, a four-point area method showed how a hand surgeon could pick four specific points, two on the scaphoid and two on the lunate, to represent the most important locations on the carpal bones that the hand surgeon would use to analyze the motion. Third, a solid volume was generated between the carpal bones by lofting between the cartilage areas of the bones.

Preliminary research showed the correlation between the volume and the minimum distance. The authors believe that the lofted volume can represent the ligament between the bones and be very valuable in the diagnosis of ligamentous injuries. Further research is needed to determine related applications. An add-in to SolidWorks, ORTHOPEDICS, was developed to implement all of the aforementioned scapholunate-gap calculation methods. Gap data can be collected automatically for all frames of a motion. The results of the gap data in this study showed that changes due to DIC or ST sectioned alone could not be detected. Furthermore, detection of major SL gap changes may be best detected in wrist ulnar deviation and flexion.

The methodology in the study can be applied to the analysis of any human or animal joint injury. Future study is needed to collect data from real patients, explore application fields, and develop stand-alone software.

References

- [1] Garcia-Elias, M., A.L. Lluch, and J.K. Stanley (2006), Three-ligament tenodesis for the Treatment of Scapholunate Dissociation: Indications and Surgical Technique. *Journal of Hand Surgery*, 31A: p. 125-134.
- [2] Manuel, J. and S.L. Moran (2007), The Diagnosis and Treatment of Scapholunate Instability. *Orthopaedic Clinics of North America*, 2007. 38: p. 261-277.
- [3] Fischer, K.J., Manson, T.T., Pfaeffle, H.J., Tomaino, M.M., Woo, S.L.-Y., 2001. A method for measuring joint kinematics designed for accurate registration of kinematic data to models constructed from CT data. *Journal of Biomechanics* 34, 377–383.
- [4] Cripton, P.A., Sati, M., Orr, T.E., Bourquin, Y., Dumas, G.A., Nolte, L.-P., 2001. Animation of in vitro biomechanical test. *Journal of Biomechanics* 34, 1091–1096.
- [5] Van Sint Jan, S., Salvia, P., Hilal, I., Sholukha, V., Rooze, M., Clapworthy, G., 2002. Registration of 6-DOFs electrogoniometry and CT medical imaging for 3D joint modeling. *Journal of Biomechanics* 35, 1475–1484.
- [6] Patterson, R.M., Nicodemus, C.L., Viegas S, F., Elder, K.W., Rosenblatt, J., 1998. High-speed, three-dimensional kinematic analysis of the normal wrist. *Journal of Hand Surgery* 23 (3), 446–453.
- [7] Asano, T., Akagi, M., Tanaka, K., Tamura, J., Nakamura, T., 2001. In vivo three-dimensional knee kinematics using a bi-planar imagematching technique. *Clinical Orthopaedics and Related Research* 388, 157–166.
- [8] You, B.M., Siy, P., Anderst, W., Tashman, S., 2001. In vivo measurement of 3-D skeletal kinematics from sequences of biplane radiographs: application to knee kinematics. *IEEE Transactions on Medical Imaging* 20 (6), 514–525.
- [9] Dennis, D.A., Komistek, R.D., Hoff, W.A., Gabriel, S.M., 1996. In vivo knee kinematics derived using an inverse perspective technique. *Clinical Orthopaedics and Related Research* 331, 107–117.
- [10] Crisco, J.J., McGovern, R.D., Wolfe, S.W., 1999. Noninvasive technique for measuring in vivo three-dimensional carpal bone kinematics. *Journal of Orthopaedic Research* 17 (1), 96–100.
- [11] Snel, J.G., Venema, H.W., Moojen, T.M., Ritt, J.P., Grimbergen, C.A., den Heeten, G.J., 2000. Quantitative in vivo analysis of the kinematics of carpal bones from three-dimensional CT images using a deformable surface model and a three-dimensional matching technique. *Medical Physics* 27 (9), 2037–2047.
- [12] Short WH, Werner FW, Green JK, et al. 2002. Biomechanical evaluation of ligamentous stabilizers of the scaphoid and lunate. *J Hand Surg* 27A:991–1002.
- [13] Raindrop Geomagic, Geomagic User Manual, Raindrop Geomagic Inc. Research Triangle Park, NC, 2000
- [14] Solidworks 99 User’s Guide, Solid Works Corporation, 1999
- [15] Jason K. Green, Frederick W. Werner, Haoyu Wang, Marsha M. Weiner, Jonathan Sacks, Walter H. Short (2004), Three-Dimensional Modeling and Animation of Two Carpal Bones: A Technique, *Journal of Biomechanics*, Volume 37, Issue 5, May 2004, Pages 757-762

Biographies

Dr. Haoyu Wang is currently an assistant professor in the Department of Manufacturing and Construction Management at Central Connecticut State University. He received his Ph.D. in mechanical engineering from Syracuse University. Dr. Wang’s teaching and research interests include GD&T, CAD/CAM, manufacturing systems, and injury biomechanics. Dr. Wang may be reached at wanghao@ccsu.edu

Prof. Frederick W. Werner is a research professor of Department of Orthopedic Surgery at SUNY Upstate Medical University. He is also an adjunct professor in the Department of Bioengineering at Syracuse University. His primary research interests are in the areas of experimental biomechanics of the upper and lower extremities as related to the function of normal, diseased and surgically repaired soft tissues and joints.

Dr. Ravindra Thamma is currently an assistant professor in the Department of Manufacturing and Construction Management at Central Connecticut State University. Dr. Thamma received his Ph.D. from Iowa State University. His teaching and research interests are robotics, linear control systems, and intelligent systems.

UTILIZING ADVANCED SOFTWARE TOOLS IN ENGINEERING AND INDUSTRIAL TECHNOLOGY CURRICULUM

Faruk Yildiz .Sam Houston State University; Recayi “Reg” Pecen, University of Northern Iowa; Ayhan Zora, University of Northern Iowa

Abstract

Engineering and technology software tools are used by professionals and companies worldwide, and in a university setting, students are given the opportunity to familiarize themselves with the operation of software packages that they will be using after they join the workforce. Many classroom projects in engineering technology curriculum that require the use of advanced software tools has increased in college and universities on both undergraduate and graduate levels. Emerging virtual applications enhance understanding both theoretical and applied experiences of engineering technology students by supporting laboratory experiments. MSC.Easy5, AMESim, SolidWorks, ProE, Matlab, MultiSim and LabView™ are some of the well known system modeling, simulation and monitoring software tools that offer solutions to many problems in mechanical, thermal, hydraulics, pneumatics, electrical, electronics, controls, instrumentation and data acquisition areas. These virtual tools also help to improve the learning pace and knowledge level of students in many applied subjects. This paper presents case studies used in applied class projects, laboratory activities, and capstone senior design projects for a B.S. degree program in electrical engineering technology and manufacturing/design technology. Many students have found software tools to be helpful and user friendly in understanding fundamentals of physical phenomena.

Introduction

The development of educational and industrial software and simulation tools has been considerably increased by the development of high speed computers. Industrial applications now concentrate on replacing expensive equipment with software and simulations tools, while a number of educational institutions are preferring simulation tools instead of purchasing expensive test equipments for their laboratories. Universities, especially engineering education departments, are incorporating industry standard programming environment tools mainly in laboratory practices, but they are also being used in research and classroom education.

In engineering education, the demonstration of high tech equipment is the most common procedure. Demonstration

engages process modeling, testing and simulation, imitates data acquisition and process control. For demonstration purposes, high level graphical user interface is required for providing efficient communication. Virtual applications may enhance both theoretical and hands-on experience for engineering technology students by supporting laboratory experiments as well. Most well-known industrial and educational software packages such as MSC.Easy5, LMS Imagine.Lab AMESim, SolidWorks, ProE, Matlab, MultiSim and LabView™ are powerful physical system simulation and monitoring software tools that offer solutions to many problems in mechanical, thermal, hydraulics, pneumatics, electrical, electronics, instrumentation and data acquisition areas. These virtual tools also help to develop learning knowledge level of students in many applied subjects. For example, one of the well-known industrial software packages used in engineering education is LabView™, is a National Instrument (NI) product [1]. The NI LabView™ is a user friendly graphical based programming environment mainly developed for data acquisition, instrumentation, and monitoring, besides process control and modeling are also supported.

There are a variety of research attempts to add simulation tools to laboratory experiments in engineering education courses. Virtual Control Workstation Design using Simulink, SimMechanism, and the Virtual Reality Toolbox was conducted in education to teach control theory principles as well as a test station for control algorithm development [2]. Authors used two workstations from Quanser Consulting for their electrical and computer engineering program student projects. Their claim was that incorporating a laboratory support into the engineering courses would enhance learning skills of the students. The discussion of the design and use of a low-cost virtual control workstation has been accomplished in the first undergraduate control theory course. The virtual workstation model from the physical, electrical, and mechanical parameters of a Quanser Consulting electromechanical system was built during the course period. The system has been used in over a dozen student projects and faculty research in the Electrical and Computer Engineering department at Bradley University. A capstone project was distributed to all faculty members. Also the learning curve of Simulink in senior capstone projects was tested by designing a six-week design project for a course that required system modeling using Simulink.

Other research incorporating the use of multimedia tools into a reverse engineering course has been presented by Madara Ogot [3]. The main goal of this study was to use multimedia as initiatives for the students to learn how to use main tools and use them in other academic activities beyond the reverse engineering class. Since a classic mechanical engineering curriculum may not offer instructions on the use of multimedia tools in the areas of computer illustration, animation, and image manipulation, this experience increased the major students' interest in these topic areas. Instruction on the use of these tools was incorporated into a mechanical engineering course at Ruther University instructors plan to send out follow-up surveys at the end of the each semester to students who have taken the class. It is expected that the results of the surveys should provide an indication as to whether providing formal instruction in the use of multimedia tools actually translates into their common use during the students' technical, oral and written communications.

Another study has been conducted to increase use of software tools such as PSCAD/EMTDC [4], an electrical power and power electronics transient studies software tool for majors in the Electrical Engineering area. The aim of this study was to familiarize students with the electrical power systems without the cost and safety issues of actual power system simulators. Introduction of the PSCAD is usually introduced in the second week of an undergraduate power systems class and training starts with two basic sessions. For this purpose two case studies were presented on PSCAD that included the simulation of a three-bus system that allowed for independent control of voltage and phase on each bus in a way that clearly illustrates the principles of power flow control [5]. The author's objective in using digital simulation software tools in power systems is that "modern teaching facilities supported with digital simulation tools and well equipped laboratories have great impact in the development of engineering programs in power systems and energy technologies."

Software Tools in Technology Education

Authors of this paper introduce a number of case studies based on the following digital simulation and modeling tools in both mechanical and electrical engineering technology areas.

The AMESim simulation package comes with very helpful demonstration models for a convenient initial start of modeling [6]. This digital software tool offers an extensive set of application specific solutions which comprise a dedicated set of application libraries and focus on delivering simulation capabilities to assess the behavior of specific subsystems.

Pro/ENGINEER Wildfire 2.0 and its "Mechanism" simulation application is used to demonstrate an interference problem between parts in the engineering assemblies by simulating the individual parts [7]. Pro/ENGINEER is another standard in 3D product design, featuring industry-leading productivity tools that promote practices in design while ensuring compliance with industry standards.

Another 3D design software is SolidWorks Education Edition, which brings the latest technologies in 3D CAD software, COSMOS Design Analysis software, and comprehensive courseware to the modern design-engineering curriculum [8]. National Instruments MultiSim [9] formerly Electronics Workbench MultiSim software integrates powerful SPICE simulation and schematic entry into a highly intuitive user friendly graphical based electronics labs in digital environments.

LabView™ is another National Instruments graphical development environment to help create flexible and scalable design, control, and test applications [1]. With LabView™, engineering and technology students can interface with real-world signals from a variety of physical systems in all engineering areas; analyze data for meaningful information; and share results through intuitive displays, reports, and the Web. Although not covered in this paper due to the length of this paper, Matlab has been one of the strongest mathematical tools in analog and digital signal and control systems design and simulation studies in the program at the University of Northern Iowa.

Case Studies

Six case studies are presented in this section of the paper. In the first case study, we will be determining the angle of inclination of a plane when the object starts moving if it is located on a flat inclined surface with a given static friction of coefficient. The second case study demonstrates how to determine the stopping distance and time of a vehicle model on inclined surfaces. The third case study is to solve interference problems between engineering models created by Pro/Engineer Wildfire based on Mechanism simulation application. The fourth case study describes Solid Works in a capstone design project to model and simulate floating calculations for a solar electric powered fiberglass boat developed at the University of Northern Iowa. The fifth case study is using MultiSim, Electronics Workbench in simple RLC circuits for measurement purposes. A low pass filter study, Bode Plot for stability, and full-wave bridge rectifier simulation studies by MultiSim are also briefly reported. The last digital tool covered in this paper is LabView™ for data acquisition and instrumentation of a 1.5 kW wind-solar power system where AC and DC voltage, current, power, wind speed values are monitored and recorded precisely.

A. Angle of Inclination Study

Figure 1 depicts a schematic of the simulated system. An object with mass, m , is located on a flat surface. One edge of the surface is lifted to form an angle, α , with the ground. The static friction coefficient, μ_s , is given. The purpose of this test is to determine the angle of inclination when the object starts the motion by using a digital simulation tool.

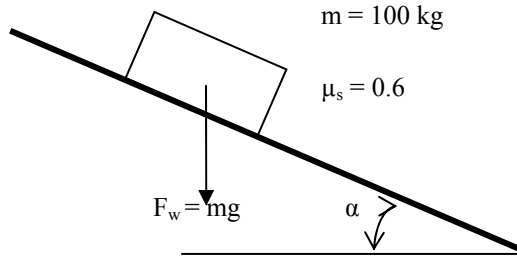


Figure 1. Object on inclined surface.

LMS.Imagine.Lab 7b is used to simulate the system [6]. In the mechanical library there exists a component called “linear mass with 2 ports and friction”. The user can apply external forces through the ports; for our purpose the external forces are set to zero. Figure 2 illustrates the simulation model where attachments from both sides of the mass represent the zero external forces.

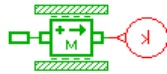


Figure 2. Simulation model of the object on inclined surface.

Parameters of the mass component are populated as demonstrated in Figure 3. The first two parameters are state variables that are calculated internally; the user is supposed to provide only the initial conditions. Initial velocity and displacements are set to zero. As a selected mass of 100 kg starts the motion, initial velocity and displacement values are set to calculated values by the model. Since stiction force is good enough for calculations selected, the other three friction inputs, coefficient of viscous friction, coefficient of windage, and Coulomb friction force are all set to zero values.

The formula for the stiction force is given as:

$$F_{fs} = \mu_s mg \cos\left(\frac{\alpha\pi}{180}\right) \quad (1)$$

where $\mu_s = 0.6$ coefficient of friction
 $m = 100 \text{ kg}$ mass
 $g = 9.81 \text{ kgm/s}^2$ gravitational coefficient
 α (degree) angle of inclination

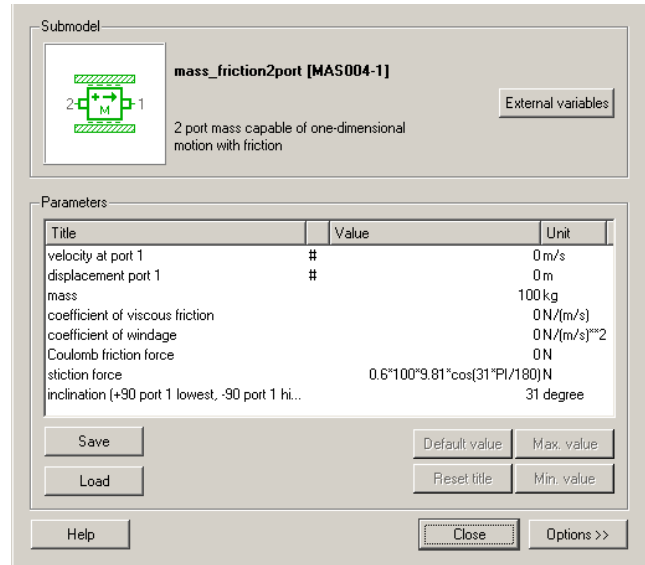


Figure 3. Parameters input to mass component.

The angle of inclination in the stiction force formula and the inclination in the following line must be identical. Several runs are conducted with different inclinations for 10 seconds and velocity of the mass has been observed to determine a motion. The results are given in Table 1. According to this study, the angle of inclination is determined as 31 degree.

Table 1. Results of the simulation model for angle of inclination

The angle of inclination(degree)	Mass Velocity(m/s)
0	0
15	0
30	0
31	5.1
40	6.3

An analytical formula to calculate the angle of inclination is given as follows [10]:

$$\mu_s = \tan \alpha \quad \text{or} \quad \alpha = \arctan \mu_s \quad (2)$$

where μ_s coefficient of friction
 α (degree) angle of inclination

Since $\mu_s = 0.6$, the angle of inclination can be calculated as $\alpha = \arctan(0.6) = 30.96^\circ$. This result validates our simulation model.

This simple case and several other cases that are introduced in lectures and labs have alleviated the instruction of a complicated engineering software tool (such as AMESim) used students who are taking beginning level of engineering or engineering technology courses. It is observed that the modeling approach has helped students grasp of more advanced engineering subjects.

B. Vehicle Traveling Distance Study

Because it is an introductory level engineering technology course, the subject of the Power Technology class includes a basic level of mechanical power transmission calculations such as gears, pulleys, inclined plane, etc. Vehicle level design and analysis are generally covered in higher level courses at junior or senior levels. Moreover, testing such vehicles in labs or in the field is always hard to conduct for even an experienced technician and it is expensive to maintain such facilities for a teaching institute. Using software tools may improve instruction of more difficult subjects at lower level courses.

One of the problems presented as part of a computer lab assignment was determining stopping distance and time of a vehicle model on an inclined ground profile. The schematic of the problem is shown in Figure 4. An initial torque profile, as depicted in Figure 5, is applied to vehicle first 22s of the test, and the travel distance and the elapsed time until the vehicle comes to a complete stop must be determined at the given ground slopes of 5%, 10%, 15% and 20%. The vehicle model consists of an engine, vehicle, transmission, differential and tire components.

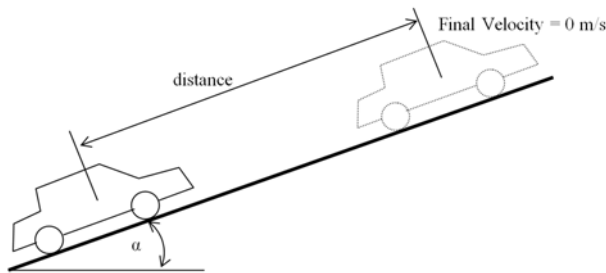


Figure 4. Schematic of vehicle and ground profile.

The AMESim simulation package offers an extensive set of application specific solutions which comprise a dedicated set of application libraries and focus on delivering simulation capabilities to assess the behavior of specific subsystems. The current portfolio includes solutions for internal combustion engines, transmissions, thermal management systems, vehicle systems dynamics, fluid systems, aircraft ground loads, flight controls, and electrical systems. AMESim comes with very helpful demo models for a convenient initial start of modeling.

“VehicleTire.ame” is a demonstration model in their power train library which consists of differential, vehicle and tire models. While the engine has been represented by a simple torque curve, a transmission model has been completely ignored. For part of the lab work, the students were expected to integrate a transmission model to the demonstra-

tion vehicle model. They are instructed to use the variable gear ratio component from AMESim mechanical library for a simplified transmission model. The component allows the user to specify any gear ratio externally. A diagram of the modified vehicle model is demonstrated in Figure 6.

Breaking torque is set to zero for the purpose of this study. The Gear ratio of the transmission has been increased from 0 to 1 by 0.25 increment for each 5 s as depicted in Figure 7. The other parameters except the slope input have been left at the default parameters from the demonstration model. The model is run twice for 5%, 10%, 15% and 20% of ground slopes. The results are shown in Table 2. It is obvious that as the slope increases, the vehicle stops earlier.

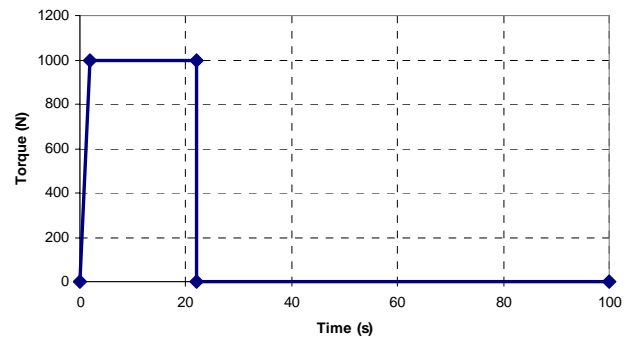


Figure 5. Engine torque profile.

Interestingly, at 20% slope, the vehicle did not move towards up to hill, instead it moved back after the engine torque was released at a time of 22s of the simulation. This gives the student an opportunity to investigate the system capabilities. The model can be used further in a detailed discussion and analysis of the vehicle behavior. For example, the car body longitudinal velocity and acceleration for 5% ground slope (Figure 8). The vehicle is accelerating and reaches to maximum velocity until time 22 second when the engine torque is set to zero as seen in Figure 8.a. The accelerating scheme (Figure 8.b) during this period looks like a step function since gear ratios are suddenly increased at times of 5, 10, and 15 s of simulation. The slight decrease in acceleration through the end of each step is because of the drag losses that were set to nonzero by default.

C. Solving an Interference Problem with Pro Engineer Wildfire 2.0

Pro Engineer Wildfire 2.0 is an engineering modeling and design program capable of creating solid models, drawings, and assemblies. Pro/Engineer comes with different application program packages to help in the design and modeling process.

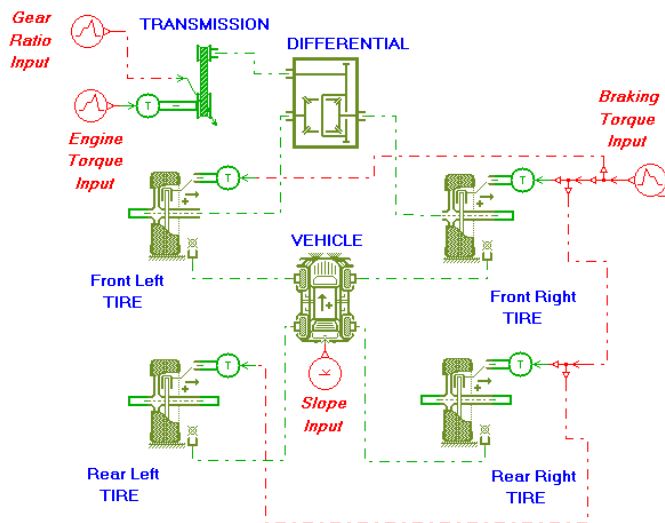


Figure 6. Vehicle simulation model.

Table 2. Results of the vehicle simulation model.

Ground Slope (%)	Stopping Distance (m)	Stopping Time (s)
5	1304	85.96
10	454	47.38
15	111	32.4
20	n/a	n/a

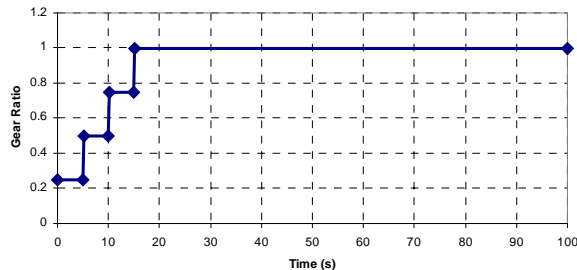
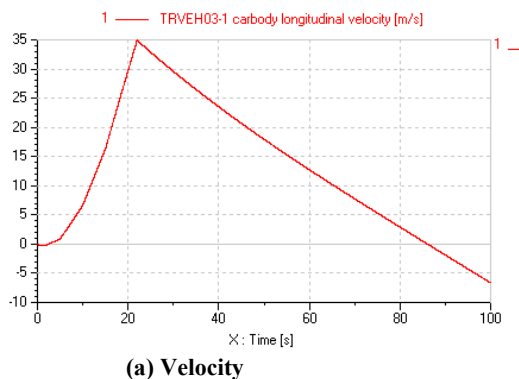
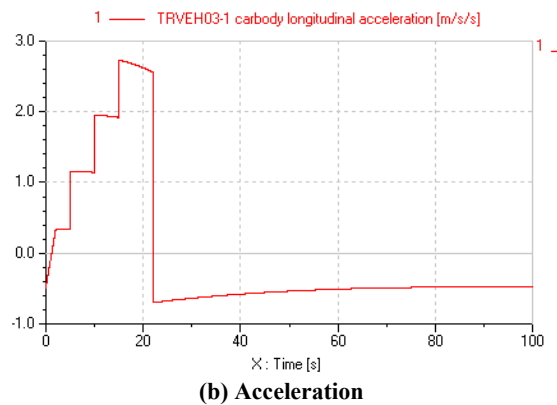


Figure 7. Gear ratio of transmission in a vehicle simulation model.



(a) Velocity



(b) Acceleration

Figure 8. Car body longitudinal velocity and acceleration.

These application programs aid engineers in testing parts, models, and assemblies from early to advanced development stages. Applications include cabling, piping, welding, sheet metal, mechanics, mechanism, animations, plastic advisor, finite element analysis etc. Student groups who are familiar with Pro/Engineer can be divided into small interest groups to make projects using application packages depending on their area of interest. For instance, cabling applications can attract an electrical engineering major student to learn how to design an electrical cabling of the system. The piping application package can be an interesting part of modeling for students who want to model air, gas, hydraulic and fuel pipes and hoses for the automotive industry. In fact, learning fundamentals of how to use Pro/Engineer applications definitely enhance students' knowledge. Fundamentals of each application help students to understand the basic terminology, tasks, and procedures so they can build their own models efficiently and share information, ideas, and processes with other students.

In this case study, a small group of engineering students were required to solve an interference problem between two parts by providing a new design solution. For this purpose, the Pro/Engineer "Mechanism" application was used to find out where the interference occurs. Pro/Engineer Mechanism can define a mechanism, make it move, and analyze its motion. In the Mechanism application, engineering students create connections between parts to build an assembly with the desired degrees of freedom, then apply motors to generate the type of motion the student wants to study. Mechanism Design allows designers to extend the design with cams, slot-followers, and gears. When the movement of the assembly is completed, the students can analyze the movement, observe and record the analysis, or quantify and graph parameters such as position, velocity, acceleration, and force. Mechanism is also capable of creating trace curves and motion envelopes that represent the motion physically. When the movement ready, mechanisms can be brought into

“Design Animation” to create an animation sequence. Actual physical systems such as joint connections, cam-follower connections, slot-follower connections, gear pairs, connection limits, servo motors, and joint axis zeros are all supported in “Design Animation.”

Initially, the dimensions of four different parts were provided to the students to model in Pro/Engineer. The parts were named with appropriate explanations to alleviate the modeling process for them. The dimensions of the ball adapter and main structure plate were intentionally changed to cause interference in between when operating in the assembly. In this case, the students used a mechanism application by changing the assembly type and using joint connections to move the parts in the assembly. Figure 9 depicts a Pro/Engineer assembly of four different parts; ball adapter, connection pin, tightening pin, and main structure plate.

As a result of modeling and assembling the aforementioned parts together, students realized that there was interference between the internal sides of the main plate and the ball adapter. The interference amount was found by making a model clearance analysis with Pro/Engineer (depicted in Figure 10 with red lines). Second interference occurred when testing the ball adapter using the mechanism application. When the ball adapter moved down 65-degree angle there was interference between the narrow edge of the main structure plate and the round shape of the ball adapter.

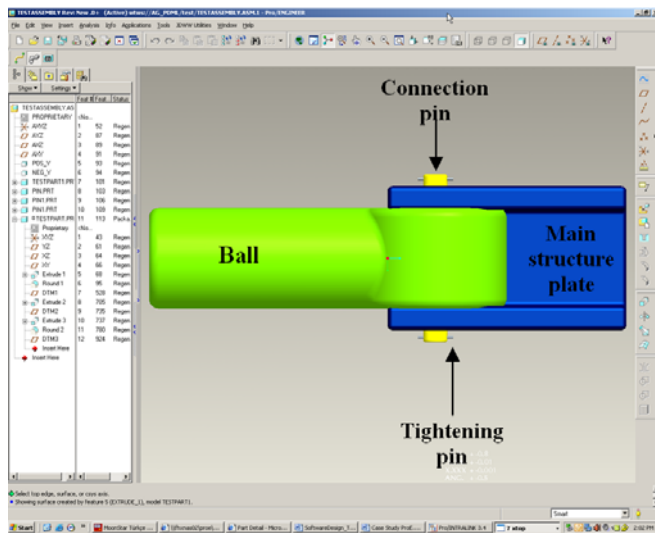


Figure 9. Pro-Engineer assembly to test assembly for interference control

This was obvious when testing with mechanism only; otherwise the interference was not visible without moving the ball adapter. Second interference diagnosed by mechanism application is shown in Figure 11 with red lines and 65-

degree angle. In this example, the 65-degree angle was given initially to indicate that the ball adapter is supposed to move a maximum 65 degree angle to avoid interference of other parts in the assembly.

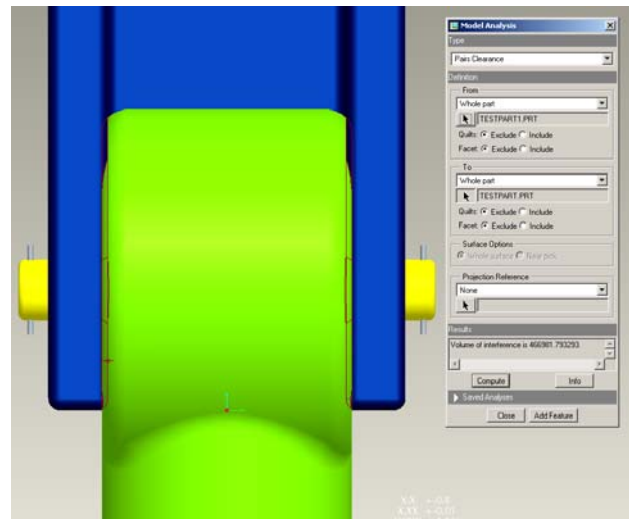


Figure 10. Interference between main plate and ball adapter without moving the parts

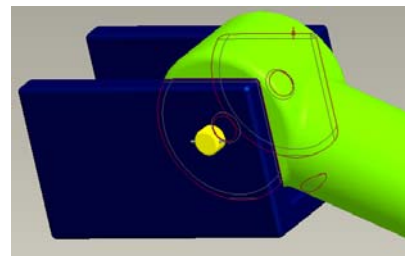


Figure 11. Interference between main plate and ball adapter when moved 65 degrees

After diagnosing the interference problems, the thickness of the main structure plate and the diameter of the round shape of the ball adapter were decreased enough to avoid the problems. This case study motivated students to involve more model analysis with other applications of Pro/Engineer. Students gained skills in how to model, assemble, and analyze their designs with Pro/Engineer and its applications.

D. Using Solid Works in Solar Electric Boat Design and Floating Calculations

The UNI solar electric boat team used both Solid Works and Pro-E to model the new solar electric boat in 2007. With the team’s extensive use of CAD, it was easiest to change the material of the hull to water and have Solid Works automatically to calculate the new mass as shown in

Figure 12 by using properties of the assigned materials from library. Buoyancy is created by the displacement of water. As modeled, the boat displaces 288 pounds of water when submerged. Calculations by Solid Works indicate the weight of the hull composed of foam material to be only 40 pounds. With all other components taken into account, the assembly of the boat weighs approximately 230 pounds in race trim. This yields a safety factor (SF) as follows:

$$SF = (288 - 230) / 288 = 0.2014 \text{ or } 20.1 \%$$

These calculations together with SolidWorks modeling show that the UNI solar electric boat, in the event of capsizing, will not sink and has a safety margin of 20.1 %.

E. Using NI MultiSim in a variety of EET Applications

Although actual hands-on analog laboratories must be included in EET curriculum, students using electronics software tools in the EET majors may also gain some initial skills and depth in knowledge without exposing themselves to the higher voltage/current values in the circuits before the actual lab day. Using virtual labs with graphical metering tools is particularly important in terms of selecting appropriate circuit components to avoid any overheating and damage to the circuit parameters.

A number of circuit simulation tools now offer low cost student versions that may provide user friendly access from student's personal computer to the laboratory circuits before the class day. Figure 13 depicts a simple RLC circuit and how to connect appropriate meters to measure voltage, current, and power.

Figure 14 shows a simple passive low pass-filter circuit and its frequency response in MultiSim using a cut-off frequency of $f_c = 2,192 \text{ Hz}$. Similarly, Figure 15 depicts a Notch filter design, its frequency response, and Bode plots in MultiSim.

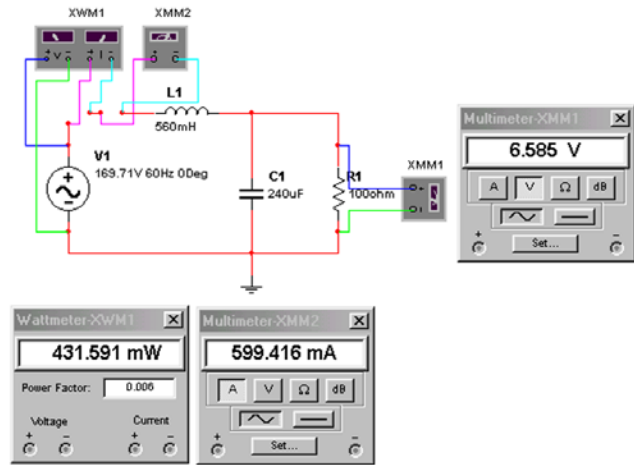


Figure 13. Voltage, current, and power measurements in MultiSim for a simple RLC circuit

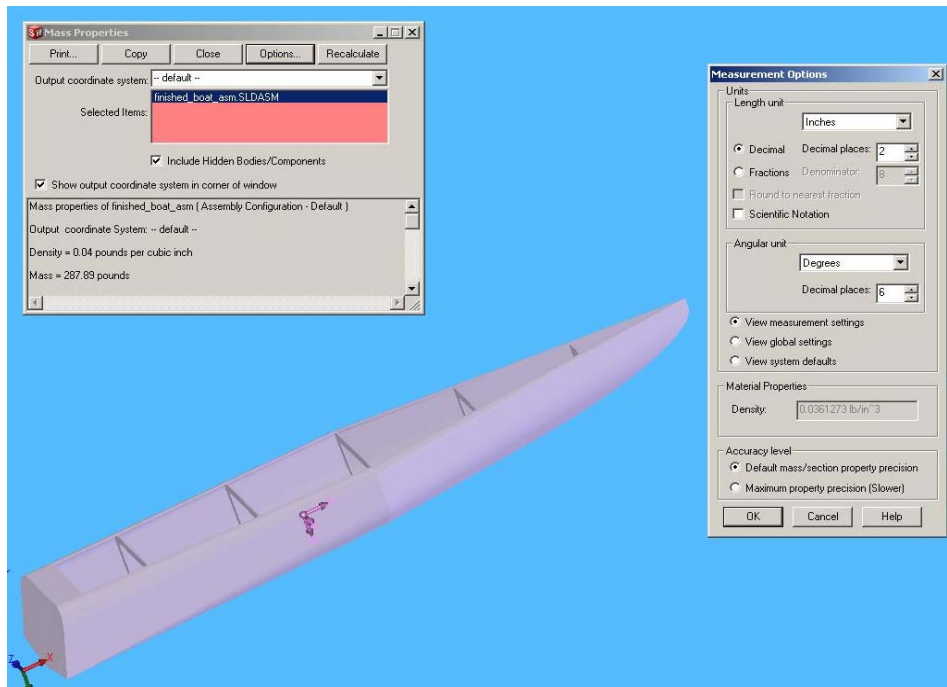


Figure 12. Solid Works model of UNI solar-electric boat

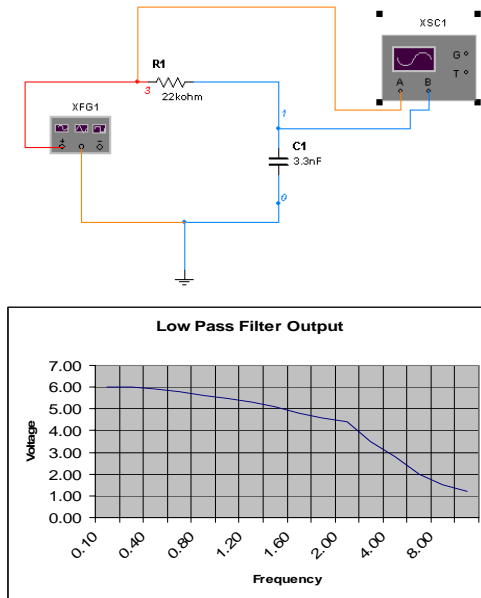


Figure 14. A simple passive low-pass filter and its frequency response using MultiSim

Figure 16 indicates another example of MultiSim applied to the simulation of a full-wave bridge rectifier in a power electronics class. Students safely gain in-depth knowledge of a high-power AC/DC converter before ever entering the lab. This also includes instrumentation connections in a virtual environment, waveform monitoring and overall circuit operation in steady-state. Figure 17 depicts a DC waveform output with numerical readings from the same bridge-rectifier circuit shown in Figure 16.

F. Using LabView™ in Computer Based Data Acquisition and Instrumentation Classes and Capstone Design Projects

Figures 18 and 19 show a LabView™ based data-acquisition virtual instrument diagram and graphical outputs, respectively, for a 1.5 kW hybrid wind-solar power system, where AC/DC voltage and current values, wind direction, wind speed and AC/DC power values are measured and monitored precisely.

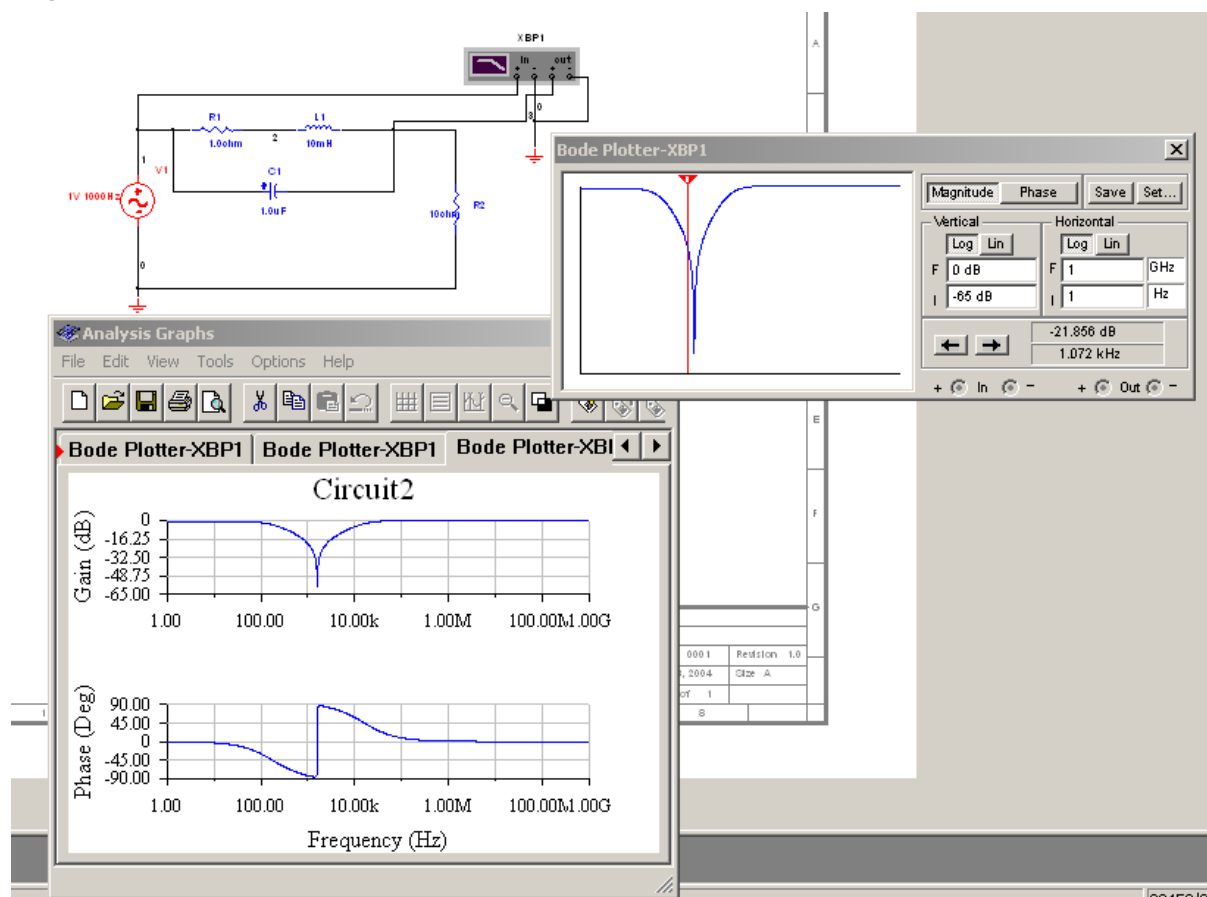


Figure 15. A notch-filter design and its Bode plots in MultiSim

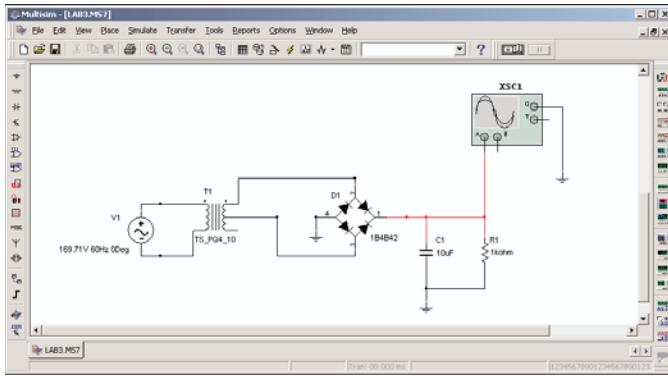


Figure 16. A full-wave bridge rectifier in MultiSim

The instrumentation phase of the wind-solar power station includes the following hardware: One CR4110-10 True RMS AC Current Transducer, one CR5210-50 DC Hall-Effect Current Transducer from CR Magnetics, voltage- and current-divider and scaling circuits, one wind-monitoring device called an anemometer, a LabView Professional Development System for Microsoft Windows, one PCI-6071E I/O board, NI-DAQ driver software, one SH 100100 shielded cable, SCSI-II connectors, one NI SCB-100 DAQ (shielded connector block), one isolation amplifier circuit, and a PC.

A Young 05103V anemometer provides two voltage signals corresponding to wind speed and wind direction. These wind signals are fed to AD210AN isolation amplifiers and the output is applied to National Instrument's SCB-100 data acquisition board (DAQ).

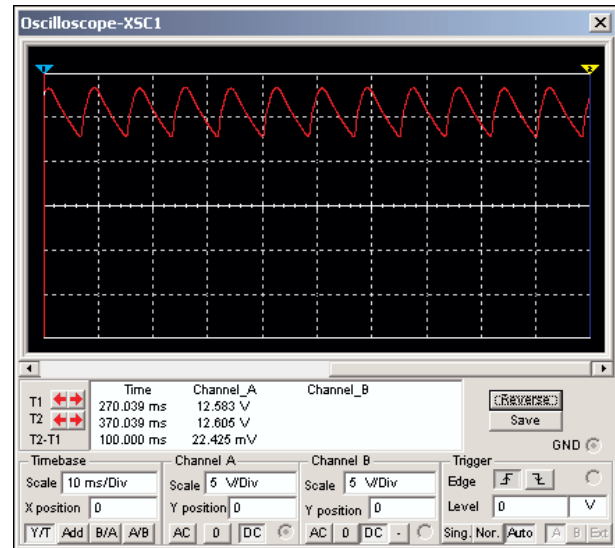


Figure 17. DC output waveform of the bridge-rectifier circuit

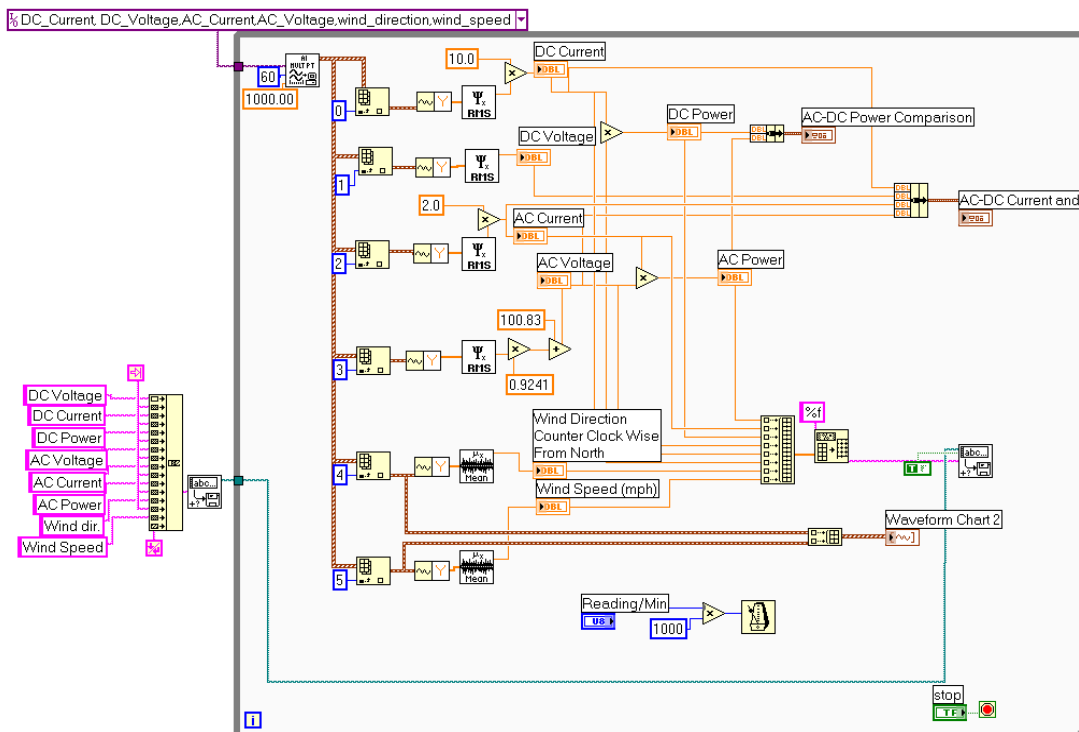


Figure 18. Overall diagram of the LabView™ data-acquisition virtual instrument (VI)

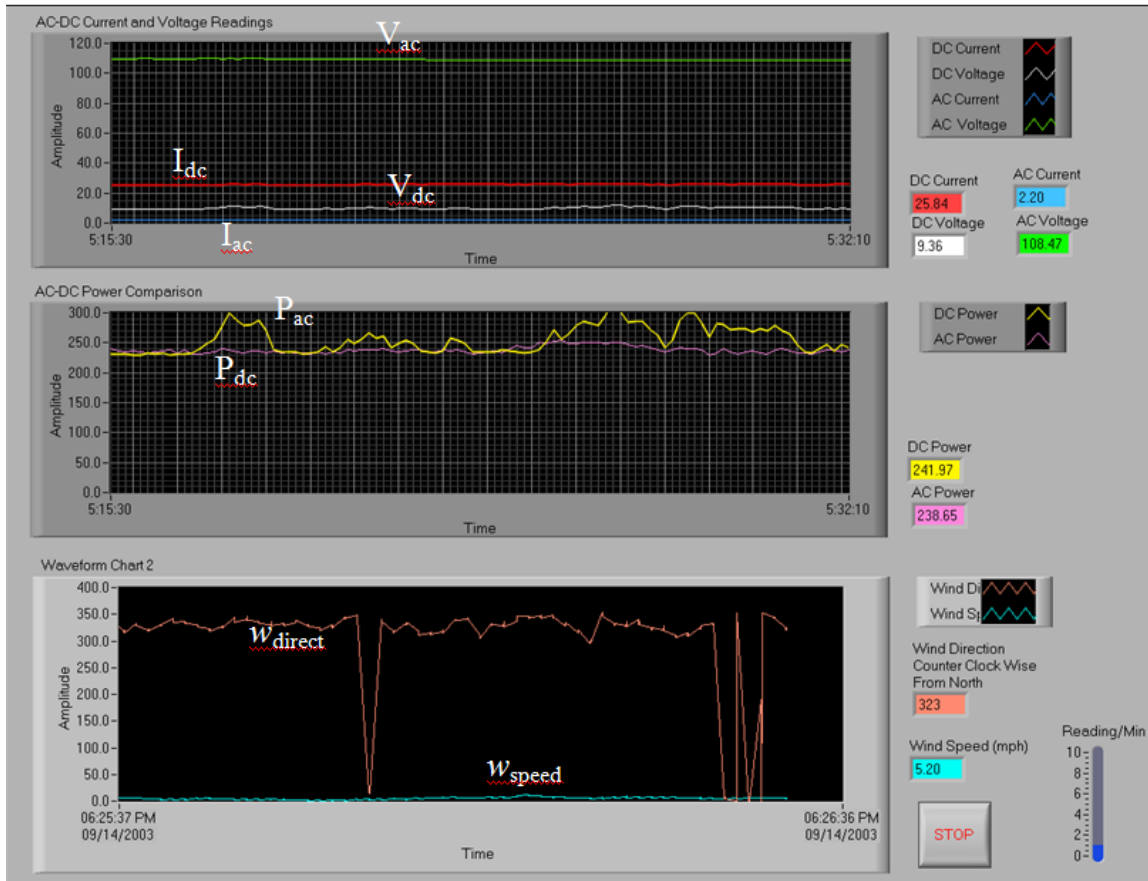


Figure 19. Front panel of the data-acquisition VI for a 1.5 kW wind-solar power system

Conclusion

Computer-aided engineering education is a valuable solution for increasing the quality of laboratory environments of engineering education courses. The classroom education process, similar to laboratory exercises, may be further visualized by introducing more advanced simulation tools. Several case studies have been demonstrated using LMS Imagine.Lab AMESim—a professional grade, integrated platform for 1-D multi-domain system simulation, Pro Engineer Wildfire—a well-known three-dimensional CAD/CAE software tool, SolidWorks—another 3-D digital simulation tool, NI MultiSim—formerly Electronics Workbench software integrating powerful SPICE simulation and schematic entry into a highly intuitive user-friendly graphical-based electronics lab in digital environments, and LabView™—another National Instruments graphical development environment to help create flexible and scalable design, control, and test applications in electronics and electromechanical systems.

Many students have found the software tools to be very helpful and user-friendly in understanding the fundamentals of physical phenomena in engineering technology areas. A number of students have increased their knowledge and experience with the aforementioned software tools as a valuable bridge to many internship and part-time student positions in local electronics and machinery manufacturing industries. Our industrial advisory board members have repeatedly mentioned their satisfaction with our students' achievements and their valuable experience with digital modeling and simulation tools.

References

- [1] National Instruments, <http://www.ni.com/labview/>
- [2] Kain Osterholt, et al., "Virtual Control Workstation Design Using Simulink, Simmechanics, and The Virtual Reality Toolbox", *Proceedings of American Society for Engineering Education*, 2006-567.

-
- [3] Madara Ogot, "Integration of Instruction on the use of Multimedia Tools into a Mechanical Engineering Curriculum", *Proceedings of the 2003 American Society of Engineering Education Annual Conference & Exposition*, 2003-1566.
 - [4] <http://pscad.com/> Professional Power System Design and Simulation
 - [5] F. Chalkiadakis, "Classroom Studies in Power Flow and Transmission Lines by Means of PSCAD/EMTDC", *Proceedings of the 2003 American Society of Engineering Education Annual Conference & Exposition*, 2007-321.
 - [6] LMS Imagine.Lab AMESim, <http://www.lmsintl.com/imaginelab/amesim/>
 - [7] Pro/ Engineer WildFire 4.0, <http://www.ptc.com/>
 - [8] Solid Works, <http://www.solidworks.com/>
 - [9] <http://www.ni.com/academic/multisim.htm>
 - [10] J. Harter, "*Electromechanics: Principles, Concepts, and Devices*", Prentice Hall Publishing, 1995.

Biographies

FARUK YILDIZ is an Assistant Professor of Industrial Technology at Sam Houston State University. He earned his B.S. (Computer Science, 2000) from Taraz State University, Kazakhstan, MS (Computer Science, 2005) from City College of The City University of New York, and Doctoral Degree (Industrial Technology, 2008) from the University of Northern Iowa. Dr. Yildiz is currently teaching Electronics and Computer Aided Design related classes at Sam Houston State University. His interests are in energy harvesting, conversion, and storage systems for renewable energy sources. Dr. Yildiz may be reached at fx001@shsu.edu

AYHAN ZORA is a senior engineer at John Deere Power Systems. The company specializes in off-road machinery (Agriculture, Constructions, Forestry, Turf, etc). He received his bachelor's degree in Mechanical Engineering, master's degrees in both Mechanical and Industrial Engineering, and a doctoral degree in Industrial Technology. He has been working as a researcher since 2003. He has conducted research in a variety of topics including mechanical and hydraulic systems simulation, hybridization and electrification of vehicles and exhaust after treatment systems. Dr. Zora may be reached at ayhanzor@uni.edu

REG PECEN holds a B.S.E.E. and an M.S. in Controls and Computer Engineering from the Istanbul Technical University, an M.S.E.E. from the University of Colorado at Boulder, and a Ph.D. in Electrical Engineering from the University of Wyoming (UW, 1997). He has served as graduate assistant and faculty at UW, and South Dakota State University. He is currently an Associate Professor and

program coordinator of the Electrical Engineering Technology program at the University of Northern Iowa. He serves on the UNI Energy and Environment Council, College Diversity Committee, University Diversity Advisory Board, and Graduate College Diversity Task Force Committees. His research interests, grants, and publications are in the areas of AC/DC Power System Interactions, distributed energy systems, power quality, and grid-connected renewable energy applications. He is a member of ASEE, IEEE, Tau Beta Pi National Engineering Honor Society, and ATMAE. Dr. Pecen was recognized as an Honored Teacher/Researcher in "Who's Who among America's Teachers" in 2004-2009. He was also nominated for the 2004 UNI Book and Supply Outstanding Teaching Award, March 2004, and nominated for 2006, and 2007 Russ Nielson Service Awards, UNI. Dr. Pecen is an Engineering Technology Editor of the American Journal of Undergraduate Research (AJUR). He has been serving as a reviewer on the IEEE Transactions on Electronics Packaging Manufacturing since 2001. Dr. Pecen has served on ASEE Engineering Technology Division (ETD) in Annual ASEE Conferences as a paper reviewer, session moderator, and co-moderator since 2002. He is serving on ASEE Energy Conversion and Conservation Division, advisory boards of International Sustainable World Project Olympiad (isweep.org) and International Hydrogen Energy Congress. Dr. Pecen may be reached at r.pecen@uni.edu

SECURING VIRTUALIZED DATACENTERS

Timur Mirzoev, Georgia Southern University; Baijian Yang, Ball State University

Abstract

Virtualization is a very popular solution to many problems in datacenter management. It offers increased utilization of existing system resources through effective consolidation, negating the need for more servers and additional rack space. Furthermore, it offers essential capabilities in terms of disaster recovery and potential savings on energy and maintenance costs. However, these benefits may be tempered by the increased complexities of securing virtual infrastructure. Do the benefits of virtualization outweigh the risks? In this study, the authors evaluated the functionalities of the basic components of virtual datacenters, identified the major risks to the data infrastructure, and present here several solutions for overcoming potential threats to virtual infrastructure.

Introduction

The past few years have seen a steady increase in the use of virtualization in corporate datacenters. Virtualization can be described as the creation of computer environments within operating systems allowing multiple virtual servers to run on a single physical computer. Many datacenters have adopted this architecture to increase the utilization of available system resources, which resulted in a decreased need for additional servers and rack space. There are substantial savings in energy, cooling, administration and maintenance expenses. But these advantages are somewhat tempered by the additional complexities, performance and security complications in virtualization environments. According to a recent survey from 531 IT professionals [1], concerns about security was considered one of the top issues in adopting virtual technology (43%) and the main reason that organizations were slow in the deployment of virtualization (55%). It is therefore necessary to examine the security risks associated with virtualization and the potential countermeasures.

Presented here are the key components that make up a virtual datacenter, followed by the analysis of virtualization security threats including virtual machine security, hypervisor security, network storage concerns, and virtual center security. Finally, the authors present possible solutions, guidelines and recommendations for enhancing security in virtualized datacenters.

Components of Virtual Datacenters

Virtual technologies have a broad range of contexts: operating Systems (OS), programming languages and computer architecture [12]. Virtualization of OS and computer architecture significantly benefits any disaster-recovery process and improves business continuity due to the fact that images of virtual machines can be quickly restored from different physical servers without waiting on the hardware repair. A virtual datacenter is a type of infrastructure that allows for sharing physical resources of multiple physical servers across an enterprise. This aggregation of resources becomes feasible when a suite of virtualization software is installed on the various components such as physical servers, network storage and others. As shown in Figure 1, the major elements of the virtualized datacenter include virtual machines, hypervisors, network resources, and datastores – Network Attached Storage (NAS), Storage Attached Network (SAN) and IP Storage Attached Network (IP SAN).

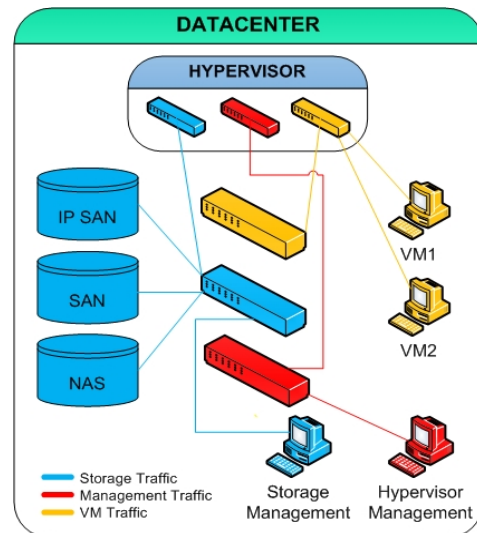


Figure 1. Datacenter components

It should be noted that this discussion of virtual infrastructure is independent of specific brands of virtualization suites. Different virtualization vendors tend to use different names when referencing the various components, although they all equate to the same basic principles.

A. Virtual Machines

The concept of virtualization is not new. It is based on a time-sharing concept originally developed by scientists at

the Massachusetts Institute of Technology (MIT) in 1961 [2]. Time-sharing creates an opportunity for concurrently managing multi-hardware and multi-user environments on a single physical machine. Today, many vendors such as IBM, VMware, Oracle, HP and others have taken this time-sharing concept even further and developed virtualization schemes of various types including Integrity VM by HP [5]. The advantages of modern technologies such as Integrity VM allow any operating system to run inside VM that supports the Integrity VM platform. An example of how virtualization is applied in a hosted virtualization model is shown by Figure 2.

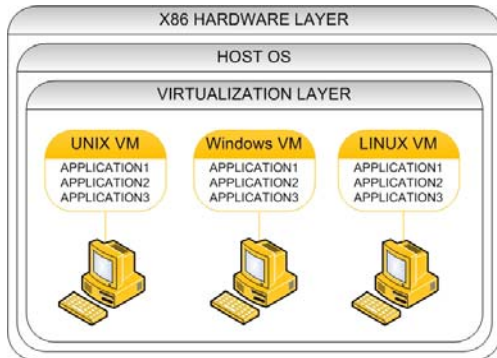


Figure 2. Hosted approach for virtual servers
Source: Adapted from [4]

Virtual machines (VMs) are sets of files that support operating systems and applications independent of a host operating system. Typical VMs include BIOS, configuration and disk files. In other words, they are software-only implementations of computers that execute programs just like conventional systems. Figure 3 lists a number of examples of VMs containing virtual hardware components such as CPU, memory, hard drives, network adapters and many others.

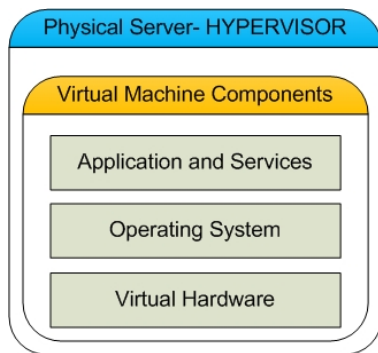


Figure 3. Elements of Virtual Machines

Nowadays, the detection of a virtualized OS is a fairly new technique, so most virtual OS environments are not detected by common operating systems such as Windows XP, Vista, and a few Linux operating systems. This offers a great deal of flexibility in the deployment of virtual infra-

structures. Another essential property of virtual machines is OS isolation – if a virtual computer gets infected with a virus other virtual machines should not get infected. Popek and Goldberg [8] describe a virtual machine as “an efficient, isolated duplicate of a real machine.”

It is possible to run multiple virtual machines on a single physical server without any interaction between operating systems. Thus, if a virtual machine crashes, it would not affect the performance of the other virtual machines on the same physical server. Because of these properties, virtual machines are considered one of the building blocks of virtualized datacenters.

B. Hypervisors

A hypervisor, also known as physical host, is a physical server that contains hardware and virtualization layer software for hosting virtual machines. Hypervisors use existing physical resources and present them to virtual machines through the virtualization layer. Virtualization is neither simulation nor emulation. To share resources, hypervisor runs in a native mode, directly representing the physical hardware. Additionally, hypervisors effectively monitor and administer shared resources given to any virtual machine. Groups of similar hypervisors may be organized into clusters. Clusters allow for aggregation of computing resources in the virtual environment and allow for more sophisticated architectures. Typically, specific software manages a cluster of hypervisors.

C. Network Configurations

Virtual datacenters, like traditional datacenters, require network infrastructure. A hypervisor can use multiple network interface cards (NICs) to provide connectivity. In fact, it is highly recommended that several NICs be used for a single hypervisor in order to separate networks and various functions. Furthermore, as virtualization of I/O devices takes off, the IT industry will see another sharp turn towards fewer cables, NICs and other devices. Each Ethernet adapter can be configured with its own IP address and MAC address manually or automatically. A hypervisor or a virtual machine can be configured with one or more virtual NICs to access different physical or virtual networks (see Figure 4).

Virtual switches allow virtual machines to communicate with each other using normal TCP/IP protocols without using additional physical network resources internal to hypervisor. Virtual switches may be configured to have the same functionality as a physical switch, with the exception that direct interconnection between virtual switches is not available in some configurations.

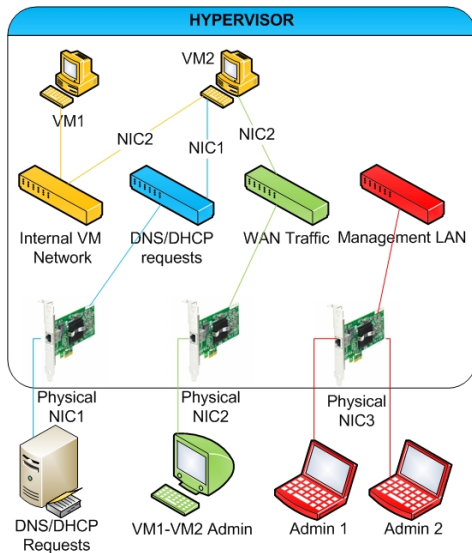


Figure 4: Hypervisor and virtual machine networking

D. Network Storage

Most datacenters rely heavily on Fiber Channel SAN, iSCSI arrays, and NAS arrays for network storage needs. Servers use these technologies to access shared storage networks. Storage arrays are shared among computer resources enabling essential virtualization technologies such as live migration of virtual computers and increased levels of utilization and flexibility. Within a virtual datacenter, network storage devices may be virtualized in order to provide distributed shared access among virtual machines. Moreover, it is recommended that files containing the virtual machines be placed on shared storage. This is because most current virtualization server products will not support a live migration of a virtual machine from one physical server to another physical server if the virtual machine is located on a storage area that is not accessible by all hypervisors.

Several options are available for the creation of datastores such as NAS, SAN, local storage, etc. Shared network storage is an essential component for any virtual infrastructure, and applying different storage technologies typically requires a balance between cost and performance. But regardless of whether it is a NAS or SAN array, securing network storage should always be at the top of the security policy for any datacenter. It is critical to separate network storage traffic from virtual machine traffic.

Virtualization Security Threats

In this section, the security threats to a datacenter's key components in a virtualized environment are discussed.

A. Virtual Machine Threats

It is a common misconception that the security risks of virtual machines are much higher than those of physical computers. Virtual machines have the same, if not fewer, levels of security risks as their physical-computer counterparts. This is due to the fact that physical connectivity, software updates and networking employ the same logical infrastructure. The key difference lies in the fact that VMs are running on top of a virtualization layer instead of the actual hardware. Virtual machines should be protected by antivirus software and should be patched on a regular basis just like any physical computer. However, there are several virtualization-specific threats that require the attention of datacenter administrators:

1) **Suspended Virtual Machines.** When a virtual machine is not running, users typically assume there are no security threats since the VM is powered off. Throughout tests in our lab environment, an observation was made that un-patched and unprotected Windows 2000 Servers, running in an earlier version of a virtualized product, were actually infected by the Blaster Worm even when a VM was not running. To make matters worse, it was able to duplicate itself and infiltrate other unprotected suspended virtual Windows 2000 Servers. It was felt that the problem was due to security flaws in how the virtualized networking environment was implemented, but there were no validated hypotheses generated. Another observation was made regarding a virtual machine running as a DHCP server that continued to hand out IP addresses even when it was powered off. It is important then to realize that suspended virtual machines should not be ignored as security targets in virtual datacenter environments.

2) **Resource Contention.** When multiple virtual machines run on the same physical server, they will inevitably be competing for hardware resources such as CPUs, RAMs, I/O, and network. Additionally, all of the server and client operating system updates are typically applied at the exact same time. When multiple virtual machines demand the same physical resources simultaneously, they may cause performance degradation across the datacenter and could even lead to some virtual machines not being able to power on. VM-specific countermeasures must be utilized to alleviate resource contention among virtual machines.

3) **VM Sprawl.** With the help of current virtualization products, the creation of new VMs is quick and easy. It is a common malpractice that whenever there is a need for a certain service, a dedicated VM is immediately created. It then becomes a problem noted as VM Sprawl, where too many virtual machines are created without careful planning, management and service consolidation [9]. The biggest threat

associated with VM sprawl could be the cost of resources: storage space, CPU and RAM resources may become scarce and additional software licenses and network service may be required. From a security of point of view, if a virtual data-center is abused by the creation and deployment of unnecessary virtual machines, the entire infrastructure may become too complex to manage, thereby posing a dangerous, unsecure environment. And if any virtual machine is not carefully protected or it is placed on a wrong network, it may put the entire virtual datacenter in jeopardy.

B. Hypervisor Threats

Hypervisor is a thin layer that runs directly on top of the physical hardware and provides isolation between different virtual machines that run on the same physical server. It is, therefore, vital to protect hypervisor from being compromised or attacked. Anything happening at the hypervisor level is not visible to virtual machines and will eventually render the traditional OS hardening or protection techniques completely useless. Lately, a number of interesting research efforts have been made to address the possible security threats to hypervisors:

1) **Virtual-Machine-Based Rootkit (VMBR)**. Samuel T. King et al. [11] developed proof-of-concept VMBRs that can be inserted underneath the targeting virtual machines if an attacker gains administrative privileges on a virtual machine. Once the rootkit is successfully installed and configured, it functions as a modified hypervisor on the infected physical server and loads all virtual machines. As a result, an attacker will have a great possibility of controlling every virtual machine that runs on that hypervisor.

2) **Blue Pill Attack**. Joanna Rutkowska [6] presented a highly sophisticated attack at the 2006, annual Black Hat Conference. The basic idea of a Blue Pill attack is to exploit the AMD64 SVM virtualization instruction sets—code name Pacifica. If the attack is successful at the chip level, it will also install its own hypervisor to intercept the communication between virtual servers and the hardware. The author also claimed that it is quite likely that similar attacks can be implemented against Intel's VT-x instruction sets—code name Vanderpool. Unlike VMBRs, the Blue Pill attack can be installed on the fly without modifying the BIOS, and there are no noticeable performance penalties associated with the attack. As a result, it becomes extremely difficult to detect such types of attacks.

C. Virtual Infrastructure Threats

Virtual infrastructures with clusters of hypervisors are highly sensitive to internal attacks. Frequently, the response

to internal threats is such that “nothing can be done”. That is exactly the reason why internal attacks still exist. If there are no preventive measures that are taken towards internal threats, then internal attacks should be expected. Specifically, the following security threats should be addressed:

1) **Single Point of Control**. A single administrator may be implementing permissions, authentications and privileges to cluster-wide environments of hypervisors, or virtual centers. Such a person becomes the biggest threat to the company's assets, should this super administrator become dissatisfied with the company for any reason.

2) **Physical Access**. If a person gains physical access to a hypervisor, the damage could be much worse because the entire virtual infrastructure can quickly be copied, modified or even removed.

3) **Licensing Server**. Typical virtualization server products are activated and unlocked by the presence of valid license files. If for any reason the license server fails, IT administrators should respond as quickly as possible to get the license server back online. Otherwise, when the grace period expires—for some vendors this can be 14 days—certain features will be disabled, leading to a chaotic environment in the datacenter.

D. Virtual Network Threats

From a design point of view, there are no essential differences between virtual and physical networking. If network administrators have proven networking skills in dealing with physical networks, there should be no problem in designing virtual networking for VMs and hypervisors. The major challenges are the capabilities of security tools and sound designs of network configurations.

1) **Security Tools**. Conventional networking security tools, such as Intrusion Detection System (IDS), Intrusion Prevention System (IPS), are typically running on a physical network and are able to check all of the traffic coming in and out of the area being monitored. They are not capable of examining traffic flowing through internal virtual switches within hypervisors.

2) **Configuration Tools**. Configurations of physical networks can be easily designed by using well-established tools and techniques. But configurations of virtual networks are not easily accessible to network and security professionals making it difficult to validate network designs. In fact, Kim [7] pointed out that a major security risk associated with virtualization is incorrect configuration. It is essential to have a set of best practices in place to ensure that virtual switches and virtual networks are appropriately configured.

Countermeasures

This section provides practical solutions for hardening virtualized environments.

A. Hardening Virtual Machines

From a security point of view, virtual machines should be protected just like physical computers. Antivirus applications should be installed and patches should be applied as often as required for physical machines, even if some of those virtual machines remain suspended most of the time, i.e., VMs serving as templates. If applicable, it is better to patch templates and then deploy VMs from templates than patching each VM individually. There should also be a clear organizational policy set up to dictate when to create a new virtual machine so that VM-sprawl problems can be mitigated. Additionally, it is a good idea to schedule tasks from hypervisors for each virtual machine to conduct a full system security scan or a full system backup. It is also advisable to schedule such tasks in a staged manner or during times when physical resources are not heavily utilized.

B. Protecting Hypervisors

A hypervisor is the foundation of a datacenter and a virtual machine. It must be properly protected from attacks; otherwise, virtual machines will not be able to detect any illegal behavior happening underground. One of the current trends in securing hypervisors is to validate them under the framework of trusted computing. It is advisable to check the integrity of a hypervisor before it can be trusted and deployed [3]. The main challenge here is that trusted computing works only if the underlying hardware, such as CPUs and chipsets, supports Trusted Platform Modules (TPM).

Thus far, no significant security threats directly targeting hypervisors have been discovered. This does not mean that current hypervisor implementations are protected. Attacks on hypervisors tend to be much more difficult than attacking the virtual machines. To counter theoretical attacks such as Subvirt and Blue-Pill threats described earlier more secured virtualization implementations at the chipset level are needed from both Intel and AMD. Another possible solution is to make the hypervisor very thin so that it is easier to validate and can be pre-installed onto the hardware components with read-only capabilities (BIOS-like approach).

C. Securely Managing Virtual Infrastructure

An effective security policy is a must for any datacenter, whether virtualized or physical. Several levels of permissions can be set in a datacenter. Such levels include datacenter, virtual center, host and virtual-machine, and are represented in Figure 5. The following suggestions are particularly important to enhance the security of virtual infrastructures:

1) **Separate Permissions.** To alleviate the problem of the single point of control, the super administrator, it is best to separate permission policies as the following example indicates [10]:

- Administrator 1 (A1) may reinstall hypervisor OS;
- Administrator 2 (A2) may specify networking for hypervisors and VMs;
- Administrator 3 (A3) may deploy VMs without permissions to modify VMs' local user access and group policies;
- Administrator 4 (A4) manages the distribution of physical resources for a datacenter; and
- A1, A2, A3 and A4 work together as a group to specify administrative tasks for a datacenter.

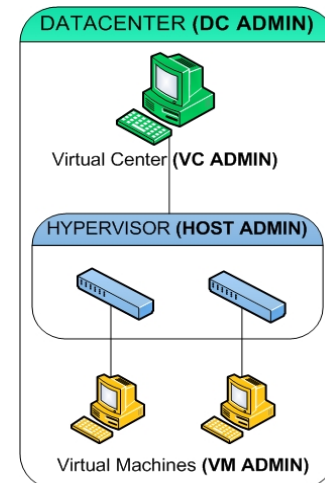


Figure 5. Levels of permissions and privileges in a virtualized datacenter

2) **Physical Access.** Physical access to a datacenter is essential: bad practices such as easily accessed codes, access cards and even open doors should be prevented at all times.

3) **Protecting Licensing Servers.** In an enterprise virtual datacenter environment, it is necessary to protect the availability of the licensing server. One solution may be implementing a redundant licensing server.

4) **Securing VM Management Console.** If an attacker gains control of a virtual server management console, either locally or remotely, all hypervisors and VMs that they manage are easily compromised.

D. Protecting Virtual and Physical Networks

There are crucial steps to be taken when designing a network for a virtualized environment. The following list represents the minimum requirements for configuring networks in virtualized datacenters:

1. Hypervisor management traffic or service console traffic must be restricted and separated from other networks such as virtual machine network, storage (if applicable), etc.
2. Network storage traffic must be separated from virtual machine networks. In other words, network storage access needs to be configured at the hypervisor level, where only the hypervisor has the ability to access datastores and grant access to datastores for VMs. Additionally, SAN administrators need to coordinate access control for hypervisors within datacenters (LUN masking, zoning and others). Most successful secure implementations of Fiber Channel SAN include both hard and soft zoning.
3. Setting security policies on virtual switches is important. Third-party virtual network switches can be used to expand network security.
4. VLAN tagging may be a good option in a limited network resources environment.

Figure 6 depicts a network configuration example for hypervisors.

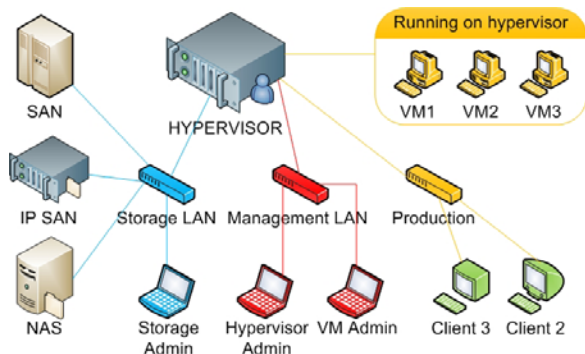


Figure 6. Separation of network Traffic (without VLANs)

E. Recent Virtualization-Aware Security Technologies

Virtualization vendors have recently begun to offer a set of Application Programming Interfaces (APIs) to end users

and third-party IT companies. The availability of the hypervisor-level APIs creates an opportunity to build a virtualization-aware security framework because it has the potential to monitor resource usage at both virtual-machine level and physical-machine level. It also makes it possible to examine network traffic passing through the virtual machines and virtual-network interfaces. An overview of such a security platform is shown in Figure 7, where a dedicated security VM is shown being created in a virtual datacenter.

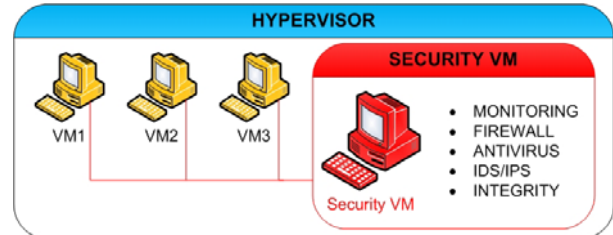


Figure 7. A model for virtualization security with hypervisor level APIs

This security VM will be loaded with many security technologies/products such as firewall, Intrusion Detection System (IDS), Intrusion Prevention System (IPS) and anti-virus agents, etc.

The security VM will communicate with the APIs to collect security-related information about each single virtual OS. As a result, it is possible to run a single antivirus agent on the security VM to fully scan multiple virtual VMs. Since hypervisor-level APIs can provide network visibility at the virtual-switch level, traditional firewall and IDS/IPS products can be installed inside the Security VM to protect the virtual datacenter just like they are protecting physical servers. It is the authors' belief that those hypervisor-level APIs can allow the IT industry to quickly arm their virtual datacenters with conventional security tools.

Conclusions and Recommendations

The current state of virtualization technologies is not more vulnerable than physical servers, but the damage to a virtualized datacenter could be much quicker and more severe than providing services in separate physical environments. However, virtualization technologies present both opportunities and risks. When virtualizing datacenters, all personnel should be involved: server administration teams, networking teams, security, development and management. There should be no difference between protecting VMs and physical computers.

The following may be used as the best practices to enhance virtualization security:

1. Create an effective security policy for the virtualized environment.
2. Define trusted zones and separate servers either at the hardware level or at a VM level.
3. Eliminate single point of control - use separation policies for datacenter administrators.
4. Employ a separation policy for hypervisor administrators and VM administrators.
5. Enforce extremely strict control for virtual center permissions and privileges.
6. In hypervisor cluster settings, provide high availability for license servers and virtual centers – have a primary and a backup copy of Virtual Center and License servers.
7. If no I/O virtualization is deployed, separate physical networks for management and administration of hypervisors, storage, and virtual machines.
8. Disable/remove all unnecessary or superfluous functions and virtual hardware.
9. Prevent virtual machines from utilizing physical resources - do not create and use extra virtual devices such as CPUs, media drives, RAM; never over-allocate any physical resources as this leads to resource-contention problems.
10. Deploy virtual security appliances such as virtual IPS/IDS systems, firewalls, antivirus agents and others in virtualized datacenters.

Acknowledgments

The authors are grateful to the IJERI reviewers and editors for their valuable feedback and support in the development of this document.

References

- [1] Centrifly, "Market Dynamics and Virtual Security Survey", published on Sep 1st, 2009, <http://www.centrifly.com/resources/survey.asp>
- [2] Corbató, F., Daggett, M., Daley, R. "An Experimental Time-Sharing System", <http://larch-www.lcs.mit.edu:8001/~corbato/sjcc62>
- [3] Dalton, C., Gebhardt, C., and Brown, R., "Preventing hypervisor-based rootkits with trusted execution technology", *Network Security*, vol. 2008, no. 11, pp. 7-12.
- [4] Goldworm, B., Skamarock, A., "Blade Servers and Virtualization", John Wiley and Sons, Inc.
- [5] Herington, D., Jacquot, B., "The HP Virtual Server Environment", Pearson Education, NJ 07458. Copyright © 2006 Hewlett-Packard Development company L.P.
- [6] Rutkowska, J., "Subverting Vista Kernel For Fun and Profit", Aug 2006, Black Hat conference. <http://blackhat.com/presentations/bh-usa-06/BH-US-06-Rutkowska.pdf>
- [7] Kim, Gene, "Practical Steps to Mitigate Virtualization Security Risks", White Paper, Tripwire, <http://www.tripwire.com/register/?resourceId=9803>
- [8] Popek, G., Goldberg, R. , "Formal Requirements for Virtualizable Third Generation Architectures". *Communications of the ACM* 17 (7): 412 –421.
- [9] Reimer, D., Thomas, A., and et al., "Opening black boxes: using semantic information to combat virtual machine image sprawl", *Proceedings of the fourth ACM SIGPLAN/SIGOPS international conference on Virtual extension environments*, pp 111-120, 2008.
- [10] Rushby, J., Randell, B., "A distributed secure system", Retrieved in April, 2010 from <http://www2.computer.org/portal/web/csdl/doi/10.1109/MC.1983.1654443>
- [11] Samual, T. King, and et. al., "SubVirt: Implementing malware with virtual machines", *Proceedings of the 2006 IEEE Symposium on Security and Privacy*, pp 327-341
- [12] Smith, J., Nair, Ravi., "The Architecture of Virtual Machines", *Computer*, 38(5): 32-38, IEEE Computer Society

Biographies

TIMUR MIRZOEV in 2003 received the M.S. degree in Electronics and Computer Technology and in 2007 the Ph.D. in Technology Management (Digital Communication) from the Indiana State University. Currently, he is an Assistant Professor of Information Technology at Georgia Southern University. His teaching and research areas include server and network storage virtualization, disaster recovery, storage networks and topologies. Dr. Mirzoev has the following certifications VMware Certified Instructor (VCI), VMware Certified Professional 4 (VCP4), EMC Proven Professional, LefthandNetworks (HP) SAN/iQ, A+. He may be reached at tmirzoev@georgiasouthern.edu

BAIJIAN YANG received the Ph.D. in Computer Science from Michigan State University in 2002. Currently, he is an Assistant Professor in the Department of Technology at Ball State University. His teaching and research areas include Information Security, Distributed Computing, Computer Networks, and Server Administration. He is also a Certified Information System Security Professionals (CISSP). Dr. Yang can be reached at byang@bsu.edu

PRACTICAL SOFT-SWITCHING HIGH-VOLTAGE DC-DC CONVERTER FOR MAGNETRON POWER SUPPLIES

Byeong-Mun Song, Baylor University; Shiyong Lee, The Pennsylvania State University
Berks Campus; Moon-Ho Kye, Power Plaza, Inc.

Abstract

A new soft-switching, high-voltage dc-dc converter for magnetron power supply application is presented in this paper. The proposed dc power supply consists of three main circuits: front-end flyback converter, high-frequency transformer, and high-voltage diode rectifier circuit. The front-end flyback dc-dc converter employs a soft-switching technique to minimize switching losses. Two high-frequency transformers with five secondary windings were developed to obtain a high voltage. Experimental results are provided to verify the superiority of the proposed converter under 200W and 4kV magnetron operations. The developed magnetron power supply, based on the proposed soft-switching converter topology, achieved an overall efficiency of 85%.

Introduction

The magnetron is a high-powered vacuum tube that generates microwaves. Typical applications of such microwaves include heating and drying in industry and home [1]. Heating and drying with microwaves provide fast, efficient and accurate control of power over the conventional thermal-based system. A high-voltage power supply, which can supply several kV, is required to operate a magnetron.

High-voltage dc-dc converters are widely used for magnetron power supplies. As these converters are very expensive, they are usually limited to applications that are the most demanding. One current challenge is to develop a low-cost dc-dc converter to drive magnetron lamps. Since these dc-dc converters transfer low-voltage power to high-voltage power, traditional converters have to utilize low-frequency ac transformers and rectifiers, resulting in low performance.

Recently, the development of a new class of low on-resistance power metal-oxide semiconductor field-effect-transistor (MOSFET) switching devices and high-frequency core materials has led to more compact dc-dc converters. They operate at higher frequencies and power densities than the traditional dc-dc converters [1], [2]. In order to improve efficiency, some converters have been using a soft-switching technique to reduce switching loss and stress on the switch

[3], [4]. However, for safety, these high-voltage converters require high-voltage insulation and the high-voltage transformers are usually mounted on a board. Therefore, they tend to be large and bulky converters, resulting in a lower efficiency of 75% with 4kV for a magnetron power supply.

This study focused on the development of a cost-effective, soft-switching, high-power density dc-dc converter for a magnetron power supply that can achieve a reduced size and weight, improved efficiency, accurate voltage regulation, and effective power delivery to the output dc. The major accomplishments of this work were

- The development of a cost-effective, high-voltage dc-dc converter using quasi-resonant flyback soft-switching dc-dc converter topology. The converter reduces the turn-on loss of the power MOSFET switching devices. The main switching device is efficiently powered at high voltages and low currents with low power consumption.
- The development of a current-mode pulse-width modulation (PWM) controller using a commercially available off-the-shelf (COTS) switch-mode power supply (SMPS) control integrated circuit (IC) TEA1533 from NXP Semiconductors [5]. The controller regulates a constant output voltage to maintain the magnetron lamp current. Using the COTS SMPS control IC reduces the system cost, while providing several advantages such as precise current regulation, resistance to breakdown, and extremely efficient soft-switching operation at the high power levels.
- The development of sensory and control logic to enable anode current control in the magnetron. This practical design and implementation of the high-voltage converter created a compact power stage in addition to safe voltage insulation and accurate current and voltage control.
- Improvement of the overall efficiency of the 200W and 4kV magnetron power supply to 85% by reducing the turn-on switching loss of the main device, using a new high-voltage transformer design and its compact power packaging.

Proposed DC-DC Converter

The simplified block diagram of the overall configuration of the proposed dc power supply to drive the magnetron is shown in Figure 1. The power supply, which provides 4kV and 40mA of output power, consists of an EMI filter, continuous-mode power factor correction (CMPFC) [10] - [13], quasi-resonant flyback dc-dc converter, and two

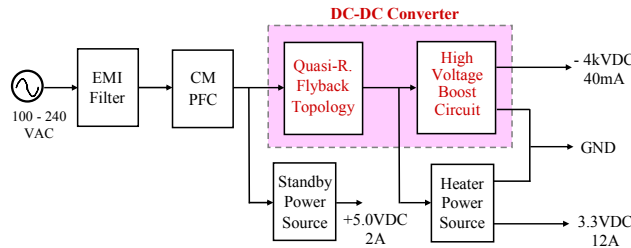


Figure 1. Overall block diagram of the proposed magnetron power supply

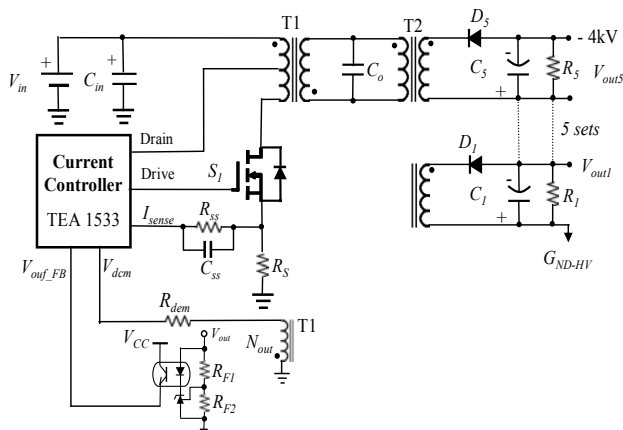


Figure 2. Proposed high-voltage dc-dc converter topology and its controller

outputs for the standby and heater power. The input to the power supply has a universal operating range of 100V to 240V. Figure 2 shows the proposed soft-switching dc-dc converter topology for the magnetron lamp drive. The converter consists of two power stages: low- and high-voltage.

The low-voltage stage contains quasi-resonant flyback topology with only one MOSFET switch and a flyback transformer. It is possible to allow the operation of the converter with critical conduction mode control, so that the converter achieves soft switching for the main switch, S_1 , by using the leakage inductance in the transformer. The high-voltage stage is connected to the isolated two-stage windings of the transformer for high-voltage insulation.

An output filter bank is composed of five series-connected capacitors, C_1 through C_5 , with the rectifying diode connected to each side of the load. At this stage, the high-voltage ac produced by the transformer is rectified and converted back to high-voltage dc. The output is then filtered by a capacitor bank to produce a low-ripple dc.

The switching sequence of the converter, based on the switch-voltage and current waveforms, is shown in Figure 3. The converter has four operational modes to achieve the desired output voltage waveforms at steady-state operation. The TEA1533 SMPS control IC was selected to achieve the zero-voltage switching (ZVS) operation [5]. The converter was operated under ZVS in valley switching technology. In order to achieve the soft-switching operation, a time delay is

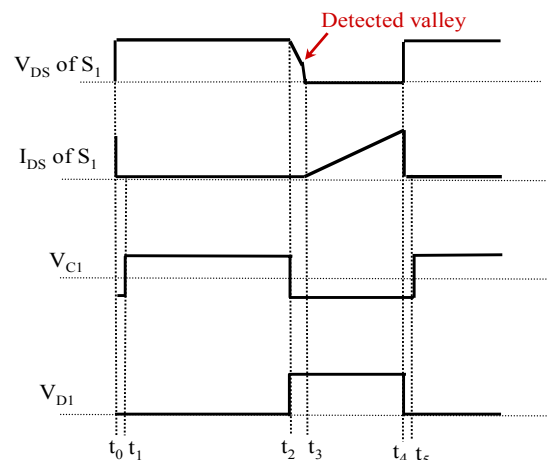


Figure 3. Voltage and current waveforms of the main switch

inserted between the turn-off of the freewheeling diode and turn-on of the main MOSFET switch, S_1 . At the valley voltage region, an L-C resonance is formed by the leakage inductance on the primary winding of the transformer and the device capacitance across S_1 .

For effective ZVS operation, it is necessary that the converter controller accurately detect the voltage drop and turn on the main switch at valley points. In the converter, the two high-frequency transformers have one winding with a turns ratio of 1:1 and five windings connected in series with a turns ratio of 1:9 in order to meet the high-voltage safety requirement. Since this converter has quasi-resonant flyback topology, the switching frequency was varied up to 250kHz, depending on the load condition. In this converter, a frequency of 50kHz was selected for full load. The configuration of the implemented high-voltage transformer is shown in Figure 4.

Design of current Controller and System Operation

The current controller block-diagram with secondary voltage sensing is shown in Figure 2. The current controller was operated with a TEA1533 device that consists of an input filter, a transformer with a third winding, and an output stage with a feedback circuit [5]-[9]. The TEA1533 current controller regulates the output voltage. The turn-on time of the main switch, S_1 , is controlled by the internally-inverted

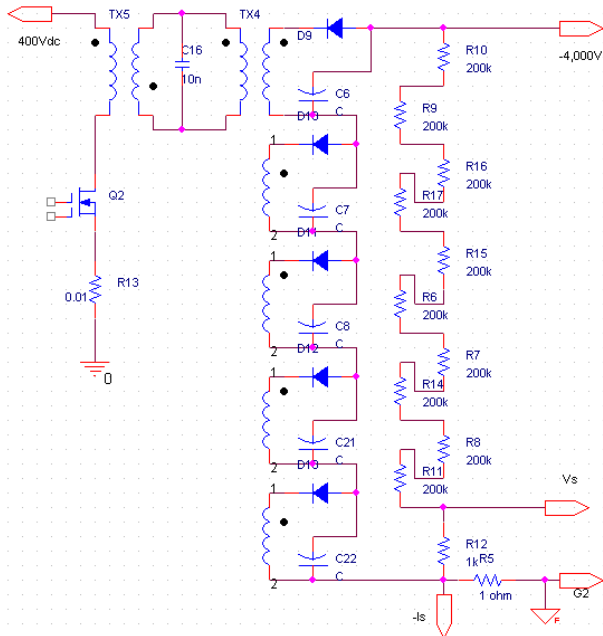


Figure 4. Overall configuration of the implemented high-voltage transformer

control voltage, which is compared with the primary-current command. Also, the primary current was sensed across an external resistor, R_s . The sense resistor converts the primary current into a voltage at the I_{sense} pin. The value of the sense resistor was determined by the maximum primary peak current.

The operational requirement of the dc power supply to drive a magnetron lamp is shown in Figure 5. The sequence of operation for the proposed power supply is as follows: During T_1 , the power supply must provide the control signal to activate the magnetron lamp when the converter is turned on and its output voltage reaches 4kV. When the magnetron lamp is turned off, the power converter should be turned off with a time delay. Even though an ac line is removed, the converter must have the capability to turn the magnetron lamp off safely.

For the high-voltage operation of the magnetron lamp, the controller of the converter should be designed with at least a 200ms time delay at startup. After period T_2 , the fast response of the controller is required for impedance matching between the front-side quasi-flyback converter and the transformer secondary output. In addition, the response bandwidth of the converter for the change of input control voltage should be designed within approximately 20ms for a T_5 period. The fall time for the constant anode current should not be greater than 2ms. Thus, the controller can actively regulate the output current for controlling the magnetron lamp. Table I describes the output-current and voltage requirements for the magnetron power supply.

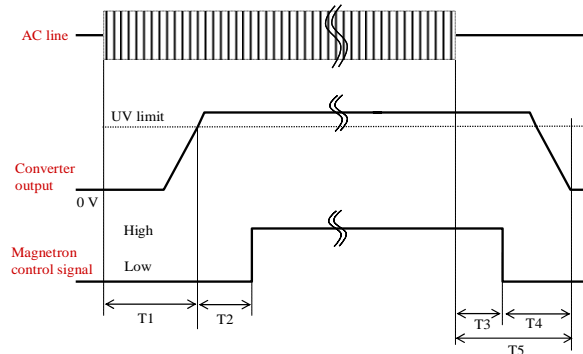


Figure 5. Magnetron control voltage pattern.

TABLE 1. OUTPUT CURRENT AND VOLTAGE REQUIREMENTS TO THE MAGNETRON POWER SUPPLY

Output Current [mA]	Output Voltage [kV]
0	0
10	3.82
20	3.87
30	3.93
40	4.0

Experimental Results

In order to validate the proposed converter operation, various experiments were conducted. The parameters of the output filter capacitors, C_1 through C_5 , and a resonant capacitor, C_o , were selected as $0.1\mu\text{F}/1\text{kV}$ and $6.8\text{nF}/1\text{kV}$, respectively. A total of five $0.1\mu\text{F}$ capacitors are connected to five transformer secondary taps. For the high-voltage balance, two $1.2\text{M}\Omega, 0.5\text{W}$ resistors were also connected in series across each tap.

The experimental waveforms during the magnetron lamp operation are shown in Figure 6(a). The time delay for startup was measured to 200ms, which matches the design target. Figure 6(b) shows the voltage and current waveforms during

ac power line turn off. Figure 5 shows that the waveforms satisfy the design specification.

The experimental waveforms of the input current and input voltage of the converter are shown in Figure 7. It can be clearly seen that the voltage and current are synchronized in-phase under near unity power factor (PF). The PF was measured at 0.98 under 230V ac input and full load, including a cooling fan. Note that the current spike near the zero crossing originates from the cooling fan to manage the thermal issues. The measured current and voltage of the primary winding of the transformer are shown in Figure 8. It should be noted that the current was well-regulated, and the active switch

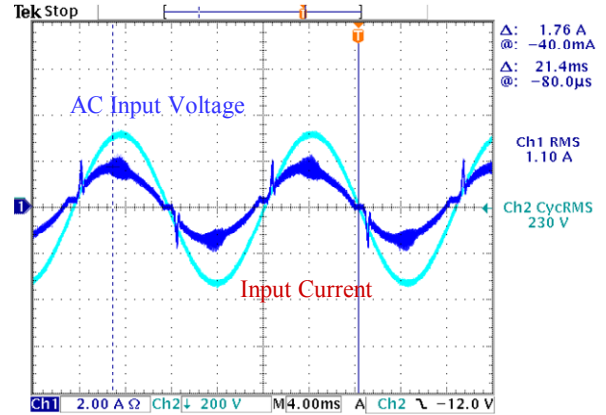
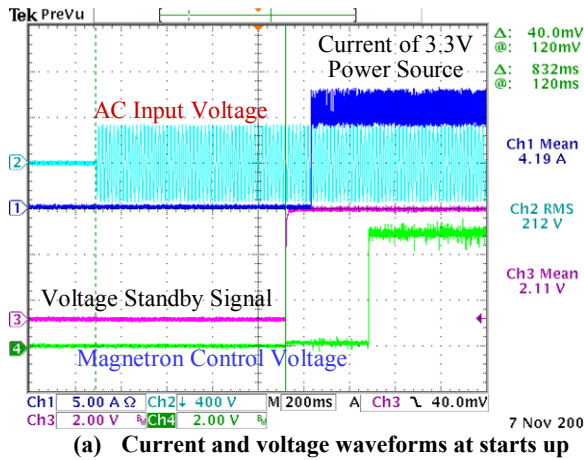


Figure 7. Input voltage and current waveforms at 230Vac under full load (PF = 0.98)



turned on at the lower valley voltage, as explained in Figure 3 [9]. Figure 9 shows the results of the conductive EMI/EMC test for the developed power supply. It is clear that the proposed soft-switching power supply met the minimum 4dB margin for the conductive EMI level at 230V ac. The layout of the major components, which are required for 8kV high-voltage insulation, is shown in Figure 10. The integrated prototype power supply is shown in Figure 11. The power in the major circuitry was measured with 230V ac nominal input voltage under full-load conditions. The measurement shows that the proposed dc-dc converter achieved 85% conversion efficiency.

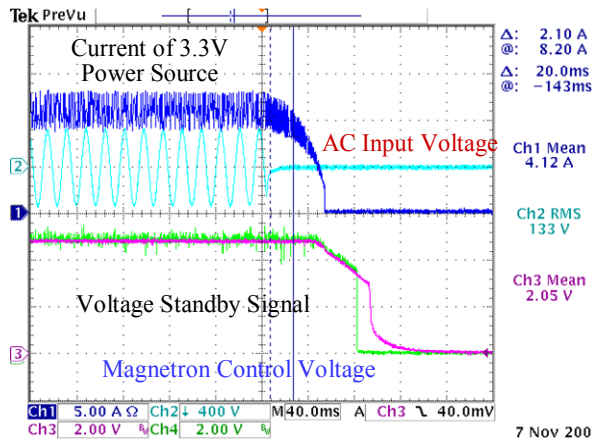


Figure 6. Timing and sequence of operation of the converter

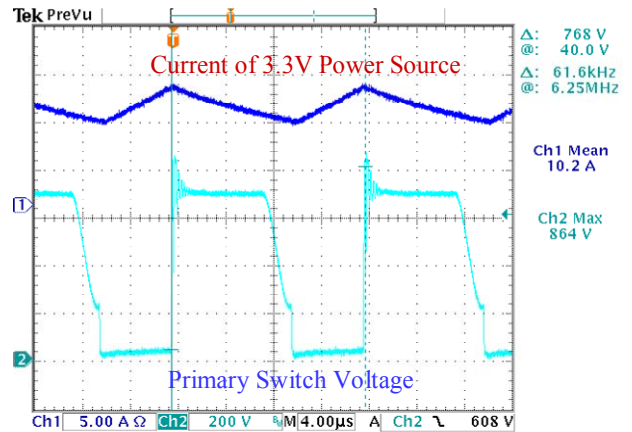


Figure 8. Output current and voltage waveforms of the transformer primary winding

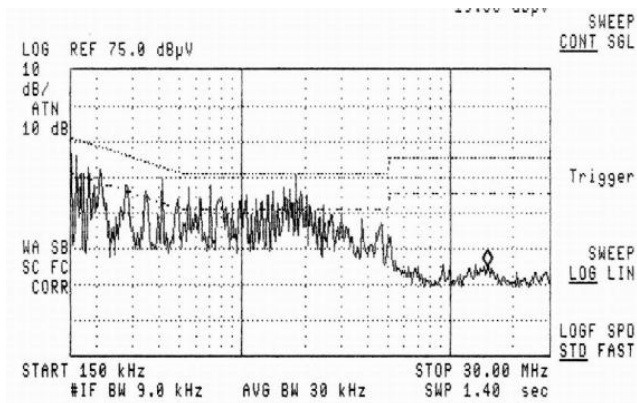


Figure 9. Measured conductive EMI/EMC for the developed power supply

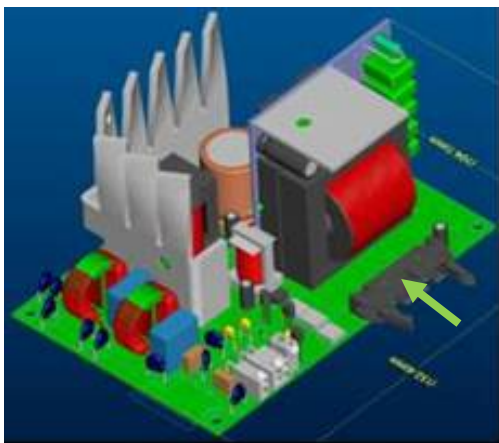


Figure 10. Component layout of the proposed power supply

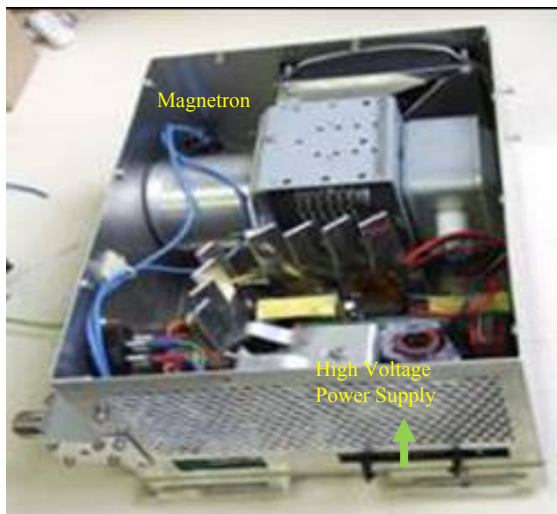


Figure 11. Integrated high voltage power supply and a magnetron

The measurement details are as follow:

- Total input power: 235W,
- High-voltage output power: 160W (4.0kV, 40mA),
- Magnetron filament power: 35W (3.4V, 10.3A),
- Cooling fan power: 4.6W,
- Standby power: 1.0W (5V, 0.2A).

Conclusion

A cost-effective soft-switching high-voltage dc-dc converter for a magnetron power supply is presented in this paper. The proposed dc-dc converter employs a quasi-resonant flyback soft-switching topology to reduce the turn-on loss of the power-MOSFET switching device. The main switching device efficiently powers at high voltages and low currents with low-power consumption. Using the COTS SMPS control IC reduced the system costs, while providing several advantages such as precise current regulation, resistance to breakdown, and extremely efficient soft-switching operation at high power levels.

The various practical design criteria, including a new high-voltage transformer, main switching device, and current controller were supported by experimental results. The quasi-resonant flyback converter achieved an overall efficiency for the 200W and 4kV magnetron power supply of 85% by the reducing the turn-on switching losses of the main switching device without any additional auxiliary circuitry.

References

- [1] B.M Hasanien, Khairy F.A. Sayed, "Current Source ZCS PFM DC-DC Converter for Magnetron Power Supply," *12th International Middle-East Power System Conference*, March 2008, pp.464-469.
- [2] J. S. Lai, B. M. Song, R. Zhou, A. R. Hefner, Jr., D. W. Berning, and C. C. Shen, "Characteristics and Utilization of a New Class of Low On-Resistance MOS-Gated Power Device," *IEEE Transactions on Industry Applications*, vol. 37, no. 5, September/October 2001, pp. 1182-1289.
- [3] F. Canales, P. Barbosa, and F. C. Lee, "A Zero-Voltage and Zero-current Switching Three-Level DC/DC Converter," *IEEE Transactions on Power Electronics*, vol. 17, no. 6, Nov. 2002, pp. 898-904.
- [4] B. M. Song, R. McDowell, A. Bushnell, and J. Ennis, "A Three-Level DC-DC Converter with Wide-Input Voltage Operations for Ship-Electric-Power-Distribution Systems," *IEEE Transactions on Plasma Science*, Oct. 2004, pp. 1856-1863.

-
- [5] NXP Semiconductors, "TEA1533P *GreenChip SMPS Control IC Datasheet and Application Note AN10268_1*", August 2002.
 - [6] R. -J. Wai, C.-Y. Lin, R.-Y. Duan, and Y.-R. Chang, "High-efficiency DC-DC converter with high voltage gain and reduced switch stress," *IEEE Transaction on Industrial Electronics*, vol. 54, no. 1, Feb. 2007, pp. 354-364.
 - [7] H. S. -H. Chung, W.-L. Cheung, and K.S. Tang, "A ZCS Bidirectional Flyback DC/DC Converter," *IEEE Transactions on Power Electronics*, vol. 19, no. 6, Nov. 2004, pp. 1426 -1434.
 - [8] T. Funaki, M. Matsushita, M. Sasagawa, T. Kimoto, and T. Hikihara, "A Study on SiC Devices in Synchronous Rectification of DC-DC Converter," *Conf. Record of IEEE APEC 2005*, Feb. 2007, pp. 339-344.
 - [9] H. Terashi and T. Ninomiya, "Analysis of Leakage-Inductance Effect in a Flyback DC-DC Converter using Time Keeping Control" *Conf. Record of IEEE 26th International Telecommunications Energy Conference (INTELEC)*, Sept. 2004, pp. 718 – 724.
 - [10] J. W. Baek, M. H. Ryoo, T. J. Kim, D. W. Yoo and J. S. Kim, "High Boost Converter using Voltage Multiplier," *Conf. Record of IEEE 31st Industrial Electronics Conference (IECON) 2005*, Nov. 2005, pp. 567-572.
 - [11] T. Matsushige, et al., "Voltage-Clamped Soft Switching PWM Inverter-Type DC-DC Converter for Microwave Oven and Its utility AC Side Harmonics Evaluations," *The Third International Power Electronics and Motion Control Conference*, vol. 1, August 2000, pp. 147-152.
 - [12] N. Vishwanathan, and V. Ramanarayanan, "High Voltage DC Power Supply Topology for Pulsed Load Applications with Converter Switching Synchronized to Load Pulses," *The Fifth International Conference on Power Electronics and Drive Systems*, vol. 1, November 2003, pp. 618-623.
 - [13] V. A. Vizir, et al., "Solid State Power Supply Modulator System for Magnetron," *The 14th International Pulsed Power Conference*, vol. 2, June 2003, pp. 1462-1464.

the Department of Electrical and Computer Engineering, Baylor University, Waco, Texas. His interests are in the design, analysis, simulation and implementation of high performance power converters, motor drives, and power electronics systems. Dr. Song is a Senior Member of IEEE.

SHIYOUNG LEE is currently an Assistant Professor of Electrical Engineering Technology at The Pennsylvania State University Berks Campus, Reading, PA. He received his B.S. and M.S. degrees in Electrical Engineering from Inha University, Korea, his M.E.E.E. in Electrical Engineering from the Stevens Tech., Hoboken, NJ, and his Ph.D. degree in Electrical and Computer Engineering from the Virginia Tech., Blacksburg, VA. He teaches courses in Programmable Logic Controls, Electro-Mechanical Project Design, Linear Electronics, and Electric Circuits. His research interest is digital control of motor drives and power converters. He is a senior member of IEEE, as well as a member of ASEE, ATMAE, and IJAC.

MOON-HO KYE received his B.S. degrees in Electronics Engineering from Hanyang University, Korea, in 1982 and M.S. degrees in Electrical Engineering from Changwon National University, Korea, 1993, respectively. He has over 25 years of experience working in the areas of power supply design and development. He was with the Korea Electrotechnology Research Institute, Century Electronics, Martek Power, Nao Tech, Comarco, and PowerPlaza. As a technical consultant, he is working for several companies in USA. His interests are in the high performance power supply design and cost-effective digital power solutions.

Biographies

BYEONG-MUN SONG received his B.S. and M.S. degrees in Electrical Engineering from Chungnam National University, Korea, in 1986 and 1988, respectively, and his Ph.D. degree in Electrical Engineering from Virginia Polytechnic Institute and State University, Blacksburg, VA in 2001. After working at the Korea Electrotechnology Research Institute for 10 years and General Atomics for 3 years, in 2004, he established his own venture company, ActsPower Technologies, San Diego, CA and served as the CEO/President and CTO. In August 2009, Dr. Song joined

A NEW METHOD FOR A NON-INVASIVE GLUCOSE-SENSING POLARIMETRY SYSTEM

Sunghoon Jang, New York City College of Technology of CUNY; Hong Li, New York City College of Technology of CUNY

Abstract

Current methods of monitoring blood glucose use invasive technologies such as collecting blood samples. Development of an accurate non-invasive method will present a great advantage over current methods. Our research group developed a non-invasive glucose-sensing polarimetry system within physiologic glucose levels by applying advanced optoelectronics technology. The authors of this study demonstrated accurate results with the system presented here. In a previous study, the authors were successful in detecting the optical rotation of in-vivo and ex-vivo glucose concentrations within the physiologic range of 0-500 mg/dl due to a highly sensitive and stable closed-loop polarimetry system. Although preliminary results from this system were successfully demonstrated by the authors in a previous study, the complication of a closed-loop system creates issues for future applications because it will require more components and it is more difficult to design and analyze the system. The authors introduce here a new, simplified open-loop non-invasive glucose-sensing polarimetry system. Theories of the proposed method are introduced and preliminary results are demonstrated. This study investigated the development of an open-loop optical glucose-sensing system that used a simpler method to distinguish blood glucose levels within this physiologic range by using the aqueous humor of the eye. This is because it has extremely fast response and recovery profiles without significant delay, when compared with glucose concentrations in blood plasma. The results demonstrate that not only is this non-invasive glucose-sensing detector capable of monitoring glucose accurately enough to satisfy medical-use criteria, but is also capable of employing a more simplified method than existing conventional closed-loop optical glucose-sensing technologies.

Introduction

Diabetes mellitus is a serious disease when the human body does not produce or properly use insulin. It has been one of the major health problems in society. Often, diabetes can lead to many serious medical problems including blindness, kidney disease, nerve disease, limb amputations, and cardiovascular disease (CVD). According to the American Diabetes Association, the estimated cost of diabetes-related health care in the United States is approximately \$91.8 billion, annually, including \$23.2 billion in direct medical costs [1]. The recent studies [2] of multi-center National Institute of Health (NIH) [2] indicated that the health risks associated with diabetes are significantly reduced when

blood glucose levels are properly and frequently controlled [3]. It is clearly indicated that it is prudent to measure blood glucose as often as five or six times a day. Thus, it is very important that proper monitoring should be done by diabetics at home or at work [4] [5]. At present, all existing methods of home blood-glucose monitoring require obtaining a blood sample by pricking a fingertip with a needle. This method strongly discourages patients' compliance, and has serious drawbacks because of its associated pain, inconvenience, and invasive nature [6].

A non-invasive method of monitoring blood glucose would present major advantages over current methods using invasive technologies. The authors attempted to develop and demonstrate accurate results with a non-invasive closed-loop optical-glucose system, within the physiologic glucose range of 0-500 mg/dl. The proposed open-loop glucose-sensing opto-electronic system used in this study also needed to be capable of monitoring very low glucose levels with the accuracy and precision that would satisfy medical-use criteria; this method is also expected to be fast and simple. The cost of the proposed testing device would be significantly lower than for existing methods because only a monitor with an optical sensor would be required, and the high monthly expense of testing strips would be avoided. In addition, patient acceptance for this methodology was expected to be high, due to its non-invasive nature, and the fact that it would be a simple and safe testing procedure.

There has been an increased demand for continuous, non-invasive glucose-monitoring techniques [7], due to the increasing number of people diagnosed with diabetes and the recognition of the fact that the long-term outcome of these patients can be dramatically improved by a careful, frequent and accurate glucose-monitoring method with control. In a previous study [8] [9] [22], the authors reviewed several of the newest, minimally invasive and non-invasive glucose-monitoring technologies under development or recently introduced. These include near infrared spectroscopy (NIR) [10], mid infrared spectroscopy (MIR) [11], radio wave impedance, optical rotation of polarized light [11], fluid extraction from the skin [12], and glucose-sensing contact lenses with fluorescence detection [11]. Although recent advances in basic research and clinical applications in non-invasive optical glucose monitoring are very encouraging for the future of this field, none of the attempts with non-invasive optical glucose-sensing techniques have resulted thus far in the development of a sensor, which allows monitoring of

glucose with sufficient accuracy and precision [7], [23]. Therefore, it is necessary to develop a new technique to satisfy criteria such as accuracy, low cost, simplicity in sampling and testing, portability, and safety.

Theory and Plan of Study

The first precision optical polarimeter using the Faraday effect was introduced by Gilham [13], [14] in 1957. Rabinovitch and March [15] introduced the concept of using the aqueous humor glucose as a detector of the blood glucose concentration by measuring the polarization rotation. Subsequently, Cote, Northrop, and Fox [16], [17] developed a true phase optical-glucose sensor to monitor glucose concentration. In 1997, Jang and Fox [18], [19] demonstrated that a closed-loop polarimeter could be realized with a single Faraday rotator.

In previous studies [18], [19], the authors introduced new, simplified non-invasive glucose-sensing polarimetry technology by introducing theories and demonstrating preliminary results. Conventional optical glucose sensors [7], [11], [20], [21] are very complicated in systemic design and performance because they adopted outdated closed-loop systems, which are inefficiently designed and implemented using additional optical components and electronic devices including a beam splitter, photo detectors, polarizers, Faraday modulators, and lock-in amplifier with additional analyzing devices. In this study, the authors attempted to investigate and develop the open loop-optical glucose-sensing system due to its simplicity for achieving higher accuracy and stability, while ensuring system sensitivity. The optical rotation due to the glucose cell will be proportional to the concentration of the glucose and the path length of the cell. The entire system sensitivity can be controlled by changing the gain constant of the lock-in amplifier.

Figure 1 shows a basic open-loop polarimetry system. The linearly polarized wave is emerging from the first polarizer, where θ represents the axis of the first polarizer. \hat{x} is the horizontal component of θ and \hat{y} is the vertical component of θ . The linear polarization of the interrogating beam is modulated by the optical chopper, which replaced the Faraday modulator used in previous research, and is then transmitted through a glucose cell, second polarizer, photo detector, and lock-in amplifier, respectively. As illustrated in Figure 1, the linearly polarized wave emerging from the first polarizer, can be represented as the following vector equation,

$$\mathbf{E}_1 = E \sin\theta \hat{x} + E \cos\theta \hat{y} \quad (1)$$

The linear polarization of the interrogating beam is modu-

lated by the action of the modulating optical chopper such that $\phi = \phi_c \cos \omega_c t$. Then, equation (1) becomes,

$$\mathbf{E}_2 = E \sin(\theta + \phi_c \cos \omega_c t) \hat{x} + E \cos(\theta + \phi_c \cos \omega_c t) \hat{y} \quad (2)$$

When $\theta = 0$ and ϕ_c is small,

$$\mathbf{E}_2 \cong E \sin(\phi_c \cos \omega_c t) \hat{x} + E \hat{y} \quad (3)$$

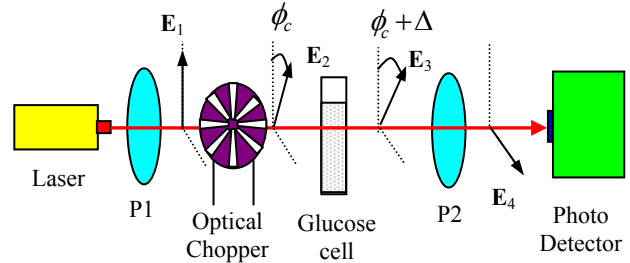


Figure 1. Block diagram of an open-loop glucose polarimetry system including glucose cell with first polarizer (P1) and second polarizer (P2)

The 'x' component of the electric field can be expanded to yield,

$$E_x \approx E \phi_c \cos \omega_c t \quad (4)$$

The frequency-doubling effect for crossed polarizers, where the axis of the second polarizer is at a right angle with respect to the axis of first polarizer, can be demonstrated by the following development, since optical detectors are sensitive to the intensity of light

$$I_x = |E_x|^2 \cong |E \phi_c \cos \omega_c t|^2 = E^2 \phi_c^2 \cos^2 \omega_c t = E^2 \phi_c^2 \frac{1}{2} (1 + \cos 2\omega_c t) \quad (5)$$

The change ' Δ ' in linear polarization due to the optical rotation effect is

$$\mathbf{E}_3 = E \sin(\Delta + \phi_c \cos \omega_c t) \hat{x} + E \cos(\Delta + \phi_c \cos \omega_c t) \hat{y} \quad (6)$$

It was found that the detected intensity will be

$$\begin{aligned} I_x &= |E_x|^2 \approx |E(\Delta + \phi_c \cos \omega_c t)|^2 \\ &= E^2 (\phi_c^2 \cos^2 \omega_c t + 2\Delta \phi_c \cos \omega_c t + \Delta^2) \\ &\approx E^2 \left[\frac{1}{2} \phi_c^2 (1 + \cos 2\omega_c t) + 2\Delta \phi_c \cos \omega_c t + \Delta^2 \right] \\ &\approx E^2 2\Delta \phi_c \cos \omega_c t \quad \text{for small } \Delta, \phi_c \end{aligned} \quad (7)$$

where: ϕ_c = optical rotation due to the optical chopper
 Δ = additional optical rotation due to the glucose cell

If a lock-in amplifier is connected to the output of the photo diode detector with a reference frequency ω_c , its DC output is

$$V_L = LE^2 \Delta \phi_c \quad (8)$$

where L is the gain constant of the lock-in amplifier and Δ directly contains information about the optical rotation due to the glucose molecule in the cell. From the above equation, we can conclude that the DC level of the lock-in amplifier in our open-loop optical-glucose sensing system will be dependent on the gain constant of the lock-in amplifier, intensity of the optical signal, and the optical rotations due to the optical chopper and the glucose medium. If we set all parameters as constant, other than the glucose medium, the system can detect the variance of DC levels due to optical rotation, which is proportional to the concentration of the glucose molecule in the medium.

The theoretical response from the lock-in amplifier as a function of the angle between the two polarizers is represented graphically in Figure 2. It was found that this open-loop polarimetry system worked efficiently when close to a 45° angle between the two polarizers. A key point is that the rotation change Δ , which is indicative of glucose concentration, is now modulated at the Faraday frequency for coherent detection.

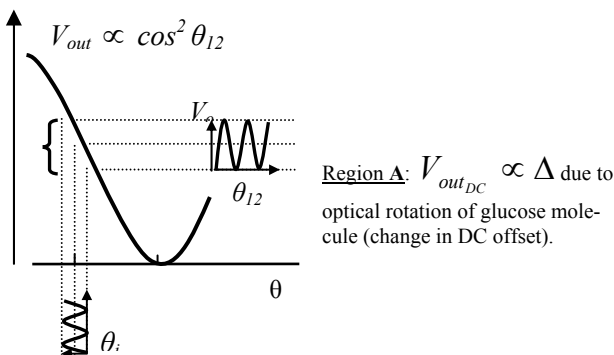


Figure 2. Graphical representation showing how the output from the lock-in amplifier depends on the angle (θ_{12}) between the two polarizers in Figure 1.

Methodology and Results

The main components of the closed-loop optical glucose sensor using the optical rotation of the glucose molecule are illustrated in Figure 3. A HeNe laser (approximately 1mW effective output after the first polarizer, 633 nm), and a first polarizer were used to provide linearly polarized light. The light was then passed through a Faraday modulator driven at about 1.2 kHz for the modulation of the polarization vector and detected by a photo diode detector after controlling its intensity by a second polarizer, which is called an analyzer. The lock-in amplifier provided an output signal, which is a DC voltage proportional to the amplitude of the 1.2 kHz present in the detected signal from the photo detector and then fed back to the Faraday modulator to close the loop. This dc output voltage is fully monitored and recorded by an

oscilloscope, and a single Faraday modulator was used as a modulator and compensator to provide modulation and feedback compensation combined within the system. Therefore, the lock-in amplifier provided phase and frequency-locked detection of the 1.2 kHz component, which itself was proportional to the net rotation between the two polarizers positioned at 45° to each other. The optical rotation due to the glucose cell, with a path length of one centimeter, is proportional to the concentration of the glucose and the path length of the cell. Thus, sensitivity of the entire system can be controlled by changing the gain constant of the lock-in amplifier.

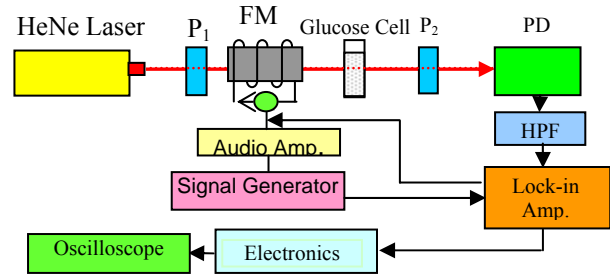


Figure 3. Block diagram of a designed and implemented closed-loop glucose-sensing polarimetry system: P_1 and P_2 are polarizers; FM is a Faraday Modulator; the glucose cell contains various glucose solutions within the physiologic range; PD is the photo diode detector; HPF is the high-pass filter

The closed-loop system was first calibrated by measuring the DC output signal from the lock-in amplifier, while applying various modulating frequencies in order to find the best fit for the current glucose-sensing system. The data shown in Figure 4 (a) was obtained from the DC output of the lock-in amplifier by changing the angle of the second polarizer. It was found that the system sensitivity was $37.01V/^\circ$, which means that every 10 millidegree of rotation gives about 370.1 mV DC offset. Since a practical glucose meter would need to detect a few millidegrees [22] of rotation, this system had a significant sensitivity. Figure 4 (b) shows a calibration run using the closed-loop system with a glucose cell containing dextrose-glucose in concentrations of 0, 100, 200, 300, and 500 mg/dl within the physiologic range. These data sets were obtained by using a single cell that was refilled with various glucose concentrations at each measurement. The averaged set of data from Figure 4 (b) was plotted after taking 10 measurements for each concentration to minimize errors due to the one-centimeter length of the glucose cell. The linear regression shown in Figure 4 (b) yielded $-5.725 - 0.006 [\text{glucose}]$, which indicates that for every 18.5 millidegree/(100 mg/dl), the dextrose-glucose molecule contributes about 0.2 millidegree of optical rotation to the system.

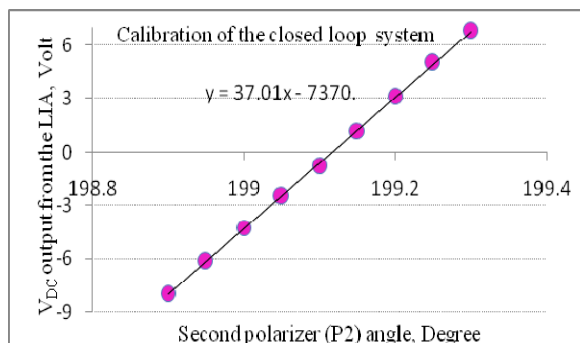


Figure 4-a. Plot of the DC output from the lock-in amplifier (LIA) as a function of the second polarizer rotation in the closed-loop optical-glucose sensor system illustrated in Figure 3

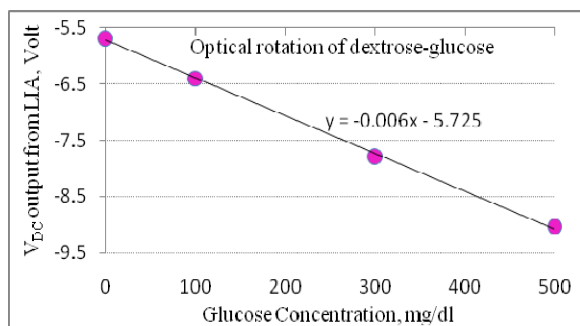


Figure 4-b. Plot of the waveforms includes DC output from the lock-in amplifier (LIA) against glucose concentration in the closed-loop glucose sensor

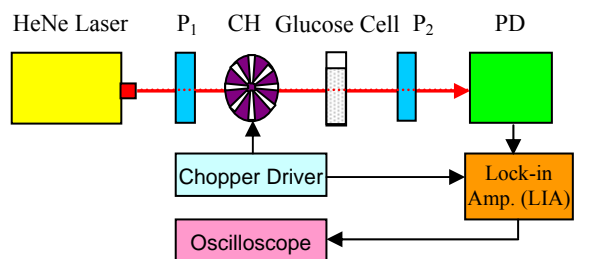


Figure 5. Block diagram and actual system of a designed and implemented open-loop polarimetry glucose sensor: CH is an optical signal chopper

The authors successfully demonstrated accurate results with the previously-designed non-invasive closed-loop polarimetry glucose-sensing system within physiologic glucose levels. This study also attempted to investigate and develop an optical glucose-sensing system, in order to achieve higher accuracy and ensure sensitivity with a simpler method using the open-loop glucose-sensing polarimetry system shown in Figure 5 by applying advanced opto-electronics technology.

The data shown in Figures 6-a to 6-i were obtained from the DC output of the lock-in amplifier with the angular orientation of the second polarizer. Various gains were also applied in order to calibrate system sensitivity and stability. Then, the system sensitivity was measured by monitoring the DC output of the lock-in amplifier using a fit of the data as shown in Figure 6-j. It was found that the system sensitivity was $6.442 \text{ V}/^\circ$, which means that every 10 millidegree of rotation gives about 64.42 mV DC offset output. This sensitivity would be enough to detect a few millidegrees of rotation for a glucose molecule.

Although the system sensitivity was lower than the previously developed closed-loop glucose-sensing polarimetry system, the authors are confident and optimistic about this new open-loop system because the system sensitivity can be improved by a factor of 10 without encountering major problems. From previous experience, the optical rotation of the glucose molecule was observed within the physiologic range at the system sensitivity, 370.1 mV DC offset for every 10 millidegree analyzing the polarizer rotation. Due to the fact that an absolutely dark room was not available for testing this system, there were certain levels of interfering optical noise involved in the current study. To improve system sensitivity and stability, future measurements will be made in an absolute dark room.

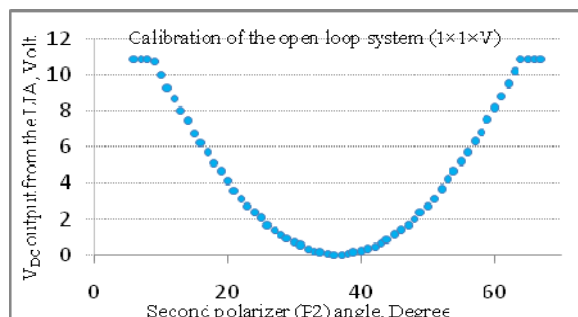


Figure 6-a

The general configuration of the system presented in Figure 7 is similar to the previous setup; however, the authors added an ex-vivo goat eye or an artificial eye to the system in order to detect penetrating light through the anterior chamber of the eye filled with aqueous humor. Also, the measured V_{DC} output depends on the glucose concentration,

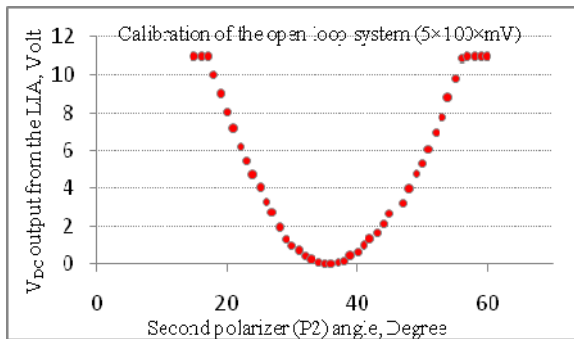


Figure 6-b

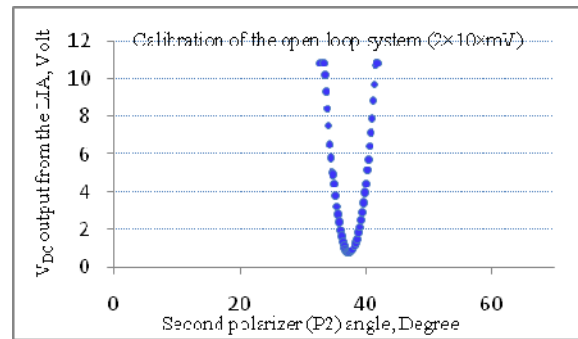


Figure 6-f

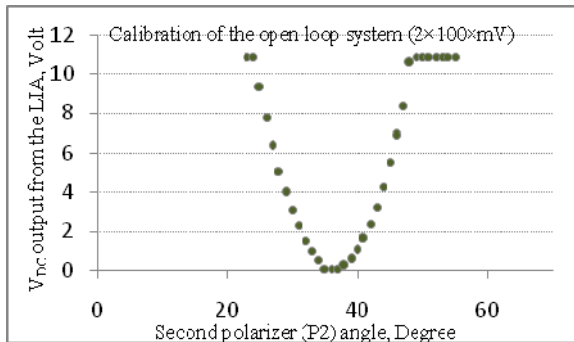


Figure 6-c

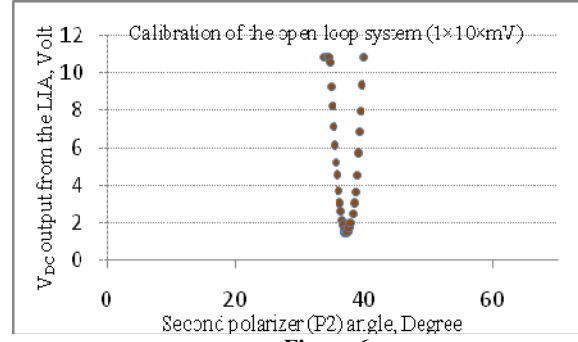


Figure 6-g

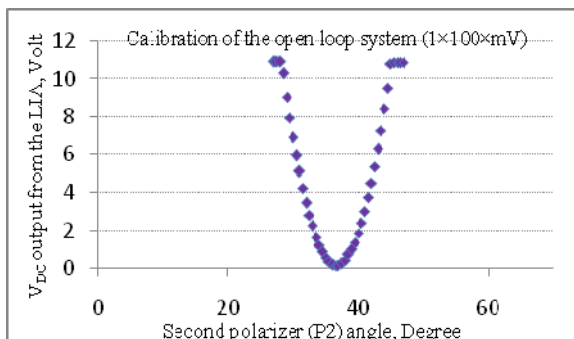


Figure 6-d

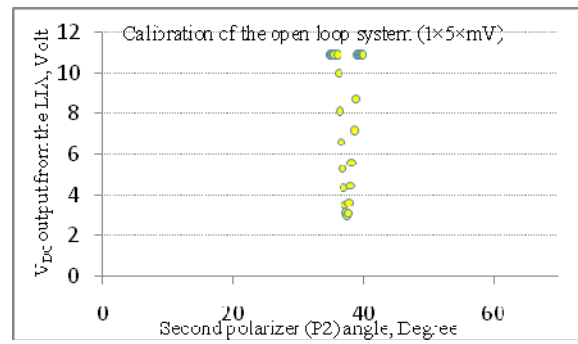


Figure 6-h

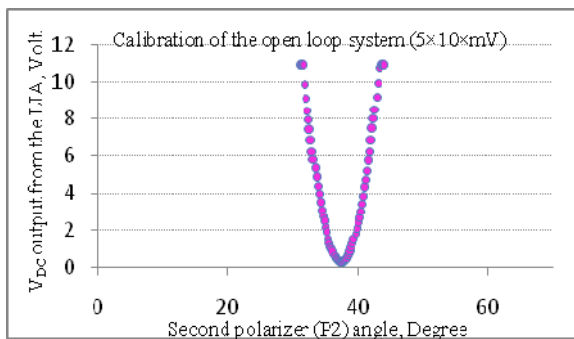


Figure 6-e

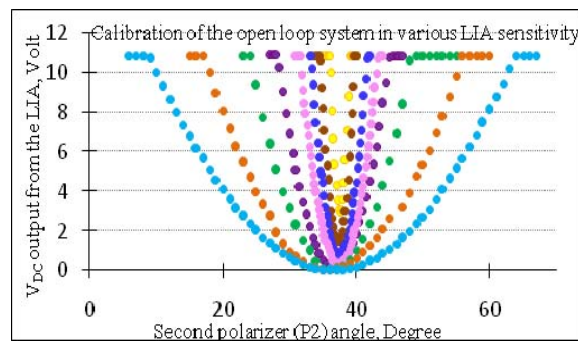


Figure 6-i

which can be detected by the lock-in amplifier. The system analysis with an ex-vivo goat eye or artificial eye will be completed in a future study. In this present study, the authors

have presented a simplified, non-invasive glucose-sensing polarimetry system by presenting theories and demonstrating preliminary results. In a follow-up study, the authors hope to achieve the intrinsic optical rotatory effect using conven-

tional optical rotation in the presence of ex vivo living tissue or an artificial eye.

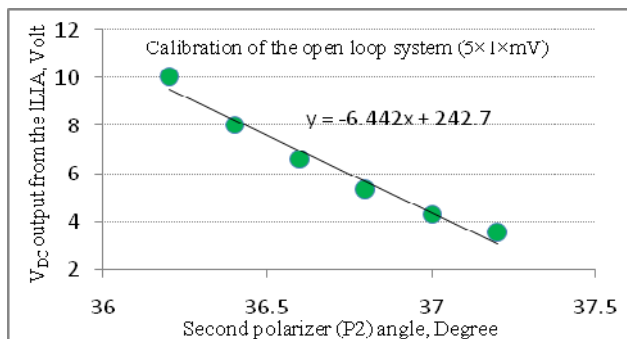


Figure 6-j

Figure 6. Demonstrated calibrations of the open-loop glucose-sensing polarimetry system. (a) to (h) are plots of V_{DC} output from the lock-in amplifier as a function of the second polarizer rotation in the open-loop system illustrated in Figure 5 at various lock-in amplifier sensitivities. (i) is a composite plot of all sensitivities in the lock-in amplifier. (j) is a plot of the V_{DC} output from the lock-in amplifier in the linear regression range at the sensitivity $5 \times 1 \times mV$

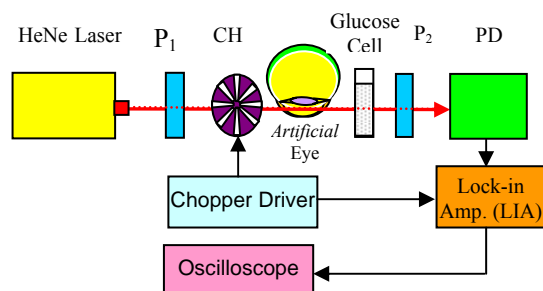


Figure 7. Schematic block diagram of the open-loop glucose-sensing polarimetry system including an artificial eye

Conclusion

Optical glucose-sensing techniques using the optical rotatory effect of glucose have many advantages over existing invasive and noninvasive methods, since the method is based on shining a brief pulse of light into the front of the eye. The authors previously showed that it is possible to isolate the lens/aqueous reflection and detect polarizational changes. However, measurements in the presence of a living eye will present many challenges because the tissues are more variable than nonliving optical components due to the nature of corneal birefringence. Further work will optimize this system in order to achieve the desired sensitivity, stability and accuracy. Once these hurdles are overcome, the optical glucose-sensing method studied and developed in this study can be miniaturized using current integrated optics, electronics, and advanced micro-fabrication technologies. This technique also has great potential for providing an inexpensive, fast,

reliable, accurate, and compact non-invasive glucose sensor for diabetic patients in the near future.

References

- [1] American Diabetes Association, "Economic Costs of Diabetes in the U.S. in 2002," *Diabetes Care*, Volume 26, number 3, Pages 917-932, March 2003.
- [2] National Institute of Health (NIH), "National Diabetes Statistics 2007" <http://diabetes.niddk.nih.gov/DM/PUBS/statistics/>
- [3] Gavin J.R., "The Importance of Monitoring Blood Glucose," *Touch Briefings*, US Endocrine Disease 2007 Issue, Pages 1-3.
- [4] Coster S.; Gulliford M.C.; Seed P.T.; Powrie J.K.; Swaminathan R., "Monitoring Blood Glucose Control in Diabetes Mellitus: A Systematic Review," *Health Technology Assessment*, 2000, vol. 4, no. 12. Pages: i-iv, 1-93.
- [5] Driskill W.T., "Diabetes Continues to be the Nation's Fourth Leading Cause of Death," *Health Educator*, 12, March 3, 1996.
- [6] Garg S.; Zisser H.; Schwartz S.; et al, "Improvement in Glycemic Excursions with a Transcutaneous, Real-Time Continuous Glucose Sensor," *Diabetes Care*, Volume 29, no. 1, Pages 44-50, January 2006.
- [7] Cote G.; Lec R.; Pishko M., "Emerging Biomedical Sensing Technologies and Their Applications," *IEEE Sensors Journal*, Vol. 3, No. 3, Pages 551-566, June 2003.
- [8] Jang S.; Ciszowska M.; Russo R.; Li H., "A New Approach to Glucose Monitoring Using a Non-Invasive Ocular Amperometric Electro-Chemical Glucose Sensor for the Diabetics," the ASEE Mid-Atlantic Section Spring 2006 Conference, Brooklyn, NY, April 28-29, 2006.
- [9] Jang S.; Russo R.; Li H., "Modifying the Existing Non-invasive Optical Glucose Sensing Device and Demonstrating the Optical Rotatory Effect of Glucose in the Presence of Glucose Medium," the ASEE Mid-Atlantic Section Spring 2007 Conference at NJIT, Newark, NJ, April 13-14, 2007.
- [10] Maruo K.; Tsurugi M.; Tamura M.; Ozaki Y., "In Vivo Noninvasive Measurement of Blood Glucose by Near-Infrared Diffuse-Reflectance Spectroscopy," *Applied Spectroscopy*, vol. 57, no. 10, Pages 1236-1244(9), October 2003.
- [11] McNichols R.; Cote J., "Optical glucose sensing in biological fluids: an overview," *Journal of Biomedical Optics*, vol. 5(1), Pages 5-16, 2000.
- [12] Klonoff D., "Non-Invasive Blood Glucose Monitoring," *Diabetes Care*, vol. 20, no. 3, Pages 433-443, March 1997.

-
- [13] Gilham E.J., "A High-precision Photoelectric Polarimeter," *Journal of Scientific Instruments*, Vol. 34, Pages 435-439, November 1957.
 - [14] Gilham E.J., "New Design of Spectropolarimeter," *Journal of Scientific Instruments*, vol. 38, Pages 21-25, January 1961.
 - [15] Rabinovitch B.; March W.F.; Adams R.L., "Noninvasive Glucose Monitoring of the Aqueous Humor of the eye," *Diabetes Care*, vol. 5, no. 3, Pages 254-258, May 1982.
 - [16] Cote' G. L.; Fox M.D.; Northrop R.B., "Glucose Sensor Development Using an Optics Approach," Proceedings of the 16th Annual Northeast Bioengineering Conference, IEEE EMBS, Penn State University, University Park, Pennsylvania, March 26-7, 1990.
 - [17] Cote' G.L.; Fox M.D.; Northrop R.B., "Laser Polarimetry for Glucose Monitoring," Proceedings of the 12th Annual IEEE EMBS Conference, Philadelphia, Pennsylvania, November 1-4, 1990.
 - [18] Fox M.D.; Censor D.; Jang S.; Welch L., "Multiple wavelength non-invasive ocular polarimetry for glucose measurement for managing of diabetes," SBIR Program Final Report 1995.
 - [19] Jang, S.; Fox M.D., "Optical Glucose Sensor Using a Single Faraday Rotator," Proceedings of the 23rd Annual Northeast Bioengineering Conference, IEEE EMBS, Durham, New Hampshire March 23-4, 1997.
 - [20] Baba J.S.; Cameron B.D.; Cote G.L., "Effect of Temperature, ph , Corneal Birefringence on Polarimetric Glucose Monitoring in the Eye," *Journal of Biomedical Optics*, 7(3), Pages 321-328, July 2002.
 - [21] Baba J.S.; Cameron B.D.; Cote G.L., "Optical Rotation and Linear and Circular Depolarization Rates in Diffusively Scattered Light from Chiral, Racemic, and Achiral Turbid Media," *Journal of Biomedical Optics*, 7(3), Pages 291-299, July 2002.
 - [22] Jang S.; Fox M.D. "Optical Sensor Using the Magnetic Optical Rotatory Effect of Glucose," *IEEE-LEOS*, vol. 12, Pages 28-30, April 1998.
 - [23] Koschinsky T.; Heinemann L., "Sensors for glucose monitoring: technical and clinical aspects," *Diabetes/metabolism research and reviews*, vol.17, issue 2, Pages 113-123, March 2001.

Electrical and Computer Engineering from New Jersey Institute of Technology, and his Ph.D. degree in Biomedical Engineering from University of Connecticut. Dr. Jang is a member of IEEE and BME. His technical areas include digital signal processing, opto-electronics, and control systems in Biomedical Engineering. He has published a number of papers in these areas. Dr. Jang teaches in Electrical and Telecommunications Engineering Technology. Professor Jang may be reached at sjang@citytech.cuny.edu.

HONG LI is currently an Associate Professor in Department of Computer Systems Technology at New York City College of Technology of CUNY. She received her M.S. degree in Mathematics from P. R. China and Ph.D. degree in Mathematics from The University of Oklahoma. Her research has been focused on system modeling and parameter estimation in variety fields of applications. She has published a number of papers with group of researchers in the fields of civil engineering and biomedical engineering. Professor Li also has years of experience of software development in industries before she joined CUNY as faculty member. Professor Li may be reached at hli@citytech.cuny.edu.

Biographies

SUNGHOON JANG is currently an Assistant Professor in Electrical and Telecommunications Engineering Technology at New York City College of Technology of CUNY. He received the B.S. degree in Electrical Engineering from the Kyung-nam University, Korea, and his M.S.E.E degree in

A SERVICE-LEARNING APPROACH IN A BASIC ELECTRONIC CIRCUITS CLASS

Fei Wang, California State University-Long Beach

Abstract

In this study, the author revised a basic electronic circuits course (EE330: Analog Circuit I) into a service-learning course with community engagement. The revised EE330 course required students to: 1) give a seminar to local high-school students on electronics topics, and 2) collaborate with local high-school students on a final project. The immediate goal of this re-design was to improve the communication skills of engineering students with a non-technical audience, and promote the awareness of engineering among future college candidates. Effectiveness of the service-learning approach was assessed through a variety of methods, including comprehensive reports and reflection responses from students, analysis of students' performance on key final exam problems, as well as surveys of high-school students and teachers. Reflection responses from college students indicated that the service-learning component enhanced their ability to communicate with a non-technical audience. It was also observed that students from the service-learning session outperformed the students from the regular session on design and complicated analysis problems. The majority of surveys from high-school students indicated that this activity stimulated their interest in choosing engineering as a college major in the future. It was also observed that female students showed less enthusiasm in technical topics when compared with their male colleagues, which suggests the needs for attention to gender differences in engineering education.

Introduction

Engineering educators are more and more aware that it is no longer acceptable to separate the teaching of engineering techniques from the social context necessary for a person to effectively contribute to society. Modern engineers must work and think both technically and socially, which requires them to acquire not only the knowledge of technology, but also the ability to communicate values and facts related to technology, mostly to audiences outside of engineering [1]-[2]

Nowadays, the service-learning method has been widely implemented in many disciplines. The specific methods may vary from project-based service [3], teaching-based service [4] and research-based service [5]. In general, when designing a pedagogy containing service learning, four basic principles need special attention. They are engagement, reflec-

tion, reciprocity and public dissemination. The engagement principle ensures that the service component meets a public good, which requires negotiation between university and community partners through outreach programs. The reflection component is especially necessary for the student to understand what they actually learn from the course. Whether the service is actually learning or not depends on whether the activity can encourage students to link their service experience to course content and to reflect upon the importance of the service. Reciprocity ensures that the students and the community teach and learn from one another. Public dissemination is basically the product of the service, which needs to be presented and delivered to the public.

While academic service learning usually provides community services, not all activities providing community services are considered service learning. Academic service learning should aim for both service and, more importantly, learning. Therefore, this study focused on the following criteria when designing the service-learning pedagogy.

- **Relevant and Meaningful Service with the Community:** This is the typical service component needed to ensure that the service provided within the community is relevant and meaningful to all parties.
- **Enhanced Academic Learning:** This is the typical learning component. The service provided must help students to reflect on and assimilate the knowledge they acquired in the course.
- **Purposeful Civic Learning:** This activity should intentionally prepare students for active civic participation in a diverse democratic society.

If any of these three criteria is missing, it is no longer a service-learning practice, but some other form of community engagement. Table 1 compares service learning with other types of community engagement. A common weakness of college students, especially engineering students, is an inability to communicate in non-technical terms with people from different backgrounds. Therefore, developing a learning environment that gives them the opportunity to articulate engineering problems or products in easy and organized terms is extremely important. Based on the NSF's survey of recent college graduates, only half of all engineering/science graduates enter engineering/science occupations after their graduation [7]. A great number of them take positions like technical marketing, sales, teaching or other related posi-

tions. These positions require great communication skills to non-technical audiences. Although engineering students receive basic communication training through general education courses required by ABET, they do not usually receive the training in technical communication, which benefits them directly. The service-learning pedagogy designed for the EE330 course targeted this issue. Therefore, a teaching-based service-learning model was used. The community partner in this study was a local high school serving mainly minorities.

Table 1 Comparison of Types of Community Engagement [6]

	Community Service	Enhanced Academic Learning	Purposeful Civic Learning
Volunteering	Yes	No	No
Internship	Yes	Yes	No
Service Learning	Yes	Yes	Yes

From a community-service point of view, K-12 students are provided an opportunity to get to know the engineering world through this activity. They also come face-to-face with electrical engineering students, who share their college experience with them. This helps the K-12 students make well-informed decisions when they need to choose a college major in the future.

From the academic department's point of view, this service-learning activity has the potential to recruit future students, who are really interested in electrical engineering. This directly helps department enrollments, and indirectly improves the quality of the program.

Curriculum Design

EE330-Analog Circuit I is a required course for Electrical Engineering majors at California State University, Long Beach. It is offered in both Fall and Spring semesters. Depending on the student enrollment, at least one session is offered each semester. EE330 has both lecture and lab components, and students are required to work on hardware lab experiments. The "required" nature and the offering frequency of this course ensures that all students graduating from the Electrical Engineering department receive technical communications practice.

The current curriculum of EE330 includes a review of linear electronic circuits, introduction to diodes, transistors and operational amplifiers, and examination of their applications in electronic circuits. Application topics include rectifiers,

DC-DC converters, amplifiers, sensors and I-V converters. During the course, students are expected to develop the ability to design and build circuits, troubleshoot them and explain the results. The addition of a service-learning component does not alter the learning objectives of the course; on the contrary, it enhances student achievement of those objectives.

The service-learning component of EE330 requires students to give a seminar to local high-school students on topics related to the course and collaborate with them on a hardware final project. Students are required to develop their presentation strategies so that youths from high school will understand. Topics selected for purposes of the seminars should be chosen very carefully, so that they are not only related to course content, but also relevant to everyday life in order to attract the attention of the audience. The hardware project, which is also the final project of the course, must reflect one of the circuit applications covered in class. Instructors suggest a few topics, but students can also choose their own topics given the instructor's permission.

The specific learning objectives of EE330 include:

1. Students should be able to describe basic electron transport phenomena, diode rectification, switching and amplification of BJT and MOSFET transistors and op-amp operation sufficiently well to convey that understanding to audiences without an engineering background. This objective is assessed through the service-learning presentation, reflection discussion and service-learning final report.
2. Students should be able to draw schematics of diode bridge rectifiers, DC-DC converters and complete power supply. This objective is assessed through exams and lab reports.
3. Students should be able to draw AC and DC equivalent circuits of bipolar junction and field-effect-transistor circuits. This objective is assessed through exams and lab reports.
4. Students should be able to mathematically analyze transistor and diode circuits and solve for Q-points using the MoHAT procedure. This objective is assessed through exams and lab reports.
5. Students should be able to design CS and CE amplifier circuits based on given design expectations. This objective is assessed through exams and lab reports.
6. Students should be able to synthesize the knowledge learned from lectures into a hardware circuit design to perform certain applications. Students should be able to troubleshoot and test their cir-

7. Students should demonstrate civic engagement with local communities to promote fundamental engineering knowledge through informal education seminars. This objective is assessed through the service-learning presentation, reflection discussion and service-learning final report.

8. Students should demonstrate their ability to recognize different audiences and be able to design their presentations accordingly. This objective is assessed through the service-learning presentation, reflection discussion and service-learning final report.

The specific requirements of the service-learning activities include:

1. **SERVICE-LEARNING PRESENTATION:** Students are allowed to choose any topic that is related to this course in order to design a seminar presentation for high-school students in grades 8-12. The presentation is evaluated through feedback surveys from 8-12 students and the PowerPoint slides of the presentation.
2. **SERVICE-LEARNING PROJECTS:** Students are required to collaborate with 8-12 students on a hardware final project. Final projects must reflect one of the circuit applications covered in class. Instructors may suggest topics, but students can also choose their own topic given the instructor's permission. Final projects should require 10-12 hours of work. The final reports and seminar PowerPoint slides will be shared with 8-12 schools for educational purposes.
3. **REFLECTION DISCUSSION:** The discussion board on beachboard.com (a subsidiary of blackboard.com designed solely for CSU Long Beach) is used as a medium for discussion. Students are required to respond to reflection questions posted by the instructor and share their learning experience with peers through board postings. At least three responses are required by the end of the semester including one before the seminar presentation, one after the seminar presentation and one during the final project. Extra credit will be granted to students, who actively participate in discussions.

Implementation

In the Fall 2008 semester, EE330 was offered as a service-learning course. The Center of Community Engagement on the Cal-State Long Beach campus was of tremendous help in terms of identifying service-learning opportunities within the Long Beach community. The New City School at Long Beach expressed their interest during the initial contact with the author of this study. Several campus visits to the New City School were conducted to identify the feasibility for

setting up the equipment. A meeting with their science teachers was conducted to coordinate the educational needs of both parties and to negotiate an appropriate class schedule of both parties.

During the first week, the instructor of EE330 conducted an introductory lecture to the EE330 students about the educational benefits and the goals and requirements of the service-learning component. This lecture also covered technical communication topics such as strategies to approach the target audience, selection of topics/project, and design of a presentation. Safety issues that students should be aware of were also covered in the introductory lecture. Students were expected to approach the community partner to make arrangements for the scheduling of their presentation and the project.

Five groups—19 students—provided service to 8-grade students in the New City School. The topics of their seminar presentations ranged from interesting applications to basic science. Some of them taught 8th-grade youths to measure current, voltage and resistance using the digital multi-meter. Some of them lectured on the behavior of diodes, transistors and their applications. Some of them brought a microcontroller board to showcase how to control a toy car.

The selected final hardware projects included: Automatic light control using a Schmitt Trigger built from an operational amplifier; a power-supply design including diode rectification and DC-DC converter; small signal amplifier design using a BJT transistor (2 groups selected this project); light insolation meter using an operational amplifier as I-V converter. The students designed, built and tested their circuits in the EE department's laboratory before their community service. On-site at the high school, they re-built their circuits with high-school students and characterized the circuits with them again. This way, the high-school students were provided a hands-on experience on electronic hardware, which was expected to stimulate their interests in electrical-engineering topics.

Students were required to have reflection discussions before and after their service so that they could reflect on what they learned during the service activities. The reflection questions were posted on beachboard.com by the instructor. Students responded to questions by adding threads to the board. Sample questions posted by the instructor include:

1. What topic did you choose for this service and why?
2. Discuss your experience about the service presentation, such as questions received, audience interest and how you dealt with the non-technical audience.

cuits. This objective is assessed through final project reports.

7. Students should demonstrate civic engagement with local communities to promote fundamental engineering knowledge through informal education seminars. This objective is assessed through the service-learning presentation, reflection discussion and service-learning final report.
8. Students should demonstrate their ability to recognize different audiences and be able to design their presentations accordingly. This objective is assessed through the service-learning presentation, reflection discussion and service-learning final report.

The specific requirements of the service-learning activities include:

1. **SERVICE-LEARNING PRESENTATION:** Students are allowed to choose any topic that is related to this course in order to design a seminar presentation for high-school students in grades 8-12. The presentation is evaluated through feedback surveys from 8-12 students and the PowerPoint slides of the presentation.
2. **SERVICE-LEARNING PROJECTS:** Students are required to collaborate with 8-12 students on a hardware final project. Final projects must reflect one of the circuit applications covered in class. Instructors may suggest topics, but students can also choose their own topic given the instructor's permission. Final projects should require 10-12 hours of work. The final reports and seminar PowerPoint slides will be shared with 8-12 schools for educational purposes.
3. **REFLECTION DISCUSSION:** The discussion board on beachboard.com (a subsidy of blackboard.com designed solely for CSU Long Beach) is used as a medium for discussion. Students are required to respond to reflection questions posted by the instructor and share their learning experience with peers through board postings. At least three responses are required by the end of the semester including one before the seminar presentation, one after the seminar presentation and one during the final project. Extra credit will be granted to students, who actively participate in discussions.

Implementation

In the Fall 2008 semester, EE330 was offered as a service-learning course. The Center of Community Engagement on the Cal-State Long Beach campus was of tremendous help in terms of identifying service-learning opportunities within the Long Beach community. The New City School at Long

Beach expressed their interest during the initial contact with the author of this study. Several campus visits to the New City School were conducted to identify the feasibility for setting up the equipment. A meeting with their science teachers was conducted to coordinate the educational needs of both parties and to negotiate an appropriate class schedule of both parties.

During the first week, the instructor of EE330 conducted an introductory lecture to the EE330 students about the educational benefits and the goals and requirements of the service-learning component. This lecture also covered technical communication topics such as strategies to approach the target audience, selection of topics/project, and design of a presentation. Safety issues that students should be aware of were also covered in the introductory lecture. Students were expected to approach the community partner to make arrangements for the scheduling of their presentation and the project.

Five groups—19 students—provided service to 8-grade students in the New City School. The topics of their seminar presentations ranged from interesting applications to basic science. Some of them taught 8th-grade youths to measure current, voltage and resistance using the digital multi-meter. Some of them lectured on the behavior of diodes, transistors and their applications. Some of them brought a microcontroller board to showcase how to control a toy car.

The selected final hardware projects included: Automatic light control using a Schmitt Trigger built from an operational amplifier; a power-supply design including diode rectification and DC-DC converter; small signal amplifier design using a BJT transistor (2 groups selected this project); light insolation meter using an operational amplifier as I-V converter. The students designed, built and tested their circuits in the EE department's laboratory before their community service. On-site at the high school, they re-built their circuits with high-school students and characterized the circuits with them again. This way, the high-school students were provided a hands-on experience on electronic hardware, which was expected to stimulate their interests in electrical-engineering topics.

Students were required to have reflection discussions before and after their service so that they could reflect on what they learned during the service activities. The reflection questions were posted on beachboard.com by the instructor. Students responded to questions by adding threads to the board. Sample questions posted by the instructor include:

1. What topic did you choose for this service and why?

2. Discuss your experience about the service presentation, such as questions received, audience interest and how you dealt with the non-technical audience.
3. If you had a chance to repeat this service, how would you improve the effectiveness?
4. Give your opinion on electronics-related service-learning topics and how you benefited from this service.

Assessment

The assessment of this service-learning activity was conducted in three ways: 1) Students' reflection responses were collected and analyzed in order to assess the learning outcome regarding technical communication; 2) Students' performance on key final-exam problems were analyzed and compared with a control session in order to assess the effectiveness of the service-learning activity in terms of enhancing the learning of technical topics; and, 3) Surveys of high-school youths (mainly 8th graders) were collected and analyzed in order to assess the effectiveness of the service-learning activity in terms of enhancing community's awareness of engineering.

• Reflection Response

This is a qualitative assessment method. All reflection responses from students were collected, analyzed and summarized on key issues. It was found that most of the students found it challenging to present the material to 8th-grade youth. The main reason was that they had a hard time attracting the youths' attention during the presentation. In addition, explaining concepts in non-technical terms was another thing they found to be challenging. The lesson they learned from this service was that the design of a presentation is extremely important when facing a non-technical audience. Some of them said that if they were to do the seminar again, they would include more hands-on demonstrations and more videos and pictures.

Those strategies attract the audience's attention more effectively, and can help them better understand the topic. Some of them mentioned taking control of the presentation pace and using an active tone during the presentation, which is also important. Regarding the learning outcome, most of them responded positively. They stated that they have to understand their project before they can explain it to others. One of the groups also mentioned that the questions they received during the service made them think about and improve the project. Another group stated that they remembered how "blind" they were when they got to choose a college major, and that they were glad that they could help others make informed choices. This comment indicated that the students started to become aware of their responsibilities to the community.

• Performance on Key Problems

Students' learning outcome on technical content was assessed quantitatively by comparing their performance on key final-exam problems with those from a regular session. When designing the two final exams, three identical key problems were intentionally included for assessment purposes. The three key problems were: a transistor analysis for dc and small signal analysis, a diode analysis problem for dc Q-point analysis, and an op-amp design problem. To exclude the psychological effects, these key problems were put in the same order for both sessions, i.e., problem 1 was the transistor analysis, problem 2 was the diode analysis, and problem 3 was the op-amp design. Problems that were not for assessment purposes were included thereafter. The average score of the assessment problems from both sessions are summarized in Table 2.

It was observed that the students from the service-learning session significantly out-performed the regular session students on design and transistor-analysis problems. This is probably because a majority of the students from the service-learning session chose final projects related to either the op-amp design or amplifier design using a BJT. Although students from the regular session were required to do similar projects, they still showed a weaker understanding on these topics. This clearly suggests that the service-learning component did enhance the students' learning outcome. While seeking a way to explain their final projects to 8th-grade youths, the students solidified their understanding on selected topics.

Table 2 Score comparison of key problems between service-learning session and regular session

	Service Learning Session	Regular Session
Transistor Analysis	71%	43%
Diode Analysis	61%	67%
Design using Op-Amp	62%	34%

• Survey to High School

The impact of the service-learning activity on the local community was assessed both quantitatively and qualitatively. The assessment surveys shown in Table 3 were distributed to 8th-grade audiences. Besides the numerical measures, audiences were also provided room to provide their comments and expectations on future presentations. High-school teachers were also invited to provide their qualitative comments on this activity.

Eighty copies of survey were distributed to the 8th-grade audience, of which 59 were returned. Among those returned,

30 were from males and 26 were from females; 3 others did not specify their gender. Some returned surveys were partially completed (20 copies) with one or two un-answered questions. The statistical results are presented in table 4. Questions 1, 5 and 6 focused on assessing the effectiveness of the service-learning activity in terms of improving high-school students' awareness of the engineering field, i.e., the audience's interest in engineering topics and enthusiasm for pursuing further study in this field. Questions 2, 3 and 4 focused on assessing the technical communication performance of college students.

From the statistical results shown in Table 4, it can be concluded that the performance of college students turns out to be positive. Their presentations gained positive responses from the audience. Overall, they were able to convey the topics they selected in non-technical terms. A significant difference between male and female audiences on Questions 2, 3 and 4 was not observed. However, regarding the level of interest in engineering topics and the enthusiasm for pursuing further study in engineering, the difference between male and female audiences becomes significant. The male audience showed stronger interests and enthusiasm in engineering topics (Question 1- 4.65, Question 5- 4.1 and Question 6- 4.1) than female audience (Question 1- 3.75, Question 5- 3.43 and Question 6- 3.2). These results tell us that, as educators, we need to pay more attention to the gender differences in engineering education.

Table 3 Assessment survey to 8th-grade audience

	Strongly Agree		Strongly Disagree		
Does the topic interest you?	5	4	3	2	1
Is the presenter well prepared?	5	4	3	2	1
Did the presenters provide interesting examples and/or demos that helped you understand the topic better?	5	4	3	2	1
Did the presenter try to communicate with the audience in non-technical terms?	5	4	3	2	1
Are you willing to learn more about Electronic and Electrical Engineering after this seminar?	5	4	3	2	1
Will you consider Electrical Engineering as your major in college?	5	4	3	2	1

The high-school teachers also gave positive feedback by stating that their students showed more enthusiasm on science topics after this activity. They received requests from multiple students about visiting the college of engineering at CSU-Long Beach after our students gave the seminar presentation. Thus, a campus visit was arranged in the same semester. High-school youths visited our electronics and micro-fabrication lab as well as some computer-aided classrooms. During the visit, the authors received multiple questions regarding the instruments in our lab as well as the admission requirements to the electrical engineering department. Visitors expressed high enthusiasm for further involvement in these kinds of activities.

Table 4 Statistical results of the assessment survey

	MALE (30 responses)		FEMALE (26 responses)	
	Mean	STD	Mean	STD
Question 1 (56 responses)	4.65	0.48	3.75	1.15
Question 2 (45 responses)	4.6	0.73	4.81	0.39
Question 3	4.42	0.94	4.6	0.61
Question 4 (41 responses)	4.53	0.82	3.94	1.03
Question 5	4.1	1.11	3.43	1.06
Question 6	4.1	1.14	3.2	1.47

Conclusion

An electronics core course (EE330-Analog Electronic Circuit I) was redesigned into a service-learning course in order to improve engineering students' ability to communicate with non-technical audiences and simultaneously promote engineering awareness among K-12 students. Students offered community service in the form of seminar presentations and project demonstrations to local high-school students. Assessment analysis show that: 1) all college students stated that the service-learning activity improved their capability to communicate with non-technical audiences; 2) students from the service-learning session outperformed the students from the regular session on key final exam problems, specifically on design and complicated analysis problems; 3) the majority of the surveys collected from high-school students indicated that they were interested in choosing engineering as their major in the future; 4) female high-school students showed less enthusiasm for engineering topics when compared with their male colleagues, which suggests the need for attention to gender differences in engineering education.

References

- [1] L. Pascail, "The Emergence of the Skills Approach in Industry and Its Consequences for the Training of Engineers", *European Journal of Engineering Education*, vol. 31, No.1, 2006, pp.55-61
- [2] W. Ravesteijn, E. de Graaff and O. Kroesen, "Engineering the Future: The Social Necessity of Communicative Engineers", *European Journal of Engineering Education*, vol. 31, No.1, 2006, pp.63-71
- [3] W. Oakes, J. Duffy, T. Jacobius, P. Linos, S. Lord, W. Schultz and A. Smith, "Service-Learning in Engineering", *Frontiers in Education*, Volume 2, 2002, pp.F3A-1 - F3A-6
- [4] W.J. McIver, Jr. and T. Rachell, "Social informatics and service learning as teaching models", *Technology and Society Magazine, IEEE*, vol. 21, No. 2, 2002, pp. 24 – 31
- [5] X. Jin, F. Wang, J. Flickinger, S. Jobe and T. Dai, "International Engineering Research Collaboration on Gallium-Nitride (GaN) Lasers and Light Emitting Diodes (LEDs)", *International Journal of Engineering Research and Innovation*, vol. 1, No.1, 2009, pp. 5-10
- [6] Service Learning Curriculum Development Resource Guide for Faculty, Center for Community Engagement, California State University-Long Beach, 2008, pp.17
- [7] "An Overview of Science, Engineering, and Health Graduates: 2006", NSF publication 08-304, 2008

Biography

FEI WANG is an assistant professor in Electrical Engineering Department at California State University, Long Beach, CA, since 2007. She was an assistant professor in EE department at California Polytechnic State University at San Luis Obispo, CA, from 2005 to 2007. She received MS and PhD degree in Electrical Engineering from University of Cincinnati in year of 2002 and 2005 respectively. She received her BS degree in Electronics and Information Science from Peking University, Beijing, China in year of 2000. Dr. Wang can be reached at fwang3@csulb.edu

TOOL CONDITION MONITORING SYSTEM IN TURNING OPERATION UTILIZING WAVELET SIGNAL PROCESSING AND MULTI-LEARNING ANNS ALGORITHM METHODOLOGY

Samson S. Lee, Central Michigan University

Abstract

The present study shows the development of a tool condition monitoring (TCM) system utilizing signal decomposition techniques in an artificial neural networks (ANNs) system. The raw signals obtained from sensors under different machining conditions were examined and reduced to multiple components. The most significant components of each signal were implemented to develop tool-monitoring systems. Over 900 neural-networks structures were tested using a multi-learning algorithm methodology to find an optimized structure for the TCM system. This technique provided systematic test results of the extended number of possible ANN structures with higher accuracy, when compared with the traditional manual trial-and-error methodology. The ANN-TCM system developed in this study showed 97% accuracy from 151 test samples with the reject flank wear size of 0.2 mm or larger. The results demonstrated the successful development of a TCM system, which can be implemented as a practical tool to reduce machine downtime associated with tool changes and to minimize the number of scraps.

Introduction

The metal cutting process, which has played an important role in modern manufacturing history, relied on highly skilled labor until the mid-1950s, when automated machining was introduced to replace traditional labor, decrease production costs, increase productivity, and enhance product quality [1]. Not long afterwards, the industry demanded another task from manufacturers. Products became more individualistic, varied, and complex to manufacture. Manufacturers needed new technologies and methods that would allow small-batch production to gain the economic advantages of mass production [2]. The development of CIM (Computer-Integrated Manufacturing) and FMS (Flexible Manufacturing Systems) seemed to be ideal solutions for increasing machining flexibility in addition to flexibility in routing, process, product, production, and expansion [3].

Although the combination of CIM and FMS technologies showed great promise as a cost-effective solution to meet

new demands, CIM-FMS systems could not be implemented until certain prerequisites were met. One major prerequisite was uninterrupted machining to achieve maximum efficiency [4]. Deteriorating process conditions, such as tool condition, often forces manufacturers to interrupt machining processes in order to respond. Thus, developing an effective means of monitoring machine conditions has become one of the most important issues in the automation of the metal-cutting process [5].

Among the many machine conditions requiring monitoring, tool wear is one of the most critical issues for ensuring uninterrupted machining. An effective monitoring system allows for effective tool-change strategies when tools deteriorate, and maintains proper cutting conditions throughout the process [6]. If the monitoring system fails to detect the true cutting-tool conditions, the cutting process could result in poor surface quality, dimensional error, and even machine failure [5]. Furthermore, a reliable tool-wear monitoring system can reduce machine downtime caused by changing the tool, thus leading to fewer process interruptions and higher efficiency. The information obtained from the tool-wear sensors can be used for several purposes, including the establishment of a tool-change policy, economic optimization of the machining operation, on-line process manipulation to compensate for tool wear, and to some extent the avoidance of catastrophic tool failure.

TCM Studies

The traditional process for predicting the life of a machine tool involves Taylor's equation for tool-life expediency: $VT^n = C$, where V is cutting speed, T is tool life based on the amount flank wear, and n and C are coefficients [7]. This equation has played an important role in machine-tool development [8]. Since advanced machining was introduced in the mid-1900s, various methods to monitor tool wear have been proposed, expanding the scope and complexity of Taylor's equation. However, none of these extensions has been applied universally, due to the complex nature of the machining process [9].

Researchers have searched for reliable methods to monitor tool wear. These methods represent an area of active research because tool condition strongly influences the surface finish and dimensional integrity of the workpiece, as well as vibration in the tool. More automated approaches were attempted using computer-numerical-control (CNC) technology. However, the CNC approach also has several obstacles to widespread implementation such as the narrow learning capability of CNC machines, limited flexibility of the CNC controller, relatively large dynamic errors encountered in CNC operations, sensor noises and variability between machines [10]. In spite of the recent introduction of open CNC and STEP-NC for providing improved architectures, where researchers can integrate sensor-signal management systems and customized applications, studies show that it is still a challenge to find proper sensor technologies and signal-process techniques for tool-condition monitoring [11, 12]. Therefore, numerous sensor techniques were introduced and tested in tool-wear-monitoring studies.

Tool-condition monitoring methods can be classified into direct and indirect methods, depending on the source of signals collected by sensors. Direct methods sense tool conditions by direct measurement of the tool. Direct methods include optical, radioactive, and electrical resistance. Alternatively, indirect methods sense the tool condition by measuring secondary effects of the cutting process, such as acoustic emission (AE), sound vibrations, spindle and feed-motor current, cutting force, and machining vibration. Direct methods are beneficial because they take close readings directly from the tool itself. By contrast, indirect methods must rely on conditions other than the tool itself to judge the condition of the tool. However, direct methods are limited because the machining process must be interrupted to make the direct measurements [13]. As a result, machine downtime increases, as do costs for tool condition monitoring.

Since indirect methods do not require access to the tool itself to measure the tool conditions, signals that indicate the tool condition can be gathered in real time, while the machine is running. However, despite the benefits of on-line measurement, indirect methods also have some disadvantages. Since the information (or signals) collected by indirect sensors does not contain direct measurements of the tool conditions, additional systems are required to correlate the indirect measurements with its tool condition. Additionally, indirect measurements are weakened by noise factors associated with the machining process. Noise factors tend to weaken or totally eliminate relationships between the indirect information and actual tool conditions. Many studies have sought to correlate indirect measurements with actual tool conditions using statistical regression techniques [14], fuzzy logic [1], artificial neural networks [15, 16, 17, 18, 19], and fuzzy-neural networks [10, 20]. In many of the

studies, the relationships between indirect signals and tool condition were weak because unknown factors and noise factors diluted the signals collected by the indirect sensors during machining.

Some studies attempted to eliminate or minimize noise factors from the signals collected by indirect sensors. Wavelet transformation methods were used to remove noise factors from the information collected by the sensors [9, 21]. These studies showed that a wavelet transformation process can increase the correlation between the reduced-noise signals and tool conditions [22]. However, these studies still did not show the relationship between the signal components, which were treated as noise factors, and tool conditions.

A limited number of sensors have been adopted in most studies involving indirect sensing systems. The most widely used indirect sensor is the dynamometer [6, 10, 23], which is not practical because of its high cost and lack of overload protection. The acoustic emission (AE) sensor is another sensing technology that has been used in a number of studies [24, 25], but it is also limited in its application due to its noise integrity. Some studies adopted multi-sensor techniques to improve tool-condition monitoring systems [26, 27, 28]. By combining multiple sensing technologies, these studies sought to develop more robust on-line TCM systems.

Experimental Setup

From the review of the past TCM studies, two cost-effective sensor technologies, tri-axial accelerometer and acoustic emission sensor, were employed in this study to detect multiple-direction vibrations and the energy generated from the interaction of tool and workpiece. The accelerometer was mounted under the shank holding the cutting tool with the AE sensor mounted under the work piece. The signals detected by the accelerometer were amplified and transferred to an A/D converter with the signals from the AE sensor, simultaneously. The signals were stored to a computer by a data-acquisition program (DaqView™ by IOtech), which was also utilized to analyze the data. Carbide insert tools (CNMG-432) with variable tool-wear amounts were mounted in a CNC lathe to cut aluminum alloy work pieces (AL 6061). Figure 1 shows the illustration of the experimental setup.

Experimental Design

The goal of this study was to develop a tool-condition monitoring system using three machining parameters (spindle speed, feed rate, and depth of cut) and the signals detected by the two sensors. To conduct the experiment, an experi-

mental design was established. A full factorial design was

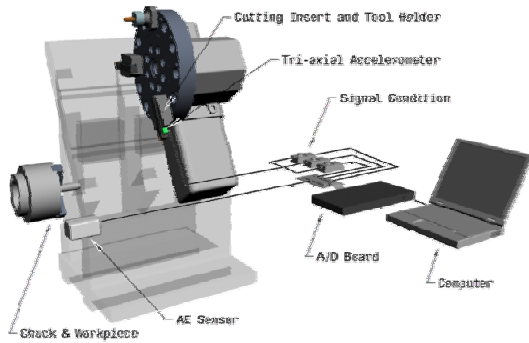


Figure 1. Experimental setup

utilized for this experiment in order to examine the full range of independent parameter combinations. A multilayered perceptron ANN model with a back-propagation learning algorithm was deployed based on the independent variables for input neurons. The independent variables utilized in this study were: 3 spindle speeds (SP), 3 feed rates (FR), 3 depths of cut (DC), and signals captured during machining (S_i). Three insert tools with different amounts of flank wear (0.010714 inch, 0.017857 inch, and 0.019643 inch) were measured under a microscope before the machining process began. The measured values were used as the outcome of the developed TCM system.

To test the flexibility of the newly developed TCM system, additional sets of machining parameters and conditions were employed. These sets includes additional values for spindle speed, feed rate, depth of cut, and tool conditions (0.007143 inch and 0.014285 inch), which are not used in the analysis and system development. After the experimental design, each cutting condition—including cutting conditions from the flexible data set—were randomly reorganized before the machining was performed in order to eliminate any systemic integration from the cutting conditions. Table 1a shows the training data set employed in this study and Table 1b shows the flexible data set employed in this study.

TCM System Development

Signal Decomposition Process

A total of 270 data sets containing raw signals were obtained from the experiment. Since the traditional time-domain analysis does not provide a clear method for analyzing raw signal data due to the randomness of each of the data points, numerous sets of conditions were tested. Among the many characteristics, the adjusted mean values of each membrane were employed to represent responses of sensors

Table 1. Experimental Design

SP		500			1,000			1,500		
FR	DC	.01	.02	.03	.01	.02	.03	.01	.02	.03
.01		S ₀₁	S ₀₂	S ₀₃	S ₁₀	S ₁₁	S ₁₂	S ₁₉	S ₂₀	S ₂₁
.02		S ₀₄	S ₀₅	S ₀₆	S ₁₃	S ₁₄	S ₁₅	S ₂₂	S ₂₃	S ₂₄
.03		S ₀₇	S ₀₈	S ₀₉	S ₁₆	S ₁₇	S ₁₈	S ₂₅	S ₂₆	S ₂₇
SP		625		825						
FR	DC	.015	.025	.015	.025					
.015		S ₂₈	S ₂₉	S ₃₂	S ₃₃					
.025		S ₃₀	S ₃₁	S ₃₄	S ₃₅					

to each of the machining conditions, including machining parameters and tool conditions. However, the raw signal data restrain other machining effects including the effects of machining parameters and machining environments. Therefore, it is necessary to reduce the raw signals into multiple components and adopt only the significant components for development of the TCM system.

Among a number of signal-processing techniques, Daubechies wavelet was employed for its fairly quick calculation results and simple programming structure under Matlab and its Wavelet Toolbox environment. In this study, a D4 wavelet program was developed. In the past, wavelet transformation methodology has been used to eliminate the noise factors. In this study, however, components of noise factors and significant responses to tool condition are indistinguishable. In order to find the most significant component of tool condition, a series of statistical data analyses were performed. Figure 2 shows an example of the reduction process. Table 2 shows the statistical analysis results of the components of each signal. The analysis results show that component 6 (C6) of the x, y, and z direction vibrations and the original raw signal of the AE sensor show stronger relationships to tool condition than the others. This indicates that by utilizing the raw signal of the AE sensor and the 6th component of the vibration signal, obtained by wavelet reduction of the raw vibration signals, a more accurate TCM system can be created.

ANNs Structural Developments

Artificial neural networks provide an artificial means of making some of the same kinds of decisions that a highly skilled machine operator would make before, during, or after the machining process [17]. Human operators learn to make accurate judgments of tool conditions based on relationships

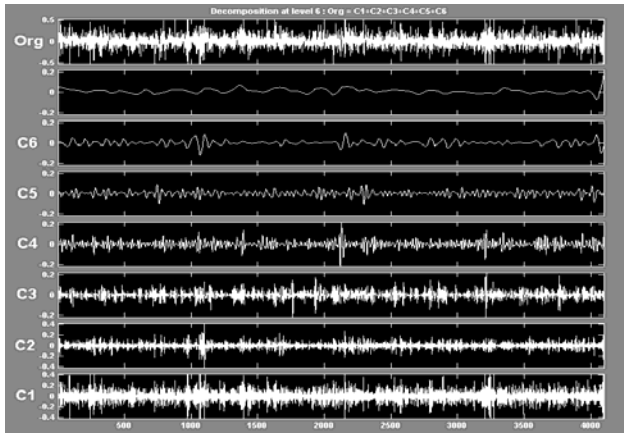


Figure 2. Example of signal reduction by wavelet transformation

Table 2. Correlation factors of tool wear and signal

Signal	Org	Cmp1	Cmp2	Cmp3	Cmp4	Cmp5	Cmp6
X	.0415	.0007	.0368	.0793	.2660	.2413	.5369
Y	.0958	.0136	.0266	.0288	.0727	.0753	.3618
Z	.0030	.0199	.0431	.0577	.1929	.2002	.5134
W	.1214	.0874	.0864	.0595	.0792	.0306	.0427

X: x-direction vibration, Y: y-direction vibration, Z: z-direction vibration, W: AE signal, Org: original signal, Com1 – 6: signal components

observed during the machining process. As human operators gain experience, their sensitivity to these relationships increases. More recent experience reinforces or adjusts the patterns developed from prior experience. ANNs work in a similar fashion, continually training themselves to accurately judge tool conditions. By adjusting the weights among neural-network nodes until the number of test errors falls to an acceptable level, the nonlinear relationships among the factors and tool condition are updated and tested.

Determining the network's structure (the number of hidden layers and nodes of each layer) that performs best is one of the biggest challenges in the process of developing ANNs. Many machining-tool studies tested only a limited number of cases by trial-and-error in order to determine the appropriate structure [15, 26]. Investigating a limited number of cases of the ANN structure often leads to a low probability of obtaining the best-performing system with the available data. In addition, in a trial-and-error methodology, the researcher has to spend a great amount of time modifying the ANNs structure, including the numbers of hidden layers and nodes; and, each structure must be trained until the test results are valid. As a result, this method requires a great deal of time in order to optimize the network training time and output results [29].

A novel method for finding the optimized ANN structure for tool-condition monitoring is proposed in this study. In order to avoid the problems of the traditional manual method (inefficient, time consuming, and potential inaccuracy) to build the ANN structure, a computer-assisted ANN-structure search methodology was employed. The proposed methodology tests all possible structures with a simplified learning process (quick-propagation) and short-training iteration, providing fitness scores for each structure to allow focus on a limited number of structures with higher scores and higher possibilities of accurate explanation of the outcome. The following is a discussion of the process of ANN-structure construction and selection.

For the input layer of an ANN-based TCM system, three machining parameters (spindle speed, feed rate, and depth of cut), three accelerometer signals (three direction vibrations), and acoustic emission (AE) sensor signals were employed. The output layer has one node (the amount of flank wear of the tool used in each cutting condition). For the accelerometer and AE signals, the best signal components of each signal were utilized since they exhibited a closer relationship with tool conditions than raw signals. In order to utilize the data in ANNs training, a preprocessing of the data is required to give equal initial weights for the input layer. All input layer node data (machining conditions and sensor signals) were transformed into the range between -1 and 1, and the output node (the amount of flank wear) was transformed into the range between 0 and 1 (normalization).

After the preprocessing, the best-performing ANN structure was determined using a computer-assisted neural-networks-structure search method. This methodology verifies the performance of all possible structures systematically, based on the criteria of interest. In this study, the number of hidden layers was limited to one and two (both cases were tested), and the number of nodes per hidden layer was limited to thirty, due to the limitations in available computing power. Therefore, the number of possible structures for the ANN system is 930. Each of these possible structures was tested and scored based on its fitness to the tool conditions. During the test, a simplified learning algorithm (quick-propagation) was utilized to shorten the learning time with a limited number of iterations. Table 3 shows the top 25 ANN structures selected by the process, based on the fitness scores of each. The results show that the structure with two hidden layers had a better performance fitness compared with the single hidden-layer structure. An irregular relationship between the degree of fitness and the structure of ANN systems (the number of nodes in each hidden layer) was also observed. From the test results, the top 22 structures (all with a fitness score of 400 or more) were studied further to determine the best fit for the TCM system.

Table 3. Summary of the top 25 ANN structures

ID	Architecture*	Number of weight	Fitness score	Train error
236	7-14-8-1	409	448.703	0.00332
195	7-29-6-1	767	431.531	0.00298
101	7-19-3-1	444	427.816	0.00312
738	7-12-26-1	605	425.111	0.00344
598	7-12-21-1	535	425.080	0.00328
852	7-14-30-1	761	423.547	0.00323
242	7-20-8-1	577	422.291	0.00336
327	7-21-11-1	674	421.018	0.00325
851	7-13-30-1	711	418.271	0.00338
351	7-17-12-1	569	411.719	0.00342
138	7-28-4-1	681	411.177	0.00300
272	7-22-9-1	657	410.725	0.00348
739	7-13-26-1	651	405.973	0.00359
239	7-17-8-1	493	404.659	0.00318
111	7-29-3-1	674	404.409	0.00345
189	7-23-6-1	611	402.797	0.00368
269	7-19-9-1	570	401.746	0.00376
150	7-12-5-1	311	401.460	0.00347
271	7-21-9-1	628	401.443	0.00326
245	7-23-8-1	661	401.366	0.00318
580	7-22-20-1	921	401.267	0.00345
267	7-17-9-1	512	401.249	0.00341
737	7-11-26-1	559	399.767	0.00366
222	7-28-7-1	771	396.488	0.00340
214	7-20-7-1	555	394.358	0.00324

* Input Layer – Hidden Layer 1 – Hidden Layer 2 – Output Layer

A new series of neural-networks training was performed with the top 22 ANN structures. A total of 405 data sets were used as training data, including three spindle speeds, feed rates, and depths of cut, with five tool conditions. A back-propagation learning algorithm was utilized as the network learning algorithm for an in-depth learning process. Learning rates and momentum values for each neural network were arranged by the negotiation of the speed of convergence and the prevention of divergence during the training. The number of iterations for training was set at 50,000 and each structure was run four times. This setup routine helped to ensure that the learning results avoid a local solution, which is a false response of neural networks during the process of node-weight adjustment during training.

During the training iterations, the convergence of the system was checked by monitoring the system training error, error improvement, and error distribution. Figure 3 shows an example of training and its monitoring process. The test results show the successful convergence of all 22 network systems with high R-squared scores, which indicates fitting level between the neural-networks outcomes and the expected outcomes. The score range was between 0.831101 (networks ID: 150) and 0.996173 (networks ID: 245), which indicated that the tool conditions used in the training procedures can be explained by the input variables up to 99.61%. However, the results could be from the learning characteristic of neural networks and does not always indicate the prediction capability of the network structures. Therefore, the prediction capability of the networks' structures was tested with the test data set, which was not used in the process of training. The 22 network systems were able to explain the test data set with an accuracy range between 73.65% (network 150) and 87.78% (network 245). From its higher accuracy, network 245 (7-23-8-1) was nominated as the best

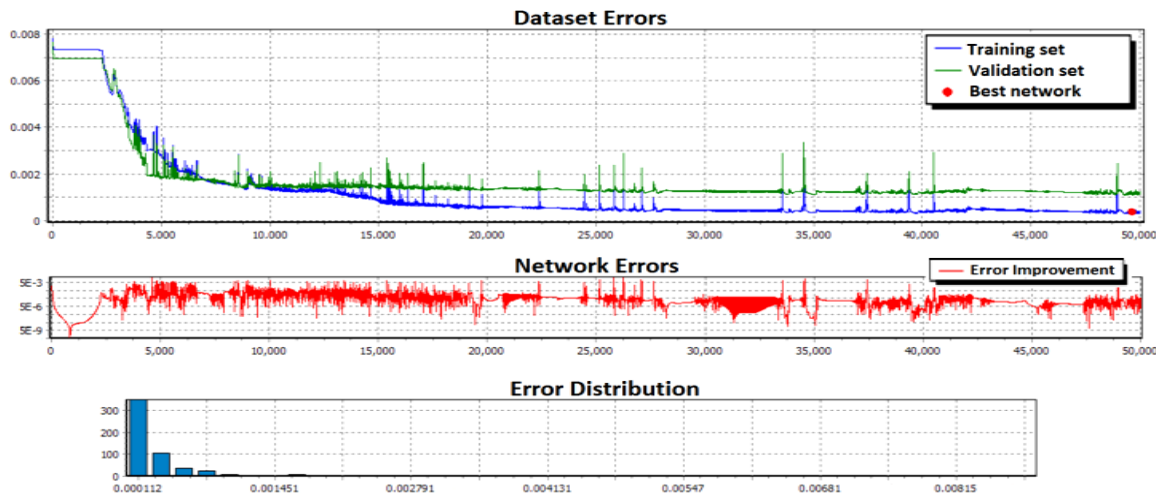


Figure 3. Summary of the training results of network 245 (Correlation: 0.99813, Training time: 0:50:50)

Results and Conclusion

With the selected ANN structure, a test was performed based on the criterion of detecting the rejecting tool condition (0.00787 inch [0.2 mm] or bigger), which could practically be adopted as a “STOP-GO” tool in the real manufacturing environment. The developed ANN-based TCM system successfully predicted 146 tests out of a total of 151. From the 62 “sharp tool” tests, five samples were predicted as a “worn tool” (Type II error). Within the 89 “worn tool” tests, zero samples were predicted as a “sharp tool” (Type I error). Overall, the developed ANN-based prediction model can identify the tool condition with 97% accuracy.

In subsequent studies, enlarging the number of machining parameters, tool conditions, types of insert tool, and different work-piece materials is recommended for more variable machining conditions. Increased numbers of hidden layers and nodes of ANN systems is also recommended with higher computational power.

References

- [1] Ming, L., Xiaohong, Y., & Shuzi, Y. Tool wear length estimation with a self-learning fuzzy inference algorithm in finish milling. *International Journal of Advanced Manufacturing Technology*, 15, 1999, pp. 537-545.
- [2] Willow, C. A feedforward multi-layer neural network for machine cell information in computer integrated manufacturing. *Journal of Intelligent Manufacturing*, 13, 2002, pp. 75-87.
- [3] Singh, N. *Systems Approach to Computer-Integrated Design and Manufacturing*. New York: Wiley, 1996.
- [4] Venkatesh, K., Zhou, M., & Caudill, R.J. Design of artificial neural networks for tool wear monitoring. *Journal of Intelligent Manufacturing*, 8(3), 1997, pp. 215-226.
- [5] Li, X., Dong, S., & Venuvinod, P.K. Hybrid learning for tool wear monitoring. *International Journal of Advanced Manufacturing Technology*, 16, 2000, pp. 303-307.
- [6] Lee, J.H., Kim, D.E., & Lee, S.J. Statistical analysis of cutting force ratios for flank-wear monitoring. *Journal of Materials Processing Technology*, 74, 1998, pp. 104-114.
- [7] Taylor, F.W. On the art of cutting metals. *Transactions of the ASME*, 28, 1906, pp. 31-35.
- [8] Kattan, I.A., & Currie, K.R. Developing new trends of cutting tool geometry. *Journal of Materials Processing Technology*, 61, 1996, pp. 231-237.
- [9] Xiaoli, L., & Zhejun, Y. Tool wear monitoring with wavelet packet transform – fuzzy clustering method. *Wear*, 219, 1998, pp. 145-154.
- [10] Chen, J. An effective fuzzy-nets training scheme for monitoring tool breakage. *Journal of Intelligent Manufacturing*, 11, 2000, pp. 85-101.
- [11] Kumar, S., Nassehi, A., Newman S.T., Allen, R.D., & Tiwari, M.K. Process control in CNC manufacturing for discrete component: A STEP-NC compliant framework. *Robotics and Computer-Integrated Manufacturing*, 23(6), 2007, pp. 667-676.
- [12] Oliveira, J., Ferraz, F., Jr., Coelho, R.T., & Silva, E.J. Architecture for machining process and production monitoring based in open computer numerical control, *Proceedings of Institution of Mechanical Engineers, Part B: Journal of Engineering Manufacture*, 222(12), 2008, pp. 1605-1612.
- [13] Bradley, C., & Wong, Y.S. Surface texture indicators of tool wear – a machine vision approach. *International Journal of Advanced Manufacturing Technology*, 17, 2001, pp. 435-443.
- [14] Choudhury, S.K., & Kishore, K.K. Tool wear measurement in turning using force ratio. *International Journal of Machine Tools & Manufacture*, 40, 2000, pp. 899-909.
- [15] Chen, J.C. & Chen, J.C. An artificial-neural-networks-based in-process tool wear prediction system in milling operations with a dynamometer. *International Journal of Advanced Manufacturing Technology*, 25(5-6), 2002, pp. 427-434.
- [16] Chen, S.L., & Jen, Y.W. Data fusion neural network for tool condition monitoring in CNC milling machining. *International Journal of Machine Tools & Manufacture*, 40, 2000, pp. 381-400.
- [17] Masory, O. Detection of tool wear using multisensor readings defused by artificial neural network. In S.K. Rogers (Ed.), *Proceedings of SPIE: Vol. 1469. Applications of Artificial Neural Networks II*, 1991, pp. 515-525.
- [18] Özel, T., & Nadgir, A. Prediction of flank wear by using back propagation neural network modeling when cutting hardened H-13 steel with chamfered and honed CBN tools, *International Journal of Machine Tools & Manufacture*, 42, 2002, pp. 287-297.
- [19] Park, K.S., & Kim, S.H. Artificial intelligence approaches to determination of CNC machining parameters in manufacturing: a review. *Artificial Intelligence in Engineering*, 12, 1998, pp. 127-134.
- [20] Balazinski, M., Czogala, E., Jemielniak, K., & Leski, J. Tool condition monitoring using artificial intelligence methods. *Engineering Applications of Artificial Intelligence*, 15, 2002, pp. 73-80.
- [21] Al-Habaibeh, A., & Gindy, N. Self-learning algorithm for automated design of condition monitoring systems

for milling operations. *International Journal of Advanced Manufacturing Technology*, 18, 2001, pp. 448-459.

- [22] Wu, Y., & Du, R. Feature extraction and assessment using wavelet packet for monitoring of machining process. *Mechanical Systems and Signal Processing*, 10(1), 1996, pp. 29-53.
- [23] Ertune, H.M., & Loparo, K.A. A decision fusion algorithm for tool wear condition monitoring in drilling. *International Journal of Machine Tools & Manufacture*, 41, 2001, pp. 1347-1362.
- [24] Li, X. A brief review: acoustic emission method for tool wear monitoring during turning. *International Journal of Machine Tools & Manufacture*, 42, 2002, pp. 157-165.
- [25] Liang, S.Y., & Dornfeld, D.A. Tool wear detection using time series analysis of acoustic emission. *Journal of Engineering for Industry*, 111, 1989, pp. 199-205.
- [26] Dimla, D.E., Jr., Lister, P.M., & Leighton, N.J. Automatic tool state identification in a metal turning operation using MLP neural networks and multivariate process parameters. *International Journal of Machine Tools & Manufacture*, 38(4), 1998, pp. 343-352.
- [27] O'Donnell, G., Young, P., Kelly, K., & Byrne, G. Toward The improvement of tool condition monitoring systems in the manufacturing environment. *Journal of Materials Processing Technology*, 119, 2001, pp. 133-139.
- [28] Schefer, C., & Heyns, P.S. Wear monitoring in turning operations using vibration and strain measurements. *Mechanical Systems and Signal Processing*, 15(6), 2001, pp. 1185-1202.
- [29] Dimla, D.E., Sr. Application of perceptron neural networks to tool-state classification in a metal-turning operation. *Engineering Applications of Artificial Intelligence*, 12, 1999, pp. 471-477.

Design, and Geometric Dimensioning & Tolerancing. Dr. Lee may be reached at samson.lee@cmich.edu

Biographies

SAMSON S. LEE received the B.S. degree in Naval Architecture and Ocean Engineering from Inha University, Incheon, Korea, in 1996, the M.S. and Ph.D. degree in Industrial Education and Technology from Iowa State University, Ames, Iowa, in 1999 and 2006, respectively. Currently, he is an Assistant Professor of Engineering and Technology at Central Michigan University. His research involves CNC machines, sensor technologies, signal processing, and artificial neural-networks. His teaching includes Engineering Graphics, Computer Aided Design and Analysis, Computer Aided Manufacturing, Computer Numerical Control, Tool

A PROCESS FOR SYNTHESIZING BANDLIMITED CHAOTIC WAVEFORMS FOR DIGITAL SIGNAL TRANSMISSION

Chance M. Glenn, Sr., Rochester Institute of Technology

Abstract

In the development of a chaotic oscillator technology to produce high-quality communication signals, the authors found a novel method for limiting the out-of-band spectral power from chaotic oscillators. This development is an important breakthrough that has allowed the authors to make a major step toward a commercially viable technology.

Introduction

In a practical wireless communication system, the signal transmitted from the antenna must be limited to a finite range of frequencies. Such signals are known as *bandlimited* signals; or, if the range of frequencies does not include dc—where the frequency equals 0 Hz—they are called *passband* signals. Typically, passband signals are bandlimited signals that occupy a small percentage of bandwidth about a center or carrier frequency. Multiple signals can then be transmitted by using passbands that do not overlap, then separating the signals at the receivers by filtering all but the passband of interest. This method of sending multiple signals, known as frequency-division multiplexing, is the basis for many multiple-user systems in use today. When many users can access a system on either a fixed- or flexible-frequency division plan, the method is known as frequency-division multiple access. Although some methods such as code division multiple access, or CDMA, do not rely upon frequency division for signal separation, the signals are still limited to a passband defined by the Federal Communications Commission (FCC) [1].

If the signals generated by chaotic systems are to be used in commercially viable systems, the transmitted signal must be bandlimited in some way. One obvious and often-used way to do this is to generate a signal that has considerable out-of-band spectral power, and then filter the signal to remove most of the power that lies outside of the desired frequency band. This method is, however, costly in many ways. Filters that effectively remove out-of-band energy, while passing the signal in-band with minimal distortion, are expensive and generally have a large footprint. The power outside of the band is also wasted, and must be dissipated as

heat. This wasted power translates into increased transmitter power requirements and faster battery drain.

In this study, development efforts to produce a commercially viable chaotic oscillator technology yielded a particularly simple and effective way to limit the out-of-band radiation from a chaotic oscillator. This method caused the oscillator itself to produce a signal with bandwidth-constrained signal power and, thus, there was no need for a filter or waste of power. In doing so, the authors applied a principle that may be used for more general signal shaping or spectral shaping.

The idea behind this bandlimited-chaotic-oscillation (BCO) synthesis method was based on the segment-hopping method of oscillator control [2]. In segment hopping, a digital source produces an analog waveform that is used to guide the transmit oscillator. The guide signal is an analog copy of a signal that could be produced by the transmit oscillator itself, except that it follows a pre-defined symbol sequence that contains the digital information being transmitted. In this scheme, the transmit oscillator is acting as an amplifier for the guide signal, because the output of the transmitter can be much higher in power than the power drawn from the guide source.

Synthesis and Analysis

A prototypical chaotic oscillator used to produce signals useful for digital communication is the Lorenz system [3]. It was the oscillator first used by Hayes [4] to introduce the notion of controlling symbolic dynamics, a process to encode digital information in the oscillations of a chaotic system. The Lorenz system is described by a three-dimensional system of equations having the form:

$$\begin{aligned}\dot{x} &= \sigma y - \alpha x \\ \dot{y} &= \rho x - y - xz \\ \dot{z} &= xy - \beta z\end{aligned}\tag{1}$$

where s , r and b are parameters that Lorenz originally set to 10, 28, and 8/3, respectively. The state-space attractor

defined by these equations takes on a double-lobed structure, which lends itself nicely to a binary-symbol partition. Figure 1 is an example of a two-dimensional projection of the solutions of the Lorenz equations, showing state-variables x and y . Two Poincaré surfaces are placed in positions piercing the focal points and extending outward beyond the boundaries of attractor.

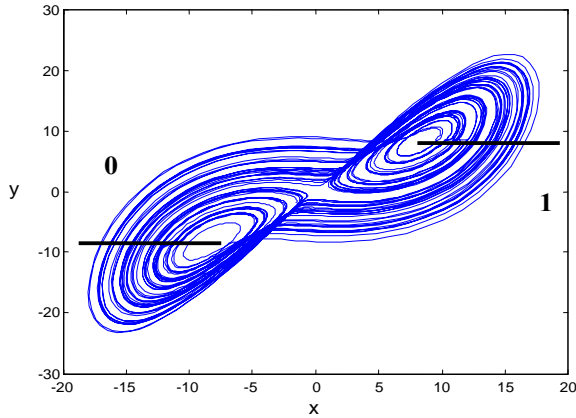


Figure 1. Two-dimensional projection of the solutions to the Lorenz equations showing state coordinates x and y and the binary partitioning of the state-space

The time-varying state-variable, $x(t)$, is a bipolar waveform well-suited for baseband transmission of digital information. Figure 2 is an example of the waveform in its generalized time coordinates, and Figure 3 is a plot of the frequency content of this signal with respect to its average cycle frequency. The average cycle frequency is the reciprocal of the average cycle time. The cycle time is defined as the time it takes a point on the attractor to travel from one Poincaré surface to the other, or back to itself. The average cycle time is the mean time, in seconds, calculated by integrating the system with a fixed integration step and collecting thousands of surface crossings. T_{avg} was found to be about 1.7 seconds, with a variance of about 1.8 seconds.

Figure 4 is a block diagram of the implementation of a bandlimited chaotic signal source. A binary sequence is fed into a discrete-time, bandlimited, segment-hopping source. This source will be described in the next section. The output signal, $y[n;t]$, is a sampled waveform used as a guide signal to synchronize a continuous-time Lorenz oscillator to it. A single state-variable synchronization method is used to lock the oscillator to the dynamics and, thus, to the embedded digital sequence of the guide signal.

Since Pecora and Carroll first introduced the concept of synchronization of chaotic oscillator circuits [5], many methods have been developed and realized.

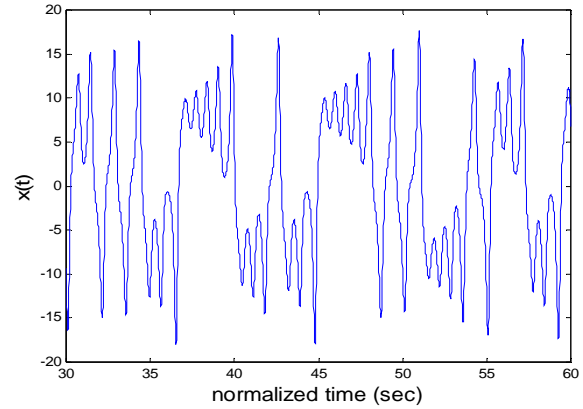


Figure 2. Time-dependent solution of the Lorenz equations for state coordinate $x(t)$

The following mathematical model works extremely well:

$$\begin{aligned} \dot{x} &= \sigma y - \alpha x \\ \dot{y} &= \rho x - y - xz + (y[n;t] - y)R \\ \dot{z} &= xy - \beta z \end{aligned} \quad (2)$$

Here, R is a coupling factor. This method works well from the standpoint of simplicity and ultimately from a circuit-realization perspective. There have been circuit realizations proposed for the Lorenz equations [6]. In such circuits this coupling method is simply a resistive feed of a voltage across, or current into, a single arm.

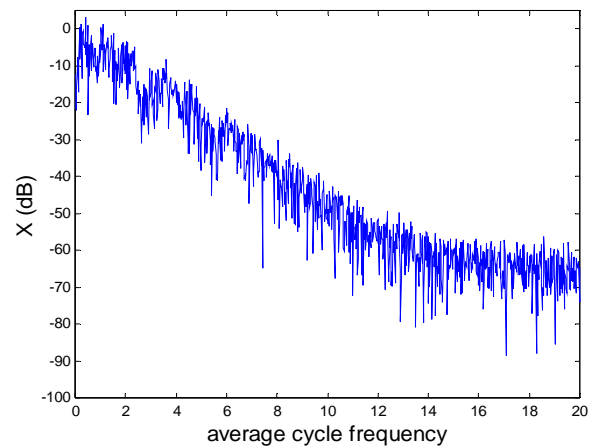


Figure 3. Frequency content of the state coordinate $x(t)$ with respect to the average cycle frequency

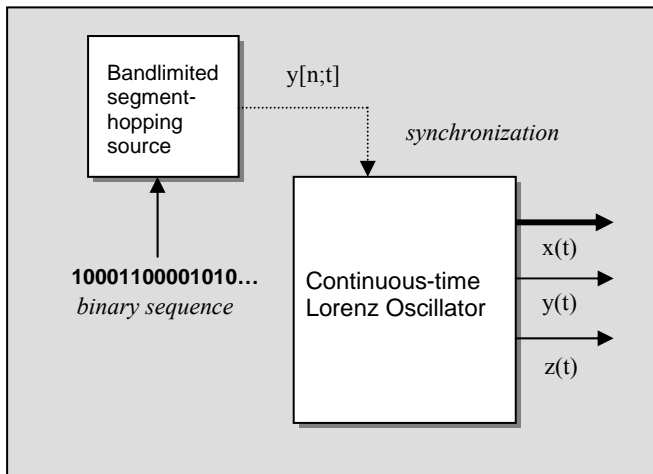


Figure 4. Block diagram of the implementation of a bandlimited digital signal synthesizer

Segment Hopping

Refer to the synthesis of the guide signal, $y[n;t]$. Two new concepts are introduced here.

1. Continuous, digitally-encoded chaos waveforms can be generated by piecing together the proper signal segments.
2. These segments can be bandlimited prior to storage, and can impress their characteristics upon a continuous-time oscillator via synchronization.

The sequencing of stored segments in memory in some pre-defined order is commonly used in arbitrary waveform synthesis. What is new and not obvious about segment hopping is that an arbitrary controlled *trajectory* of a deterministic dynamic system can be generated, even though the system produces continuous and non-repeating trajectories in state space under the action of deterministic differential equations. Furthermore, this signal can be made to carry an arbitrary sequence of digital symbols representing encoded data. Thus, the difference between this method and arbitrary waveform synthesis is that this method allows for the production of a signal carrying arbitrary data that appears to have been produced by the action of differential equations. This is achieved by putting out segments that follow the desired symbol sequence, while satisfying the grammar of the oscillator. The theoretical basis for this method of signal synthesis is the idea from ergodic theory that chaos can be approximated to an arbitrary degree of accuracy by completely deterministic mappings in state space intermediated by completely random choices [7].

For example, in an 8-bit encoding there are 256 signal pieces, or segments, that can be put together to form any desired binary-symbol sequence. The segments are assigned numbers from 0 to 255 according to the bit sequence they initiate. In a physical implementation, a segment-hopping system can be stored in a static memory device such as a ROM or EPROM and clocked out according to the input bit-sequence. A more detailed description of the segment-hopping process will be published shortly. In the following section, the authors consider a complete computer model of the BCO synthesis method.

Computer Model Results

The first, important step was to determine the amount of bandlimiting that can be achieved. Any amount of filtering will cause some distortion to the waveforms. It was then important that the binary encoding remain preserved, and that the guide signal remain capable of synchronizing the continuous-time oscillator. Given the determination of the average cycle time, T_{avg} , as stated earlier, a smooth, low-pass filter was applied to the Lorenz oscillations having a cutoff-frequency of twice the average bit rate. With the filtering applied, segments were stored that source the appropriate 8-bit symbol sequences. Figures 5 and 6 show the filter characteristics and the response of the frequency spectra and the resultant attractor.

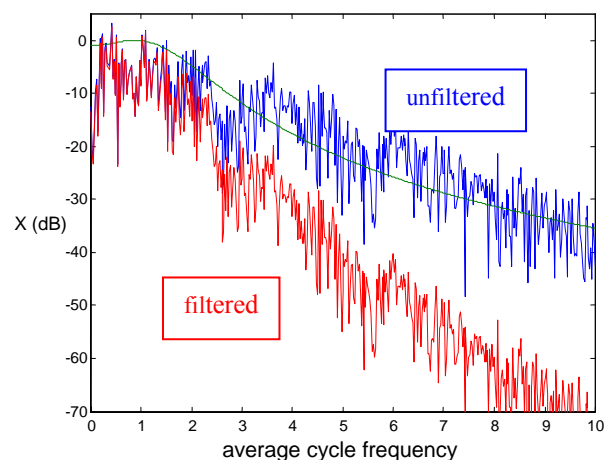


Figure 5. The result of the low-pass filtering of the state variable of $x(t)$

The filtering was applied to all three state coordinates in order to produce a new attractor. It was with this new attractor that the symbolic dynamics of the system were determined and the associated segments produced.

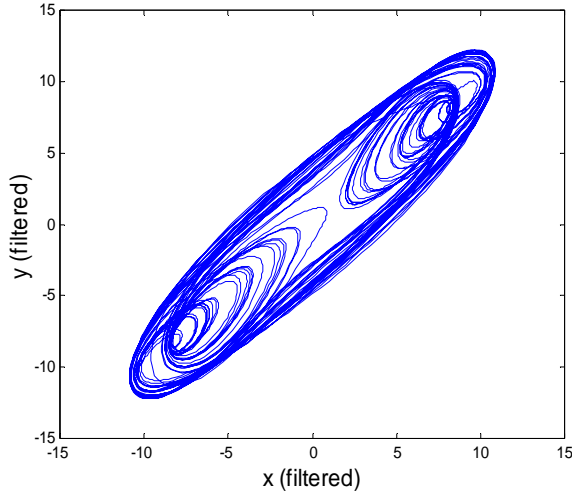


Figure 6. Two-dimensional projection of a filtered Lorenz oscillation using the low-pass filter characteristic shown by its effect on the spectrum in Figure 5

Even though only one state-coordinate was used as a guide signal, namely y , the entire attractor had to be transformed in order to synthesize the segments needed for segment-hopping control.

In the following example, the binary sequence was encoded and transmitted as

$$B = 11001101100010101111000110101100011$$

Figure 7 shows what the desired output waveform, $x(t)$, would be for a typical Lorenz oscillator. Given the bandlimited segments, the guide signal, $y[n]$, could be synthesized. Figure 8 is a plot of the frequency spectrum of the original, unfiltered transmit signal, $x(t)$, the result of which was filtered using the low-pass filter described earlier, and the frequency spectrum of the new transmit signal from the BCO synthesis method.

Note the dramatic reduction in frequency content. Particularly, there was nearly a 20 dB reduction at 3.5 times the cycle frequency and a 30 dB reduction at 6 times the cycle frequency. Earlier it was stated that it is important that binary encoding remain preserved and that the synthesized BCO guide signal be capable of synchronizing a Lorenz oscillator to it. This is demonstrated in Figures 9 and 10.

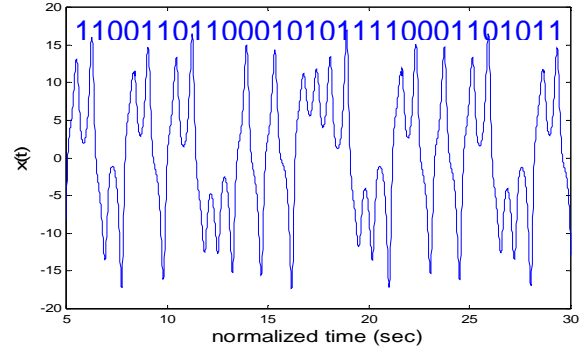


Figure 7. Typical Lorenz oscillation producing the binary sequence:

$$B = 11001101100010101111000110101100011$$

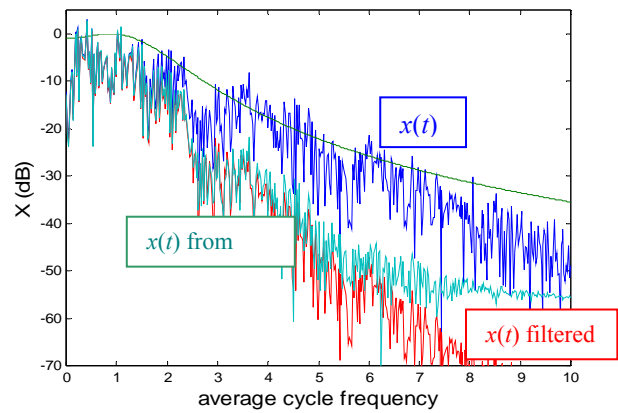


Figure 8. Frequency spectra of $x(t)$ from the Lorenz equations, a filtered version, and the output of a BCO system

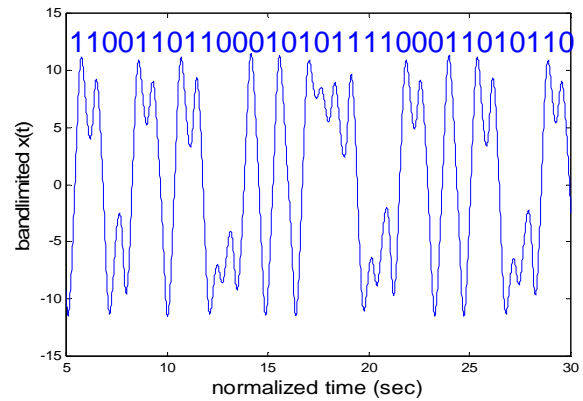


Figure 9. BCO-synthesized transmit signal with the binary encoding preserved

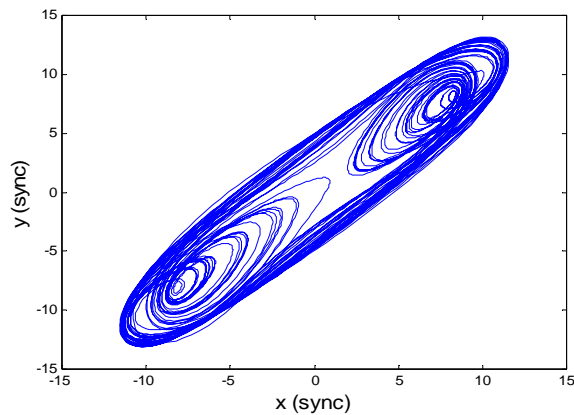


Figure 10. BCO-synthesized attractor projection

What was remarkable was how “flexible” the Lorenz oscillator can be. This was an important realization not only for this work but for synthesizing signals even more compatible with traditional communication signal formats and standards. It was demonstrated in the lab in prototypes that physical chaotic oscillators can be made to produce signals that have constant-timing intervals between Poincaré surface crossings by simply synchronizing them to an artificially-synthesized waveform having those properties. This timing regularization is of utmost importance for use in commercially-viable communication systems because it makes accurate clock-timing recovery possible. Combined with bandwidth compression, as outlined here, this solved some of the most critical technological problems for using chaotic oscillators in commercial systems.

Conclusion

What was described here in a simple example was an enabling technology. In order to use chaotic systems and processes in commercial digital communication systems, the waveforms must be restricted in bandwidth in a controllable way. The focus must shift to the *design* of waveforms and sources, and away from the use of existing, easily-constructed oscillators.

The BCO synthesis technique in this study demonstrated a simple, efficient and effective way to generate baseband signals for wireless communication. Some chaotic oscillators, such as the Colpitt’s circuit [8] and the double-scroll oscillator [9], produce signals with very different characteristics. However, this technique is a general procedure applicable to a variety of chaotic oscillators.

Another area of technology development that the authors are focusing on is in the development of oscillators that are ideally suited for given communication channels. Although the Lorenz system has excellent properties for binary baseband digital signaling in white noise, there may be oscillations better suited and which can be produced with more efficient circuitry.

Since Ott, Grebogi, and Yorke’s initial formalism for controlling chaotic processes using small perturbations [10], there has been a consistent march toward development of technological applications. Arguably, the application to communications technology has held the most promise and has been the source of the most activity. Beyond simple applications is the realm of *commercially viable* applications that have characteristics that make chaotic dynamics technology attractive to the fast-moving world of the telecommunications industry. Some of the improvement areas that make chaotic dynamics technology attractive are increases in efficiency, reduction of system complexity, increases in transmission ranges and digital transmission data rates.

References

- [1] Theodore S. Rappaport, *Wireless Communications: Principles and Practice*, Prentice Hall, Inc., New Jersey, 1996.
- [2] Scott T. Hayes, Chance M. Glenn, *Synchrodyne Amplification, Phase II Final Report*, NextWave Technologies, Contract # N00014-00-C-0044, Office of Naval Research, 2000.
- [3] Edward N. Lorenz, *Deterministic Nonperiodic Flow*, Journal of the Atmospheric Sciences, vol. 20, March 1963.
- [4] S. Hayes, C. Grebogi, E. Ott, Phys. Rev. Lett. **70**, 3031 (1993).
- [5] L. M. Pecora and T. L. Carroll, *Synchronization in Chaotic Systems*, Phys. Rev. Lett. **64**, 821 (1990).
- [6] R. Tokunaga, M. Komuro, T. Matsumoto, L.O. Chua, ‘Lorenz Attractor’ From an Electrical Circuit with Uncoupled Continuous Piecewise-Linear Resistor, *International Journal of Circuit Theory and Applications*, Vol. 17, 71-85 (1989).
- [7] Athanasios Papoulis, *Probability, Random Variables, and Stochastic Processes*, 3rd ed., McGraw-Hill, Inc., New York, 1991.
- [8] Martin J. Hasler, *Electrical Circuits with Chaotic Behavior*, Proceedings of the IEEE, vol. 75, no. 8, August 1987.
- [9] T. Matsumoto, L. O. Chua, M. Komuro, *The Double Scroll*, IEEE Trans. CAS-**32**, no. 8 (1985), 797-818.
- [10] E. Ott, C. Grebogi, J. A. Yorke, Phys. Rev. Lett. **64**, 1196 (1990).

Biography

CHANCE M. GLENN, SR. is a professor in the College of Applied Science and Technology at the Rochester Institute of Technology. He is also the founder of and senior researcher at the William G. McGowan Center for Telecommunications, Innovation and Collaborative Research. He earned his B.S. (Electrical Engineering, 1991) from the University of Maryland at College Park, his M.S. (Electrical Engineering, 1995) from the Johns Hopkins University, and his Ph.D. (Electrical Engineering, 2003) from the Johns Hopkins University as well. Dr. Glenn is also the Associate Dean of Graduate Studies for RIT. Dr. Glenn began studying nonlinear dynamics and chaotic processes as a research engineer at the Army Research Laboratory then continued to develop technology from these concepts for private commercial ventures. He holds several patents and is currently developing a complete architecture for digital communications based upon chaotic dynamical systems theory. Dr. Glenn may be reached at chance.glenn@rit.edu.

EVALUATING THE ACCURACY, TIME, AND COST TRADE-OFFS AMONG ALTERNATIVE STRUCTURAL FITNESS ASSESSMENT METHODS

Michael D. Johnson, Texas A&M University; Akshay Parthasarathy, Texas A&M University

Abstract

Development project lead time and cost are of growing importance in the current global competitive environment. During the development of physical products, one key task is often the assessment of a component's structural fitness. This paper examines the trade-offs that occur among different methods of assessing structural fitness and their associated accuracy, costs, and lead times. Results show that physical prototypes require significantly more time than analytical prototypes, where only simple calculations or finite element analyses are used. Trade-offs are further illustrated using a case study, which examines the need to meet lead-time and budgetary constraints. In this case, it is shown that it can be preferable to choose a more accurate method even if it has a higher cost and lead time. The inability to escalate to a more accurate method later and still meet time and budgetary constraints can prescribe choosing a more accurate method initially, assuming that the time and budgetary penalties for that method are not too great.

Introduction

Development is the process of creating technically feasible solutions in order to meet customer needs. In today's technologically driven world, the importance of development to the success or even survival of a firm is unquestioned. The return on investment for research and development has been shown to be more effective than capital expenditure at boosting various financial metrics [1]. However, it is not sufficient that the product-development process be effective, it must also be quick. Development lead time can affect the commercial and financial success of a product [2]-[4]. Some companies even use time-to-market as a key product development metric [5]. There is a potential conflict between trying to complete a development project quickly and producing a superior, or even acceptable, product. Design iterations increase product quality, but do so at the expense of increased lead time [6].

It is often said in product-development circles that "we never have time to do it right, but we always have time to do it twice". This remark arises from the tension between the desire of technical professionals to engineer "perfect" prod-

ucts and the business reality of needing to deliver those products in an efficient and cost-effective manner. There are usually alternative methods available to determine the acceptability of a given design solution. These range from simple analytical prototypes—such as stress calculations or the use of hand books—to comprehensive physical prototypes such as creation and testing of entire products [7]. Rapidly advancing technology in computer-aided design, manufacturing, and engineering allows for several aspects of a product throughout the realization process to be analyzed virtually. The selection of alternative assessment methods through the development process dictates alternative costs and lead times. This initial selection can also affect the costs and lead times associated with alternative assessment methods used during iterations.

There has been significant research regarding both product- and project-related risks. Product risk is defined here as an unacceptable design solution – something that does not meet technical or customer requirements. Project risk is defined as the failure to conform to time and budgetary constraints. Previous research has examined the effects of iteration on cost and lead time [6], [8]-[9]. These studies did not include the tendency to escalate to more accurate assessment methods in the event of an assessment failure. Assessment failure is defined as a method signaling an acceptable design solution, when in fact the design solution is not acceptable. This would be a Type II error. If a relatively quick and inexpensive assessment method resulted in an assessment failure, it is likely that an alternative method with putative higher accuracy will be chosen next. This switching can require significant additional time and cost.

This current study will look at 1) the tradeoffs associated with these alternative methods and switching costs, 2) a summary of related work in the areas of project lead time, risk, and simulations, 3) a presentation of the methods and results of a design and test project, 4) a case study used to illustrate the usefulness of the results, and 5) the limitations and conclusions of this current study.

Related Work

Product development lead time has long been a research focus and has been examined from various perspectives.

Some of the earliest work examined the distribution of labor over the course of a development project [10]. The effects of how tasks overlap [11] and, as noted previously, iterations have been examined. Project team resources [12] and organization have also been analyzed [13]. Product complexity and newness have been shown to increase development lead time [13]-[14]. In addition to understanding the product and project factors that affect lead time, unexpected changes in schedules or resources (project risk) have also been examined.

A significant amount of research has focused on assessing and mitigating project risk, which is usually related to lead time and budget. These previous research projects attempted to reduce unexpected delays by better understanding their causes [15] or providing frameworks that recognize risks and aim to mitigate their consequences [16]-[18]. Project simulations based on previous project data were used to examine budget and risk minimization strategies [19]. In addition to project risk, there is also technical or product risk. Similar techniques were used to assess product risk, such as examining the failure of similar products in the past [20]. Risk identification and mitigation techniques were also used for product risks [21]. Prototypes were suggested as a way to reduce both product and project risk [22]. The use of computer simulations may be another way to reduce risk and possibly decrease lead time in development projects.

There have been significant advances in computer simulation over the past two decades. Some authors have predicted that computer-aided engineering will eliminate the need for prototypes [23]. However, even a prominent proponent of finite element analysis (FEA) has expressed reservations; over a decade ago, the founder of ADINA (a FEA company) expressed concerns about the growing number of designers using FEA software [24]. This was before programs such as COSMOS (SolidWorks), Mechanica (ProEngineer), and DesignSpace (ANSYS) made FEA more accessible to designers. In addition to concerns about the training and expertise of those using FEA tools, there were questions about the reliability of the numerical simulation tools themselves. The complexity of building a reliable computer prediction was noted; when empirical data is absent, there is ignorance [25]. A necessary step of producing a reliable model is the comparison of the observed physical event with the prediction of the mathematical model; this is referred to as validation [25]-[26].

Unfortunately, this validation processes can require a significant amount of time [27]. Therefore, some trade-off must be made between lead time and method accuracy; one must choose among quicker methods, validated numerical methods, or gathering empirical data. This decision will have an impact on both product and project risk. This study

presents an explicit quantitative assessment of alternative assessment methods. The relative accuracy of two analytical prototyping methods is compared to the results of a physical prototyping method. This relative accuracy is then compared to the engineering effort (in person-hours) required to produce these results.

To illustrate the impact that assessment method selection can have on product and project risk, a case study is also detailed in the next section. This case study examines three alternative methods that were used to determine if a design solution is acceptable. The case study also incorporates the role of iterations and unique assessment-method escalation. The effect of assessment method on project-related quantities, e. g., lead time and budget, is illustrated and the product and project risk associated with the methods are presented.

Exercise and Case Study

To examine the effect of alternative data gathering methods on product and project risk, a senior design project was commissioned to mechanically evaluate a simple component. A team consisting of three students designed, performed finite element analyses, manufactured, and tested the specimen. The students were asked to design a specimen that was simple enough to structurally analyze without the use of FEA and that could be machined using manual machining equipment. Three points of interest were selected to examine the mechanical behavior of the specimen when under a load. The specimen, points of interest and loading configuration are shown in Figure 1. The span of the specimen is approximately 15cm and was manufactured from 6061 aluminum. The lower portion of the specimen was assumed to be constrained, as it would be in a fixture as shown in Figure 2. The students were asked to evaluate the specimen using three methods: simple stress calculations assuming only bending, finite element analyses, and the use of strain gages on a manufactured aluminum prototype. The students were asked to keep a diary of the time that they spent performing each of the tasks throughout the project.

Initially, the component was modeled in Pro|Engineer CAD software. Once the design for the component was finalized, the students began assessing its mechanical behavior. It was decided to test the component using 3kg, 5kg, and 7kg loads. The loads would be hung from the end of the specimen to produce a bending deformation, as shown in Figure 2. Given that the component was loaded in simple bending, it was assumed that at the three locations of interest only the principal stress, as a result of bending, would be relevant. The next step was to evaluate the mechanical behavior of the specimen using the alternative methods. The first method consisted of performing a simple bending stress calculation using:

$$\left(\sigma = \frac{My}{I} \right) \quad (1)$$

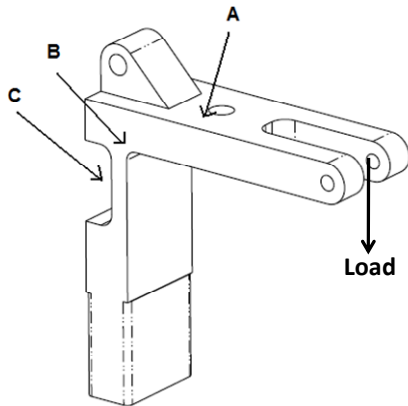


Figure 1. Diagram of specimen detailing points of interest.



Figure 2. Specimen in testing fixture

These calculations took into account the stress concentration caused by the hole at point “A” in Figure 1. Next, Pro|Mechanica—the integrated finite element program within Pro|Engineer—was used to perform the finite element analyses of the component assuming the previously mentioned loading conditions. The simulations were run and the predicted stresses at the locations of interest were tabulated. Finally, a prototype component was machined using a CNC mill. This required the generation of a numerical control program, or g-code, that was generated using the Feature-Cam program. The material was pre-cut to near net shape to minimize machining time. The prototype specimen was then instrumented with strain gages at the locations of interest and loaded in the aforementioned manner. Three samples were taken at each location for each load. These strain results were then averaged and used along with the elastic

modulus of 6061 aluminum (70 GPa) to determine the stress at the points of interest; this assumed only linear elastic bending.

For the purpose of this study, the results of the physical prototype test were assumed to be the baseline. The strain gage results were assumed to be the most representative of the physical event. Figure 3 shows the relationship between the time required to complete a given analysis and the deviation from the baseline result. Overall, the majority of the results were within 20% of the baseline. The notable exception is the finite element analysis results at location B. These results predicted stress in this location that were almost four times greater than the baseline result and the simple stress calculation. With the exception of this result, all other results were within 20% of the baseline. The majority of the results also produced what would be considered a Type I error with respect to the baseline, i.e., they predicted higher stress than the baseline. This is usually the preferred type of error in structural fitness evaluation methods as an over-engineered design is usually preferable to one that fails, though there are exceptions such as insertion or removal force for a snapfit. The only method that produced appreciable Type II errors was the simple calculation method at location B; the FEA method error at location C was less than 1%. But even this method’s 16% deviation from the baseline would be overcome with an extremely modest safety factor of 1.2. The overall trend showed that slightly more deviation resulted from methods that had a lower completion time, excluding the FEA outlier at location B.

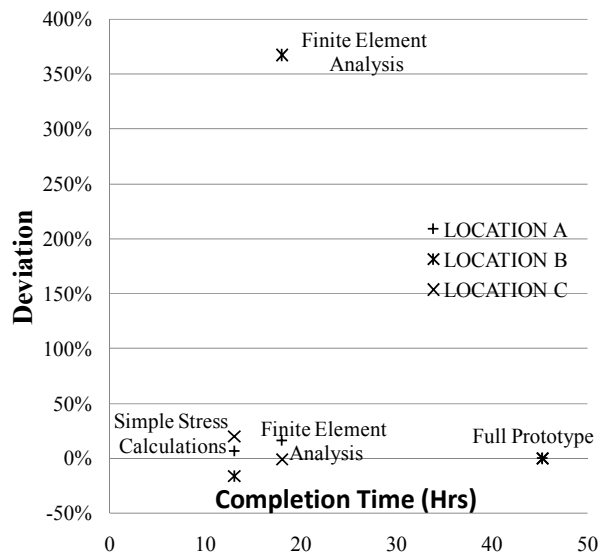


Figure 3. Deviation of stress results from those of a full prototype as compared with a full prototype tested at three locations and compared to test data gather time (hrs).

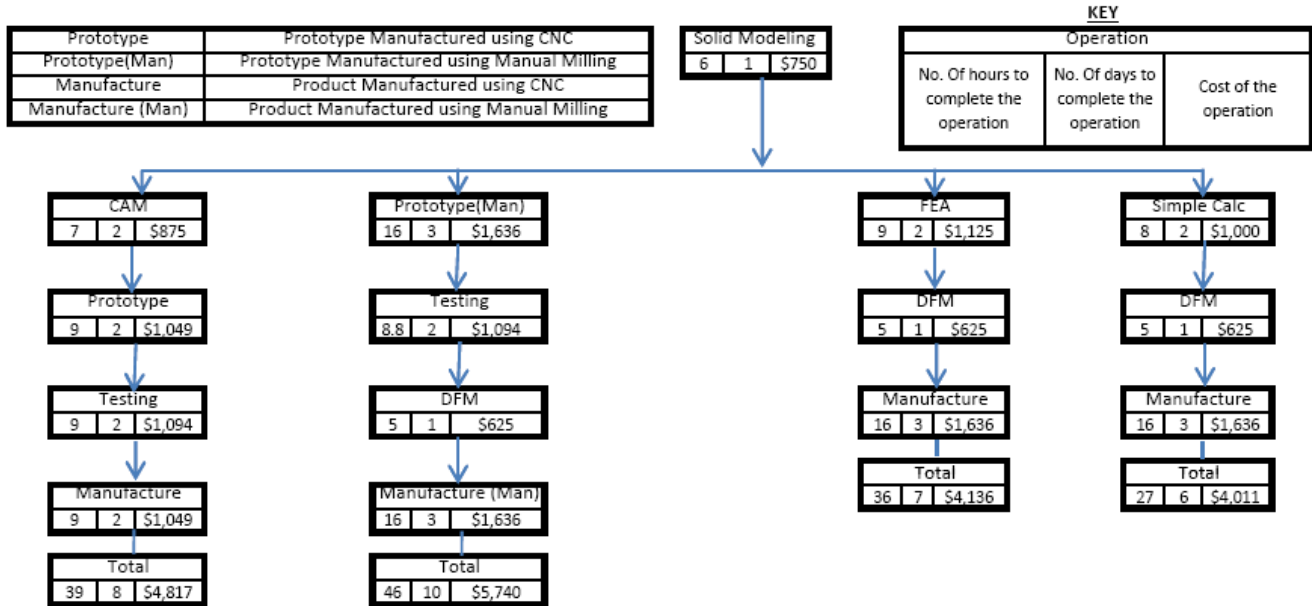


Figure 4. Process flow for alternative data gathering and manufacturing methods for the component.

While in this case the lower time-investment assessment methods produced results that compared well with the baseline, that may not always be the case. As such, the effect of product risk on project risk was still evaluated. For purposes of this project, it was assumed that the initial design would be evaluated for mechanical behavior—as detailed above—then manufactured and delivered for installation. If the component met the structural requirements as expected, the project was deemed complete. If it failed, a component that met the structural requirements had to be redesigned and delivered at no additional charge. The budget and lead time for the project were \$7500 and three weeks—15 business days, respectively.

Figure 4 shows the process plan for alternative methods of evaluating and delivering an acceptable component. All methods begin with design selection and solid modeling. The three mechanical behavior methods are detailed above: simple calculations, finite element analysis, and physical prototype testing. There are two alternative methods of manufacturing the component for both the prototype and final production: the machining can be done with a CNC mill, requiring a computer-aided manufacturing – CAM – numerical control program or it can be done manually. These two methods are noted in the process plan. It was assumed that if the manual milling operation were chosen, a design for manufacturing (DFM) analysis would be performed in order to determine a process plan and proper feed rates. The time durations shown in Figure 4 are those reported by the senior design project team. The two exceptions were the durations for the DFM analysis and the estimation

of the manual machining time, which were estimated by the authors using Boothroyd et al. [28].

It was assumed that both machining and engineering labor would have an efficiency of 60%; direct production work is being done 60% of the eight-hour work day. The fully-burdened hourly wage for engineers was assumed to be \$75; the fully-burdened wage for a machinist was assumed to be \$50. The wage and efficiency numbers are averages for engineering and production personnel found in Johnson and Kirchain [29]. There was also a \$28 hourly charge for the CNC mill and a \$16 hourly charge for the manual mill. The hourly charges for the machines were based on purchase costs of \$175,000 for the CNC mill and \$100,000 for the manual mill. It was assumed that these mills would operate 1000 hours per year and were amortized over a 10-year useful life using a 10% cost of capital to take into account the time value of money [30]. Materials were assumed to cost \$75 per part; this was based on the actual cost of material used for the project. The cost of each operation and the total for each alternative method are shown in Figure 4.

As expected, the simple calculation and FEA methods were less costly and could be performed in the shortest lead times. The two full prototype methods were more costly and required more time with the method that does not use the CNC mill, taking the longest and being the most costly. All methods were within the lead time and budgetary constraints outlined above, assuming the assessment methods were accurate and correctly predicted an acceptable design. However, if the component were installed and failed, the compo-

ment would have to be redesigned and retested. As mentioned above, this retesting would probably involve escalating to a method deemed to be more accurate. In the case of the simple calculations—the only method to produce appreciable Type II errors—escalation to the FEA method would require an updated design, an FEA analysis, the manufacture of the new component, and would require an additional six days and approximately \$3000. This assumed that the FEA method would take one-third the time of the original and that the DFM could be omitted.

This additional time and cost, combined with that of the original method, would be very close to the time and budgetary constraints. It was not possible to escalate to the manually manufactured prototype method and still meet time and budgetary constraints, which were an additional time of 9 days and an additional cost of \$4,600. It would be possible to escalate to the CNC-prototyped component and still meet the lead time constraint, but not the budgetary one of an additional time of 7 days and an additional cost of \$4,300. Overall, it would probably be preferable to choose one of the physical prototyping methods, even though they have longer lead times and cost more. It would be very difficult to escalate from one of the lower-cost and shorter lead-time methods and still meet the time and budgetary constraints in the event of Type II errors.

In summary, product risk is shown to have a significant effect on project risk and should be mitigated through the use of high-accuracy assessment methods in the presence of stringent time and budget constraints. This study examined a specific case and made numerous assumptions; as such, the results should be interpreted within certain limitations. These are discussed in the next section along with some conclusions.

Limitations and Conclusions

There are several limitations through which this work should be interpreted. First, a single and relatively simple product was examined for structural fitness. This allowed for a range of assessment options to be evaluated. In some cases, the ability to manufacture and test a component would not be feasible; in those cases, only simulation methods would be available. Second, this study assumed that all of the results from the various methods would be interpreted in a similar manner. It is possible to mitigate both the product and project risk associated with quicker methods by using larger safety factors such as over engineering to compensate for assessment risk. Next, although the students who performed this work were near the end of their professional training, they were still not experienced engineers; as such, the duration of certain activities might be longer than those

experienced in an industrial situation with more senior personnel.

Finally, this study assumed that the empirical data derived from the full prototype were assumed to be representative of the physical event. The problem with this assumption was that empirical data almost always contain errors [26]. In some cases, higher-end computer simulations may produce better results than those of simply-tested physical prototypes. Only one physical specimen was tested; the testing of multiple samples would allow for the accuracy of the empirical method to be better verified. Future studies should examine alternative components and verification methods as well as address the limitations noted above.

Technology has afforded engineers with a wide array of methods to assess the fitness of their designs. They must choose which assessment method affords them the highest probability of assessment success, while also conforming to time and budgetary constraints. In other words, they must minimize both product and project risk. This study showed an explicit, quantitative relationship between assessment-method accuracy and related engineering effort. This study also incorporated the tendency of project teams to escalate to more accurate methods, when a previous method has produced erroneous results.

It was shown that it can be preferable to choose a more accurate method even if it has a higher cost and lead time. The inability to escalate to a more accurate method later, and still meet time and budgetary constraints, prescribes choosing those methods initially, assuming that the time and budgetary penalties for them are not too great. This study showed that for assessing the structural fitness of a simple manufactured component that these penalties are in fact not too great. The methods detailed in this work can be used to explicitly and quantitatively analyze the effects assessment methods have on product and project risks.

Acknowledgments

The authors would like to acknowledge Bonner Baker, Sarah Candia, and Jonathan Croy (the senior design project team) for their efforts and contribution to this study. A previous version of this study was presented at the 2009 Integrity, Reliability, and Failure Conference.

References

- [1] P. Hsieh, *et al.*, "The Return on R&D Versus Capital Expenditure in Pharmaceutical and Chemical Industries," *IEEE Transactions on Engineering Management*, vol. 50, pp. 141-150, 2003.

-
- [2] S. Datar, *et al.*, "The Advantages of Time-Based New Product Development in a Fast-Cycle Industry," *Journal of Marketing Research*, vol. 34, pp. 36-49, 1997.
- [3] G. Kalyanaram and G. L. Urban, "Dynamic Effects of the Order of Entry on Market Share, Trial Penetration, and Repeat Purchases for Frequently Purchased Consumer Goods," *Marketing Science*, vol. 11, pp. 235-250, 1992.
- [4] D. Hall and J. Jackson, "Speeding Up New Product Development," *Management Accounting*, vol. 74, pp. 32-36, October 1992 1992.
- [5] M. A. Cohen, *et al.*, "New Product Development: The Performance and Time-to-Market Tradeoff," *Management Science*, vol. 42, pp. 173-186, 1996.
- [6] S.-H. Cho and S. Eppinger, D., "A Simulation-Based Process Model for Managing Complex Design Projects," *IEEE Transactions on Engineering Management*, vol. 52, pp. 316 - 328, August 2005.
- [7] K. T. Ulrich and S. D. Eppinger, *Product Design and Development*, 4rd ed. New York, NY: McGraw-Hill, 2007.
- [8] H. M. E. Abdelsalam and H. P. Bao, "A Simulation-Based Optimization Framework for Product Development Cycle Time Reduction," *IEEE Transactions on Engineering Management* vol. 53, p. 6, February 2006.
- [9] T. R. Browning and S. D. Eppinger, "Modeling Impacts of Process Architecture on Cost and Schedule Risk in Product Development," *Engineering Management, IEEE Transactions on*, vol. 49, pp. 428-442, 2002.
- [10] P. V. Norden, "On the Anatomy of Development Projects," *IRE Transactions on Engineering Management*, vol. 7, pp. 34-42, 1960.
- [11] T. A. Roemer, *et al.*, "Time-Cost Trade-Offs in Overlapping Product Development," *Operations Research*, vol. 48, pp. 858-865, 2000.
- [12] P. S. Adler, *et al.*, "From Project to Process Management: An Empirically - Based Framework for Analyzing Product Development Time," *Management Science*, vol. 41, pp. 458-484, 1995.
- [13] A. Griffin, "The Effect of Project and Process Characteristics on Product Development Cycle Time," *Journal of Marketing Research*, vol. 34, pp. 24-35, 1997.
- [14] K. B. Clark and T. Fujimoto, "Lead Time in Automobile Product Development Explaining the Japanese Advantage," *Journal of Engineering and Technology Management*, vol. 6, pp. 25-56, 1989.
- [15] K. G. Cooper, "The Rework Cycle: Benchmarks for the Project Manager " *The Project Management Journal*, vol. 24, pp. 17-22, 1993.
- [16] T. Gidel, *et al.*, "Decision-making Framework Methodology: an Original Approach to Project Risk Management in New Product Design," *Journal of Engineering Design*, vol. 16, pp. 1-23, February 2005.
- [17] P. S. Royer, "Risk Management: The Undiscovered Dimension of Project Management," *Project Management Journal*, vol. 31, pp. 6-13, 2000.
- [18] A. F. Mehr and I. Y. Tumer, "Risk-based Decision-Making for Managing Resources During the Design of Complex Space Exploration Systems," *Journal of Mechanical Design*, vol. 128, pp. 1014-1022, Jul 2006.
- [19] G. R. Cates and M. Mollaghasemi, "The Project Assessment by Simulation Technique," *Engineering Management Journal* vol. 19, pp. 3-10 December 2007.
- [20] K. G. Lough, *et al.*, "The Risk in Early Design Method," *Journal of Engineering Design*, vol. 20, pp. 155 - 173, 2009.
- [21] T. Kutoglu and I. Y. Tumer, "A Risk-informed Decision Making Methodology for Evaluating Failure Impact of Early System Designs," *Proceedings of The ASME 2008 International Design Engineering Technical Conferences and Computers And Information in Engineering conference* pp. DETC2008-49359, August 3-6 2008
- [22] R. L. Baskerville and J. Stage, "Controlling Prototype Development Through Risk Analysis," *MIS Quarterly*, vol. 20 pp. 481-504, December 1996.
- [23] J. K. Liker, *et al.*, "Fulfilling the Promises of CAD," *Sloan Management Review*, vol. 33, pp. 74-86, Spring 1992.
- [24] K.-J. Bathe, "What Can Go Wrong in FEA?," *Mechanical Engineering*, vol. 120, pp. 63-65, 1998.
- [25] I. Babuska and J. T. Oden, "The Reliability of Computer Predictions: Can They be Trusted?," *International Journal of Numerical Analysis and Modeling*, vol. 3, pp. 255-272, 2006.
- [26] I. Babuska and J. T. Oden, "Verification and Validation in Computational Engineering and Science: Basic Concepts," *Computer Methods in Applied Mechanics and Engineering*, vol. 193, pp. 4057-4066, 2004.
- [27] Z. Qian, *et al.*, "Building Surrogate Models Based on Detailed and Approximate Simulations," *Journal of Mechanical Design*, vol. 128, pp. 668 - 678, 2006.
- [28] G. Boothroyd, *et al.*, *Product Design for Manufacture and Assembly*. Boca Raton, FL: CRC Press, 2002.
- [29] M. D. Johnson and R. E. Kirchain, "The Importance of Product Development Cycle Time and Cost in the Development of Product Families," *Journal of Engineering Design*, vol. In Press, 2010.
-

-
- [30] R. de Neufville, *Applied Systems Analysis : Engineering Planning and Technology Management*. New York: McGraw-Hill, 1990.

Biographies

MICHAEL JOHNSON is an assistant professor in the Department of Engineering Technology and Industrial Distribution at Texas A&M University. Prior to joining the faculty at Texas A&M, he was a senior product development engineer at the 3M Corporate Research Laboratory in St. Paul, Minnesota for three years. He received his B.S. in mechanical engineering from Michigan State University and his S.M. and Ph.D. from the Massachusetts Institute of Technology. Johnson's research focuses on design tools; specifically, the cost modeling and analysis of product development and manufacturing systems; CAD methodology; manufacturing site location; and engineering education. Dr. Johnson may be reached at mdjohnson@tamu.edu

AKSHAY PARTHASARATHY is currently pursuing Master of Engineering in Industrial and Systems Engineering at Texas A&M University, College Station, Texas. He earned his Bachelorette of Engineering in Mechanical Engineering from Anna University, Chennai, India (May 2008). His interests are in statistical modeling and data analysis. Mr. Parthasarathy may be reached at akshay.p.sarathy@gmail.com

A REDUCED-CODE LINEARITY TEST FOR DAC USING WAVELET ANALYSIS

Emad Awada, Prairie View A&M University; Cajetan M. Akujuobi, Prairie View A&M University;
Matthew N. O. Sadiku, Prairie View A&M University

Abstract

In selecting Digital-to-Analog converters, overall performance accuracy is a primary concern; that is, how close does the output signal reflect the input codes. Integral NonLinearity (INL) error is a critical parameter specified by manufacturers to help users determine device performance and application accuracy. In classical testing of INL error, for an n -bit DAC, 2^n output levels must be included in the computation. This leads to a time-intensive and costly process. Therefore, the authors investigated the ability of Wavelet Transform to estimate INL with fewer samples in real-time testing. Compared with classical testing, the novel implementation of this Wavelet Transform has shortened testing times and reduced computational complexity based on special properties of the multi-resolution process. As such, the Discrete Wavelet Transform can be especially suitable for developing a low-cost, fast-test procedure for high-resolution DACs.

Introduction

In today's advanced communication systems, fast Digital Signal Processing (DSP) combined with mixed-signal Digital-to-Analog Converters (DACs) create a bottleneck in digital-to-analog conversion systems [1]. Therefore, it is important to determine the right DAC for the application. At the most basic level, converter testing would appear to be a simple matter. However, testing is extremely expensive and time-consuming, as many have agreed [1]-[8] for both static and dynamic parameters. Static parameters of DACs, such as Differential Non-Linearity (DNL) and Integral Non-Linearity (INL) errors, provide specific information that show the device output monotonicity and signal distortions. INL measurements, then, can be one of the major error characteristics of defining the overall DAC worst-case deviation [9]. This measurement can be lengthy and complicated, especially with the exponential growth in DAC internal complexity and the large number of data samples acquired per n -bit DAC [1]-[10].

Significant work has been done in the area of enhancing nonlinearity testing. Several studies proposed to reduce the number of input codes to reduce the linearity testing time. A technique was proposed to shorten the testing time by

modeling a reduced order model of DAC [4]. A reduction in the number of measurement points allows for faster statistical characteristic estimation in DAC models. However, a DAC model must feature much less than 2^n code of the actual DAC codes. Prior knowledge of the tested DAC error behavior also needs to be included in the model. This particular approach requires complicated mathematical simulation models of the DAC in order to define the influence of each code on its actual output voltage [10]. Also, DAC was modeled to show the effect of parasitic element and component mismatching on the converter performance [11]. However, other noise sources such as power supply and other hardware inputs were not included [7].

Others [10] proposed to reduce the number of samples by dividing the DAC input codes into segments. Each segment contains number of codes. Meanwhile, DAC output voltages, corresponding to different input codes within the same segment, are amplified to one value. This approach is based on the summation (averaging) of all output voltage values including noise. In addition, the separation of different errors can get harder as the number of bits increases. Others have focused on implementing new transformation techniques such as Wavelet Transform (WT) [2], [6], [7], [12]-[14]. The simulation with wavelets has shown improvements with satisfactory results in ADC testing. Thus, previous works in wavelet testing were applied through simulation process only using MATLAB. None of these investigators used LabView for real-time applications in ADC or DAC testing.

Since the problem of DAC testing persists due to lengthy processing delays caused by extremely large numbers of collected samples [10], the authors of this study investigated the ability of Wavelet Transform to estimate INL with fewer samples in real-time testing. Through actual testing, wavelets have shown improvements in characterizing DAC linearity error with satisfactory results. Wavelet Transform special properties of down sampling and multi-resolution allowed the reduction of compiled samples. No serious work has been done in this area to explore the actual strength of wavelet algorithms in real-time DAC testing. With the focus on shortening the testing process, reducing sample size, and simplifying testing complexity, wavelet computational efficiency was suitable for this application in contrast to the classical technique of estimating INL.

Theoretical Overview

Ideally, the DAC output voltage range is divided into equal segments, known as step size or Least Significant Bit (LSB), based on the device n-bit. In practice, the DAC voltage range is the difference between the output voltage of the lowest digital codes and the highest digital codes. By measuring the DAC voltage range or Full Scale Range (FSR) and dividing by the total number of codes, DAC unit separation step size can be stated as:

$$1 \text{ LSB} = \frac{\text{Voltage}[2^n - 1] - \text{Voltage}[0]}{2^n - 1} \quad (1)$$

where "n" is the DAC number of bits [7], [15]-[19].

That is, for each sequence input code, the DAC analog output is incremented by exactly 1 LSB. But, in reality, distances between codes vary due to non-linearity performance of the device, as shown in Figure 1.

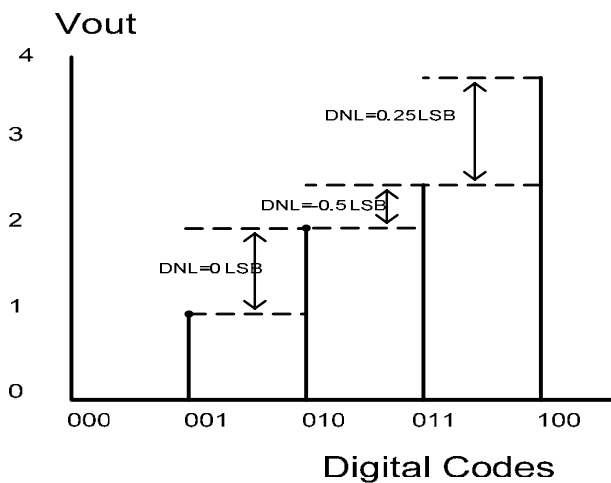


Figure 1. DAC Linearity performance in term of 1 LSB

The difference between the actual separation of adjacent individual codes and the estimated ideal step size is DNL. INL, on the other hand, is the overall linearity performance. INL measures the worst-case variation, or flatness, in the DAC analog output values with respect to an ideal straight line [15], [19]. Two straight-line methods are used in determining INL: End Point Line and Best Fit Line (linear regression). By using the End Point Line technique as shown in Figure 2, the straight line between the minimum and the maximum output value will present the ideal slope, or gain, and the INL is the deviation from this line [15]-[17].

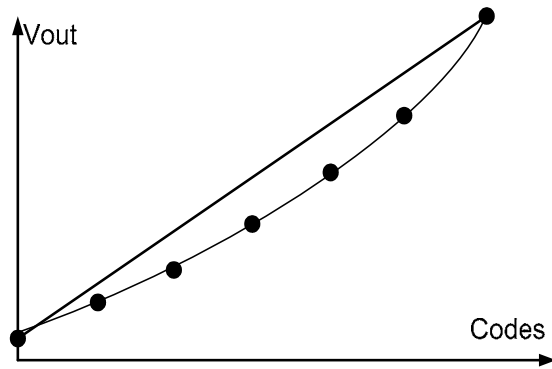


Figure 2. Endpoint Linearity Straight Line

The Best Fit Line, on the other hand, gives a representation of the DAC output linearity, based on the total sample set without looking into the smallest and largest value, as in Figure 3 [15], [16].

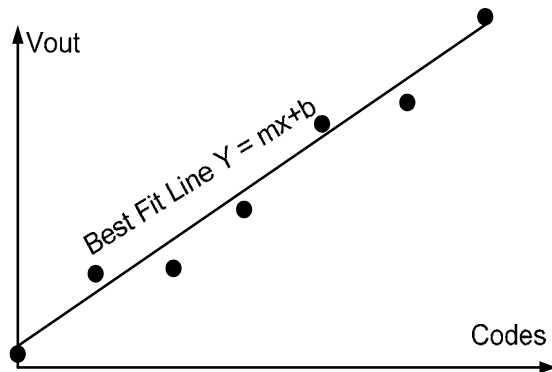


Figure 3. Best Fit Straight Line

Using either straight-line method, the INL curve can be calculated by subtracting the reference DAC straight line (End Point or Best Fit Line) from the actual output values in terms of 1 LSB. Ideally, the DAC output is linear, and the INL is equal to zero. However, in actual performance, DAC INL can be estimated as

$$INL[i] = \frac{(V[i] - V_{Ref}[i])}{V_{LSB}} \quad (2)$$

where $V[i]$ is the actual output values
 $V_{Ref}[i]$ is the straight line values
 V_{LSB} is the measured LSB

Testing Setup

The methodology of this testing experiment, shown in Figure 4, is based on generating clean, low-frequency digital

waveform codes and measuring the corresponding output voltages. This is followed by signal processing and data analysis.

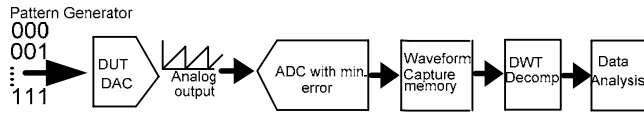


Figure 4. Model setup for DAC Wavelet analysis

In this study, a pattern generator was used to produce a ramp-up digital-waveform range from (00..0) to (11..1), based on the tested DAC number of bits. Both pattern generator and Device Under Test (DUT) DAC were triggered using the same clock to determine output analog signal frequency. The continuous output waveform, in the form of a continuous voltage, was captured and digitized using a higher-bit ADC. The digitizer resolution must be at least 2 bits greater than the resolution of the DUT DAC or one quarter the LSB [16]. In this study, a 20-bit digitizer was used, which is 6 bits higher than the DUT DAC (14-bit TI DAC2904), to allow characterization and achieve a linearity measurement accuracy of 1/64 the DUT LSB. A time-domain digitized signal was transformed into the time-frequency domain using Discrete Wavelet Transform (DWT). The transform data were used in characterizing the DAC non-linearity performance, illustrated in Fast Computation Technique section.

The hardware setup shown in Figure 5 involves supplying a digital ramp signal using a National Instruments NI-PXI-6552 pattern generator. The output analog signal was captured and digitized using a NI-PXI5922 fixable resolution digitizer to measure the output analog voltage. The clock source was routed through a NI-PXI-6552 to synchronize the DUT DAC and NI-PXI5922. A low-noise power supply was used to power the DAC testing board and to provide the digital power to trigger the bits.

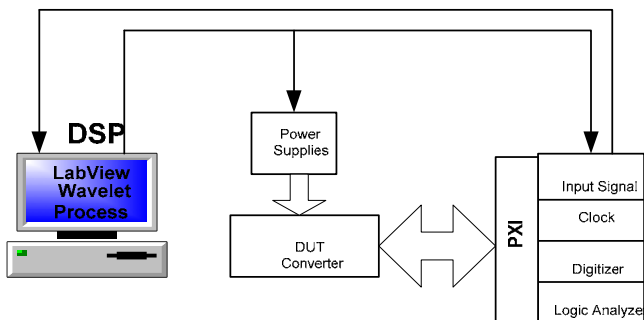


Figure 5. Experiment Hardware setup

Ramp Digital Input Codes

Non-linearity measurements were affected by the device's DC offset error, which can be caused by unsettled supply or reference-voltage input waveforms [20]. This phenomenon of unsettling requires additional time for a waveform to settle. However, testing time is often short and does not allow for settling, which may result in the DC-offset error being added to the output signal. The digital ramp signal is typically used to generate the DAC input stimulus digital waveforms and the DAC's acquired response is compared to an ideal response [16]-[20].

A computer repeatedly generates a set of ramp codes ranging from Least Significant Bit to Most Significant Bit to control a precision DAC. To eliminate waveform dead time and signal distortion, multiple ramp cycles were generated, but only one complete cycle was extracted by the digitizer. The first cycle, which could be subjected to distortion, was avoided by using derivative analysis to locate the maximum index of the derived signal and to get the starting point of the second cycle of the ramp signal.

Discrete Wavelet Transform

In most cases of signal analysis, signals are transformed and represented in a different domain. This kind of transformation, such as DWT, allows one to obtain further information in the raw signal data by localizing in frequency space and determining the position of frequency components [21], [22]. DWT is based on sub-band coding and was found to have fast computation. The computation was based on successive low-pass and high-pass filtering of the discrete time domain. Filtering was used to decompose a signal by utilizing filter banks and a down-sampling process by factor 2 (decimation) [2], [7], [22].

Assuming an output S_n , the new decomposed signal consists of two pieces, S_{n-1} and d_{n-1} for signal approximation and detail coefficients, respectively, as shown in equations (3) and (4).

$$S_{n-1,j} = \sum_k h^* s_{nk} \quad (3)$$

$$d_{n-1,j} = \sum_k g^* s_{nk} \quad (4)$$

where h and g are Wavelet Transform low-pass and high-pass coefficients, respectively

Wavelet decomposition consists of two major functions: convolution and down-sampling. In down-sampling, odd-numbered coefficients are dropped and even-numbered coefficients are renumbered by inserting a "0" in place of the

removed coefficients. The notation $(\downarrow 2)a$ denotes the sequence of down-sampling by 2 as shown in equation (5).

$$((\downarrow 2)a)_k = a_{2k} \quad (5)$$

In equations (3) and (4), output signal S_n is convoluted with wavelets low- and high-pass coefficients, as given in equations (6) and (7)

$$(h^* s_n)_j = \sum_k h^* s_{nk} \quad (6)$$

$$(g^* s_n)_j = \sum_k g^* s_{nk} \quad (7)$$

followed by down-sampling, as given in equations (8) and (9).

$$s_{n-1} = (\downarrow 2)(h^* s_n) \quad (8)$$

$$d_{n-1} = (\downarrow 2)(g^* s_n) \quad (9)$$

This process of filtering and decimation at each decomposition level reduces the number of collected samples by half of the frequency band. Starting with the largest scale (the original signal), bandwidth becomes a multiple of halves at the high-pass and low-pass filters for fast algorithms of computational and implementation processes. In other words, a signal, s_n , with a frequency 100Hz, passes through the first stage of decomposition to separate the signal into two parts: high-pass and low-pass. This results in two versions of the same signal: 0-50Hz for the low-pass portion and 50-100Hz for the high-pass portion. By taking one portion or both, this process can be repeated at multiple stages. As a result, at level 2 of the high-pass decomposition, original bandwidth can be divided into 0-50Hz, 50-75Hz and 75-100Hz, as shown in Figure 6. However, if all are combined, the original signal should be observed. Therefore, DWT is easy to implement and reduces the computation time without changing the signal.

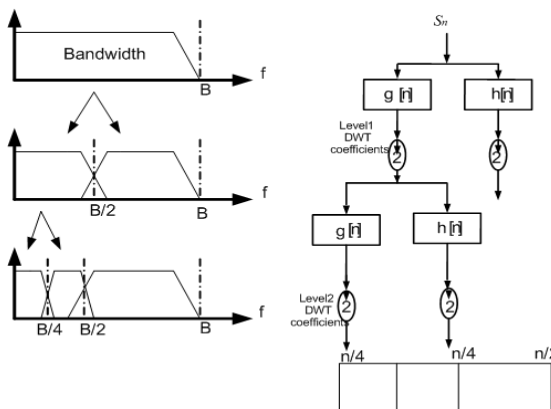


Figure 6. Wavelet Transform Multilevel Decomposition

Many types of mother Wavelets, based on the translation and scaling properties, can be used to determine signal characteristics. However, for each application, an appropriate mother Wavelet should be selected that best matches the signal [23], [24]. Selection of a specific DWT can be based on Wavelet shape, attribute, performance and signal analysis [23]. Properties of the Wavelet can be described in the time domain, (e.g., symmetry, regularity, vanishing moment, etc.), frequency domain (e.g., decaying, width of frequency window, etc.) and time-frequency domain (e.g., orthogonal, biorthogonal, fast algorithms, compact support, etc.) [23]. For example, Daubechies series are widely used in engineering applications. Using special attributes, Daubechies make conjugate quadrate filterband in multiresolutions analysis [24]. In addition, higher-order Daubechies (dbN) result in higher regularity [23]. An orthogonal wavelet with fast algorithms and computation support is a perfect match for signal spectrum analysis [23] with energy conservation.

The total energy contained in the DWT coefficients and the energy in the original signal is the same. This is suitable for signal compression and noising [21], [22]. However, unlike the orthogonal Wavelet filters (not a linear phase), biorthogonal filters can be linear-phase to allow for symmetry [21]. In this study, Haar, Coef, Daubechies (orthogonal), and biorN (biorthogonal) were used to analyze a ramp signal based on their shape characteristics, matching signal, symmetry, smoothness and phase linearity.

Fast Computation Technique

Ideally, DAC has a negligible output deviation from straight line and 0 offset voltage [15], [16]. In a non-ideal environment, a DAC analog output $\bar{x}(t)$ contains errors that distort the output signal due to noise, distortion error and heat. The output signal can be demonstrated as:

$$\bar{x}(t) = x(t) + e \quad (10)$$

where $x(t)$ = the original ramp value and e = error-value

In this study, the DWT algorithm was applied to decompose $\bar{x}(t)$ using multi-resolution techniques and a combination of low- and high-frequency components. While low-frequency components are stationary over a period of time (approximation coefficients), high-frequency components are noisy and provide detail coefficients as shown in equations (11) and (12), respectively [21].

$$\begin{bmatrix} \vdots \\ s_{n-1,-1} \\ s_{n-1,0} \\ s_{n-1,1} \\ \vdots \end{bmatrix} = \begin{bmatrix} \dots & \dots & \dots \\ \dots & \tilde{h}_{-1} & \tilde{h}_0 & \tilde{h}_1 & \tilde{h}_2 & \dots \\ \dots & \dots & \tilde{h}_{-1} & \tilde{h}_0 & \tilde{h}_1 & \tilde{h}_2 & \dots \\ \dots & \dots & \dots & \tilde{h}_{-1} & \tilde{h}_0 & \tilde{h}_1 & \tilde{h}_2 & \dots \\ \dots & \dots & \dots & \dots & \dots & \dots & \dots \end{bmatrix} \begin{bmatrix} \vdots \\ s_{n,-1} \\ s_{n,0} \\ s_{n,1} \\ \vdots \end{bmatrix} \quad (11)$$

$$\begin{bmatrix} \vdots \\ s_{n-1,-1} \\ d_{n-1,-1} \\ s_{n-1,0} \\ d_{n-1,0} \\ s_{n-1,1} \\ d_{n-1,1} \\ \vdots \end{bmatrix} = \begin{bmatrix} \dots & \dots & \dots \\ \dots & \tilde{h}_{-1} & \tilde{h}_0 & \tilde{h}_1 & \tilde{h}_2 & \dots \\ \dots & \tilde{g}_{-1} & \tilde{g}_0 & \tilde{g}_1 & \tilde{g}_2 & \dots \\ \dots & \dots & \tilde{h}_{-1} & \tilde{h}_0 & \tilde{h}_1 & \tilde{h}_2 & \dots \\ \dots & \dots & \tilde{g}_{-1} & \tilde{g}_0 & \tilde{g}_1 & \tilde{g}_2 & \dots \\ \dots & \dots & \dots & \tilde{h}_{-1} & \tilde{h}_0 & \tilde{h}_1 & \tilde{h}_2 & \dots \\ \dots & \dots & \dots & \tilde{g}_{-1} & \tilde{g}_0 & \tilde{g}_1 & \tilde{g}_2 & \dots \\ \dots & \dots & \dots & \dots & \dots & \dots & \dots \end{bmatrix} \begin{bmatrix} \vdots \\ s_{n,-1} \\ s_{n,0} \\ s_{n,1} \\ \vdots \end{bmatrix} \quad (12)$$

From the high-pass filter, detail coefficients were obtained as indicated in equation (13) and down-sampled by 2, taking the odd values as shown in (14), to end with half of the original data.

$$(\dots d_{n-1,-1}, d_{n-1,0}, d_{n-1,1}, d_{n-1,2}, d_{n-1,3}, d_{n-1,4}, d_{n-1,5}, d_{n-1,6}, d_{n-1,7}, \dots) \quad (13)$$

$$(\dots d_{n-1,-1}, d_{n-1,1}, d_{n-1,3}, d_{n-1,5}, d_{n-1,7}, \dots) \quad (14)$$

The collected detail coefficients in the first multi-resolution were used again for a second-level multi-resolution by repeating equations (12)-(15), as shown in Figure 7.

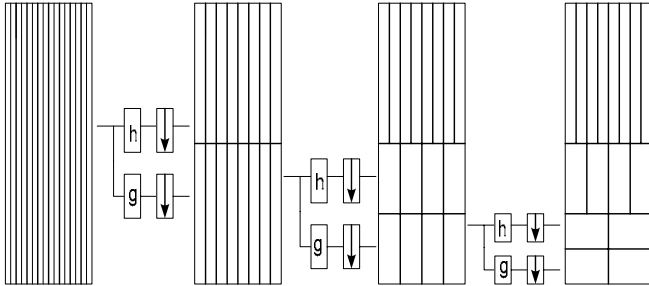


Figure 7. Data decomposition process

To compute INL using DWT coefficients, high-pass coefficients at the 2nd stage of multi-resolution were used. As in the case of computing instantaneous DNL [2], [7], instantaneous magnitudes of the high-pass filter at the 2nd level of data decomposition were used in place of the original codes for INL estimation, where codes in the time-frequency domain represented a different version of the same signal.

By applying DWT coefficients into the INL estimation, the INL was determined by subtracting the reference calculated straight line (based on instantaneous magnitudes) from the instantaneous magnitudes, and normalized by the DUT Δ_{ideal} . As a result, the instantaneous INL can be computed as:

$$INL(n) = \frac{\max \left\{ \left| d_n \right| - \left| d_{ref(n)} \right| \right\}}{\Delta_{ideal}} \quad (16)$$

where Δ_{ideal} is ideal LSB

d_n is instantaneous magnitudes

$d_{ref(n)}$ is corresponding straight-line magnitudes

Experimental Results

The proposed algorithm was implemented in LabView because of its proficiency in testing control, automation, and data acquisition [25]. A picture of the arranged bench prototype testing setup is shown in Figure 8. Testing setup consists of: 1) a National Instrument PXI 1042, capable of generating various analog and digital waveforms, built-in clock synchronization, high-resolution digitizer, and built-in logic analyzer; 2) device-under-test DAC; and, 3) PC terminal for testing engineering interfaces and interpolation of testing results.

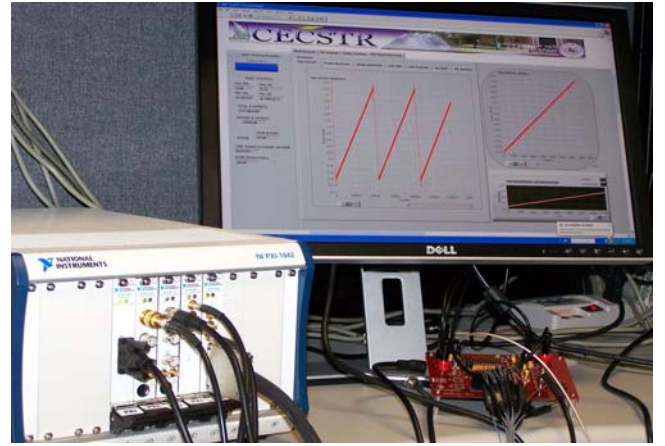


Figure 8. Bench Prototype Testing Setup

INL testing uses the classical technique as shown in Figures 9, 11 and 13 for 14-bit, 12-bit, and 10-bit DACs, respectively. Meanwhile, Figures 10, 12, and 14 illustrate the proposed DWT INL testing for 14-bit, 12-bit, and 10-bit DACs, respectively.

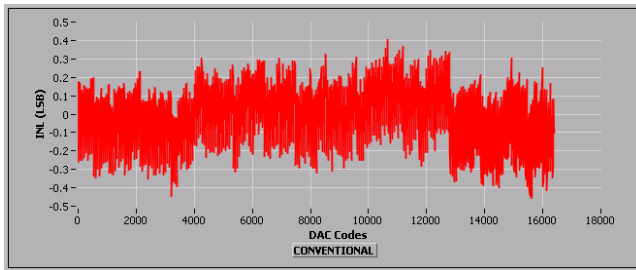


Figure 9. 14-bit DAC INL Computation

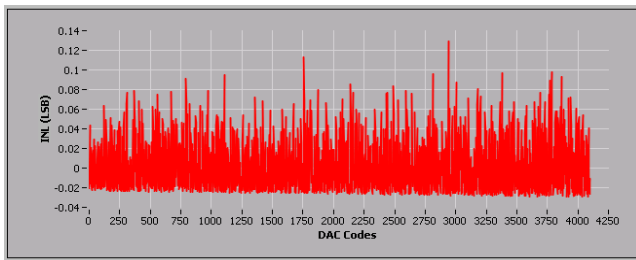


Figure 10. 14-bit INL Wavelet Based Computation

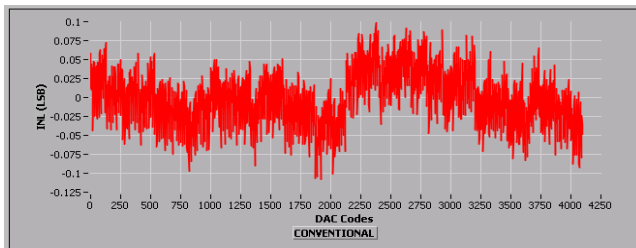


Figure 11. 12-bit DAC INL Computation

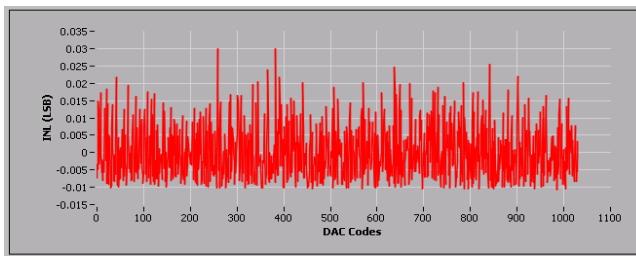


Figure 12. 12-bit INL Wavelet Based Computation

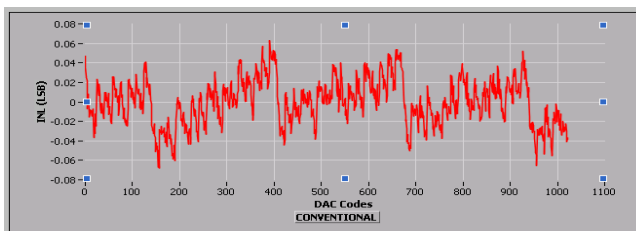


Figure 13. 10-bit DAC INL Computation

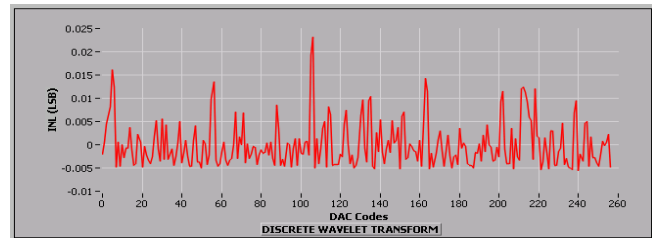


Figure 14. 10-bit INL Wavelet-Based Computation

As shown in Figures 7 and 8, for example, in classical testing of 14-bit DAC, a total of 16,383 codes were used in estimating the maximum INL, while in the DWT testing algorithm, 4,099 codes were used. In Figures 9 and 10, for the 12-bit DAC, a total of 4,095 codes were used in classical testing and 1,032 codes in the DWT algorithm. Also, for the 10-bit DAC in Figures 11 and 12, 1,023 codes were used in computing the INL, while 258 were used in the DWT algorithm. This significant reduction in the number of codes and shortened INL computation was due to the special DWT properties of dilatation and translation that allows Wavelet to zoom into signal data information, prevent redundant information during decomposition, and to possess the same amount of energy contained in the original data for signal reconstruction [21], [22].

To validate these experiment results, testing was performed using several clock frequencies and DWT mother wavelets. Results were validated with classical testing as well as device specifications as shown in Tables 1- 3 and Figures 15-17.

Table 1. INL estimation for 14-bit (DAC2904, TYP INL = ± 5)

Fclock (KHz)	C.T	db4	db2	Haar	Bior3-1	Coef1
100	0.47	0.16	0.12	0.14	0.41	0.11
150	0.42	0.11	0.13	0.13	0.46	0.13
200	0.46	0.13	0.17	0.13	0.4	0.11

C.T – Classical Testing

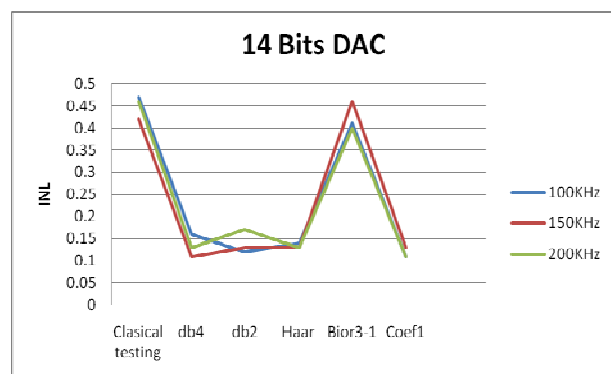


Figure 15. Illustration of INL values from Table 1

Table 2. INL estimation for 12-bit (DAC2902, Typ INL = ± 3)

Fclock (KHz)	C.T	db4	db2	Haar	Bior3-1	Coef1
100	0.16	0.03	0.08	0.03	0.22	0.07
150	0.18	0.04	0.06	0.04	0.21	0.06
200	0.17	0.04	0.06	0.04	0.21	0.06

C.T – Classical Testing

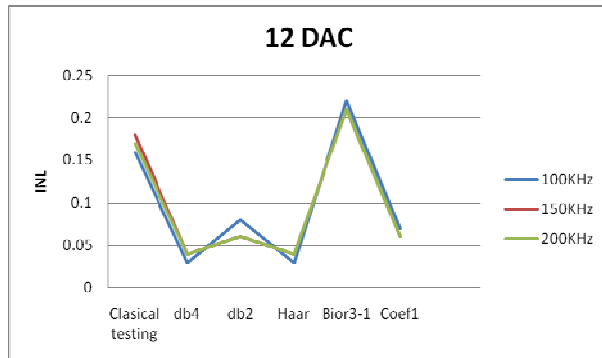


Figure 16. Illustration of INL values from Table 2

Table 3. INL estimation for 10-bit (DAC2900, Typ INL = ± 1)

Fclock (KHz)	C.T	db4	db2	Haar	Bior3-1	Coef1
100	0.08	0.01	0.03	0.02	0.11	0.03
150	0.09	0.01	0.03	0.03	0.1	0.02
200	0.09	0.02	0.05	0.02	0.15	0.02

C.T – Classical Testing

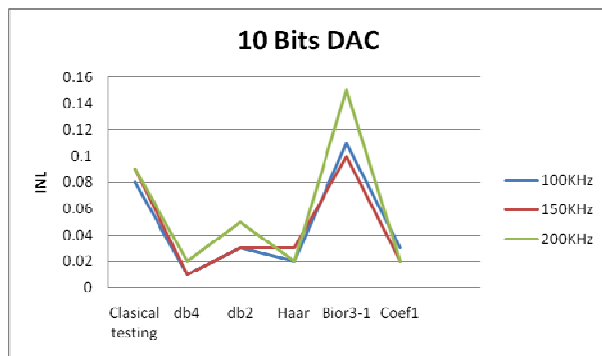


Figure 17. Illustration of INL values from Table 3.

Discussion

The Wavelet Transform showed improvements in testing INL by reducing the number of sampling data and computational complexity. As indicated in the testing process, Wavelet Transform algorithms reduced the amount of compiled data by 75% of collected data samples, which reduces the data-storage space requirements by the same amount, and shortens test duration from 312ms in conventional testing to 134ms using Wavelet algorithms.

The selection of the Wavelet was based on the Wavelet shape characteristics, matching signal, orthogonality, and filter linearity. As seen from Tables 1, 2 and 3, bior3-1 outperformed Haar and dbN Wavelets, due to the matching signal characteristics of the ramp-up signal and linear-phase filters.

Conclusion

A new method of testing INL mixed-signal DACs was presented to show the ability of DWT in analyzing output signals, and identify bit errors due to signal distortions, noise, and DC offset, that can be integrated into the output signal. This method of testing can be implemented in testing other DAC parameters such as gain and DC offset error. The benefit of Wavelet algorithms in decreasing the number of sample data can be used for a faster testing process, decreased cost, and more accurate results. DWT can be especially suitable for the incredible growing demands for high-speed, high-resolution converters, built-in self-test algorithms, and self-calibration schemes.

References

- [8] E. Balestrieri, P. Daponte, S. Rapuano, "Recent developments on DAC modeling, testing and standardization Measurement", ELSEVIER, 9th Workshop on ADC Modeling and Testing, April 2006, pp. 258-266.
- [9] T. Yamaguchi, M. Soma, "Dynamic Testing of ADCs Using Wavelet Transform" in 1997 Proc. IEEE Test Conf., pp. 379-388.
- [10] F. Adamo, F. Attivissimo, N. Giaquinto, A. Trotta, "A/D converters nonlinearity measurement and correction by frequency analysis and dither" IEEE Trans. Instrumentation and Measurement, Aug 2003. pp. 1200 – 1205.
- [11] B. Vargha, J. Schoukens, Y.; Rolain, "Using reduced-order models in D/A converter testing" in 2002 Proc. IEEE Instrumentation and Measurement Technology Conf., pp.701-706.
- [12] J.T. Doyle, L. Young; K. Yong-Bin, "An accurate DAC modeling technique based on Wavelet theory" In 2003 Proc. IEEE Custom Integrated Circuits Conf., pp. 21-24.
- [13] R. O. Marshall, C. M. Akujuobi, "On the Use of Wavelet Transform in Testing for the DNL of ADCs", In Midwest Symposium, 2002. IEEE Circuits and Systems, pp. 25-8.
- [14] C.M. Akujuobi, E. Awada "Wavelet-based differential nonlinearity testing of mixed signal system ADCs"; In 2007 Proc. IEEE Southeast Conf., pp. 76 – 81.

-
- [15] S. Cherubal, A. Chatterjee, "Optimal linearity testing of analog-to-digital converters using a linear model" IEEE Trans. Circuits and Systems I: Mar 2003, pp.317 – 327.
- [16] Y. Cong; R.L. Geiger, "Formulation of INL and DNL yield estimation in current-steering D/A converters", IEEE International Symposium on Circuits and Systems, 2002, pp. III-149
- [17] B. Vargha, J. Schoukens, Y. Rolain, "Static nonlinearity testing of digital-to-analog converters" IEEE Trans. Instrumentation and Measurement, Oct 2001, pp. 1283 – 1288.
- [18] J.J. Wikner, N. Tan, "Modeling of CMOS digital-to-analog converters for telecommunication" IEEE Trans. Circuits and Systems II: May 1999, pp. 489 – 499.
- [19] C. M. Akujuobi, L. Hu, "A Novel Parametric Test Methods for Communication System Mixed Signal Circuit Using Discrete Wavelet Transform", IASTED, St. Thomas, US Virgin Island, Nov 2002.
- [20] C. M. Akujuobi, L. Hu, "Implementation of the Wavelet Transform-based Technique for static Testing of Mixed Signal System", IASTED, CA. Palm Spring, US, Feb 2003.
- [21] A. Gandelli, E. Ragaini, "ADC Transfer Function Analysis by Means of A Mixed Wavelet-Walsh Transform" in 1996 Proc. IEEE Instrumentation and Measurement Technology, pp. 1314 – 1318.
- [22] M. Baker, "Demystifying Mixed Signal Test Methods". Newnes, Elsevier Science, 2003, pp. 147-237.
- [23] M. Burns, G. W. Roberts "An Introduction to Mixed-Signal IC Test and Measurement", Oxford University Press, New York, 2004, pp. 159-527.
- [24] J. Paul "Integrated Converters", Oxford University Press, New York, 2001, pp. 1-27.
- [25] B. Razavi "Data Conversion System Design", Wiley-Interscience, Newyork, 1995, pp 45-70.
- [26] IEEE Standard 1241, IEEE Standard for terminology and test methods for analog-to-digital converters, 2000.
- [27] J. Schat, "Testing low-resolution DACs using the Generalized Morse Sequence as Stimulus Sequence for Cancelling DC drift". in 2007 International; Conf. IEEE Circuits and Systems, pp. 371-374.
- [28] F. Keinert "Wavelet and Multiwavelets", Chapman and Hall, Boca Raton, FL. 2004, pp39-67.
- [29] O. Riouel, M. Vetterli, "Wavelet and Signal Processing," IEEE SP Mag., Volume 8, No. 4, pp. 14-38, Oct. 1991.
- [30] L. Peng, D. Jian-dong "Characteristic Analysis and Selection of Wavelets Applicable for Ultra-High-Speed Protection" in 2005 IEEE Conf. Transmission and Distribution, pp 1-5.
- [31] Y. Qing-Yu; H. Mu Long, W. Li-Yan, "Fault Line Detection of Non-Effectively Earthed Neutral System Based on Modulus Maximum Determining Polarity" in 2009 IEEE Conf. Power and Energy, pp 1-4.
- [32] C.M. Akujuobi, E. Awada, "Wavelet-based ADC Testing Automation Using LabView"; International Review of Electrical Engineering Transaction, Vol 3, pp. 922-930, Oct 2008.

Biographies

EMAD AWADA received the B.S. degree in electrical engineering from Prairie View University, Prairie View, TX. in 1998. He received the M.S. degree in electrical engineering from Prairie View University in 2006. Since then, he has been working on his doctoral degree. Mr. Emad Awada may be reached at emadawada@yahoo.com

CAJETAN M. AKUJUOBI is the founding Director of the Center of Excellence for Communication Systems Technology Research (CECSTR). He is also the founding Directors of Mixed Signal Systems Laboratory, Broadband Communication Systems Lab. His research interests are in the areas of Mixed Signals Systems, Broadband Communication Systems, Signal/Image/Video Processing and Communication Systems. He received the B.S. in Electrical and Electronics Engineering, Southern University, Baton Rouge, Louisiana 1980. M.S. in Electrical and Electronics Engineering, Tuskegee University, Tuskegee, Alabama 1983. M.B.A., Hampton University, Hampton, Virginia 1987. Ph.D. Electrical Engineering, George Mason University, Fairfax, Virginia 1995. Dr. Cajetan M. Akujuobi may be reached at cmakujuobi@pvamu.edu

MATTHEW N. O. SADIKU is presently a professor at Prairie View A&M University. He was a professor at Temple University, Philadelphia and Florida Atlantic University, Boca Raton. He is the author of over 180 papers and over 30 books including Elements of Electromagnetics (Oxford, 4th ed., 2007) and Numerical Techniques in Electromagnetics (CRC, 3rd ed. 2009), Metropolitan Area Networks (CRC Press, 1995), and Fundamentals of Electric Circuits (McGraw-Hill, 4th ed., 2009, with Charles Alexander). His current research interests are in the areas of numerical techniques in electromagnetics and computer communications networks. He is a senior member of the IEEE. Dr. Matthew N. O. Sadiku may be reached at mnsadiku@pvamu.edu

INVESTIGATION OF THE FACTORS AFFECTING SURFACE-PLASMON EFFICIENCY

Padmarekha Vemuri, University of North Texas; Vijay Vaidyanathan, University of North Texas; Arup Neogi, University of North Texas

Abstract

Group-III nitride-based semiconductors have emerged as the leading material for short wavelength optoelectronic devices. The gallium nitride/indium-gallium nitride (GaN/InGaN) alloy system forms a continuous and direct bandgap semiconductor spanning ultraviolet (UV) to blue/green wavelengths. An ideal and highly efficient light-emitting device can be designed by enhancing the spontaneous emission rate. The paper presents the design and fabrication of a visible-light-emitting device using a GaN/InGaN single-quantum-well system with enhanced spontaneous emission. To increase the emission efficiency, layers of different metals, usually noble metals like silver, gold and aluminum, were deposited on GaN/InGaN single-quantum-wells using a metal evaporator. Surface characterization of metal-coated GaN/InGaN single-quantum-well samples was carried out using Atomic Force Microscopy (AFM) and Scanning Electron Microscopy (SEM). Photoluminescence (PL) was used as a tool for optical characterization to study the enhancement in the light emitting structures. This study also compared characteristics of different metals on GaN/InGaN single-quantum-well systems, thus allowing selection of the most appropriate material for a particular application. Results show that photons from the light emitter couple more to the surface plasmons if the band-gap of the former is close to the surface-plasmon resonant energy of a particular metal. Absorption of light due to gold reduces the effective mean path of light emitted from the light emitter and hence quenches the quantum-well emission peak compared to the uncoated sample.

Introduction

Semiconductor materials play a vital role both in optoelectronics and high-speed digital circuits for computer and telecommunication applications. Silicon semiconductor technology has advanced exponentially in both performance and productivity as predicted by Moore's law [1]. These exponential advances in device integration observed over the past several decades might soon end due to fundamental physical (lithographic area not less than 100nm) and/or economic (cost of fabrication facility more than US \$2 billion) limitations [2]. The 1999 edition of the *International Technology Roadmap for Semiconductors* reported the presence of a

potential "Red Brick Wall" that could block further scaling of integrated circuits [3].

This prediction has motivated extensive efforts aimed at developing new device concepts and fabrication approaches that may enable integration to overcome the limits of conventional microelectronics technology [2]. It requires the development of an optical analogue of an electronic integrated circuit capable of routing, controlling and processing optical signals [4]. There is a strong tendency to replace big and slow electronic devices with small and fast photonic ones. Development of photonic crystals, quantum wells, and quantum dots, having key properties controlled by size, morphology, and chemical composition, represents a powerful approach that could overcome physical and/or economic limitations [2]. The photonic integrated circuit include devices such as switches, sources and interconnects to accommodate 1000 x 1000 channels on a single substrate [5]. A novel nanophotonic technology that goes beyond the diffraction limit is essential to meet the demands of the future semiconductor optoelectronic industry. Surface plasmons are an integral part of nanophotonic technology that could potentially fill a niche in the optoelectronics industry.

Surface Plasmons

Surface plasmons are trapped electromagnetic surface modes at the interface between a metal and a dielectric and are a combined oscillation of the electromagnetic field and the surface charges of the metal [6]. They are widely recognized in the field of surface science. Surface plasmons have electromagnetic fields that decay exponentially into both the metal and dielectric media that bound the interface [7]. Surface plasmons propagate along an interface between two media with dielectric constants of opposite sign (such as a metal and a dielectric). Renewed interest in surface plasmons comes from recent advances that allow metals to be structured and enable concentration and channeling of light using sub-wavelength structures. This in turn facilitates control of surface-plasmon properties to reveal new aspects of their underlying science and to tailor them for specific applications [7].

The use of surface plasmons to concentrate light in sub-wavelength structures stems from the different permittivity, (ϵ), of the metals and the surrounding non-conducting media. In order to sustain surface-plasmon resonance, the metal

concerned must have conduction-band electrons capable of resonating with light of the appropriate wavelength. Surface plasmons of lower frequency, ω_{sp} , can also be excited by high-energy electron beams or by light. Thus, using surface plasmons that are trapped at the interface, the problem of light manipulation can be simplified from three dimensions to two dimensions [8]. Surface plasmons can increase the density of states (energy levels) and the spontaneous emission rate in the semiconductor, and lead to the enhancement of light emission by surface-plasmon quantum-well coupling [9], [10].

In order to build an ideal and highly-efficient light-emitting device, it is desirable to enhance the spontaneous emission rate. Coupling the light to the surface plasmons of a metallic film can enhance spontaneous emission and thereby optical emission of the semiconductor. Metal-semiconductor surface-plasmon interaction is an effective tool for manipulating local interaction for various optoelectronic applications [11]. The purpose of this study was to design and fabricate a visible-light-emitting device using the GaN/InGaN single-quantum-well system with enhanced spontaneous emission. To increase the emission efficiency, layers of different metals, usually noble metals like silver (Ag), gold (Au) and aluminum (Al), were deposited on the GaN/InGaN single-quantum-wells using a metal evaporator. The bottom surfaces of the single-quantum-well samples (sapphire substrate) were polished to avoid scattering of light. Surface characterization of metal-coated GaN/InGaN single-quantum-well samples was carried out using Atomic Force Microscopy (AFM) and Scanning Electron Microscopy (SEM). Photoluminescence (PL) was used as a tool for optical characterization to study the enhancement of light-emitting structures. This study also compared characteristics of different metals on the GaN/InGaN single-quantum-well systems, thus allowing selection of the most appropriate material for a particular application.

Methods

The experimental procedure was divided into two sections, deposition and characterization. The first section involved deposition of thin metal films on the GaN/InGaN single-quantum-wells in an ultra-high vacuum chamber by using a metal evaporator, while the second section dealt with characterization of the metal-coated GaN/InGaN single-quantum-wells.

GaN/InGaN Single-Quantum-Wells

Three GaN/InGaN samples (growth temperatures: 780°, 800°, and 830°C) were grown at the Institute of Photonics, University of Strathclyde, Glasgow, Scotland, U.K (collabo-

ration). Metal organic-chemical vapor deposition or metal organic-vapor phase epitaxy was used to grow epitaxial structures of samples by depositing atoms on a sapphire substrate. Ammonia (NH₃) was used as a precursor for nitrogen, whereas trimethylgallium and trimethylindium were used as gallium and indium sources, respectively. Typically, the growth rate employed was one to three mono-layers per second, approximately 0.3-1 μ m/hr, although much higher growth rates can be attained. Compounds were grown in a hydrogen atmosphere where they formed epitaxial layers on the substrate as they decomposed [12]. In order to study the enhancement in light emission from metal-coated GaN/InGaN single-quantum-well samples, the samples needed to be excited from the bottom surface. Rough bottom surfaces scatter the light and drop the efficiency of light reaching the quantum wells. Hence the substrate side (bottom surface) of the samples had to be polished. Mechanical polishing is commonly used to smooth surfaces [13]. An Allied Tech Prep™ P/N 15-2000 mechanical polisher was used to polish the samples used in this study.

Sample Preparation

Samples used for metal deposition and further characterization were cleaned thoroughly for best results. The three different GaN/InGaN single-quantum-well samples were cut into four pieces each for metal deposition. The protocol for cleaning the GaN/InGaN samples is as follows:

- Rinse the samples in acetone for 5 minutes.
- Clean the samples in distilled water 2 to 3 times.
- Rinse the samples in methanol for 3 minutes.
- Clean the samples with distilled water again, 2 to 3 times.
- Place the samples in 15% (HCl+HNO₃) Aqua Regia solution and heat the solution to approximately 80°C.
- Clean the samples with distilled water 4 times.
- Blow-dry the samples with dry nitrogen gas.

Thickness Monitoring

A Maxtek TM-100 Thickness Monitor was used to monitor the thickness of the metal films during the deposition process. The thickness monitor allows improved manual control of the vacuum film deposition process by providing a direct display of film thickness and deposition rate during deposition.

Thin-Film Characterization

Physical and optical analyses were carried out on all the metal-deposited single-quantum-well samples. Scanning

Electron Microscopy (SEM) was performed using the JEOL-5800™ SEM. All samples with and without metal films deposited were physically examined under the SEM to understand their surface morphology. Atomic Force Microscopy (AFM) was used to make a physical analysis. Digital Instrument's Nanoscope-E® AFM was used in this study. A photoluminescence technique was used to perform optical analysis. Figure 1 shows the photoluminescence arrangement with a system made up of a laser (light source), lenses and spectrometer interfaced to a PC.

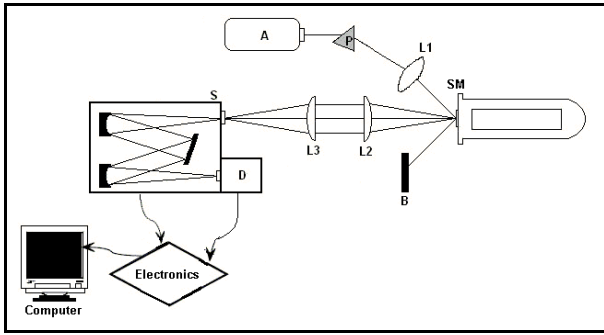


Figure 1: Simplified Photoluminescence arrangement, with Laser (A), Lenses (L1, L2, L3), Prism (P), Beam block (B), Sample (SM) inside Cryostat (C), Spectrometer (S), and Detector (D)

The enhancement of optical emission induced by surface-plasmon interaction was studied by using a two-dimensional emitter situated within the surface-plasmon penetration depth of the semiconductor light-emitting structure. For the development of efficient light emitters, the quantum-well widths were varied by growing the samples at different temperatures. Three GaN/InGaN quantum-well samples were grown with varying quantum-well widths for achieving varying emission energies. Sample preparation was carried out by first polishing the bottom surface of sapphire substrate grown, single-quantum-well samples and later by cleaning the samples for metal deposition. Thin metal (Ag/Au/Al) films were deposited using a metal evaporator.

The quantum-well samples were characterized for surface roughness using SEM and AFM. The enhancement in light emission was investigated using Photoluminescence (PL) spectroscopy. A GaN buffer layer of approximately 1.5 μ m thick was deposited on the sapphire substrate. Single InGaN quantum wells were grown on the GaN buffer layer at various temperatures measured by a pyrometer within the growth chamber. The growth run was finished by a GaN cap layer of 17nm thickness, grown at the same temperature as the InGaN quantum wells. The growth time for the cap was held at 36 s, with the GaN growth rate only slightly dependent on temperature over the range concerned. Table 1 represents the classification of samples based on their quantum-well (QW) emission and growth temperatures.

Sample A was grown at 780°C with a well thickness of 4.05nm. Sample B was grown at 800°C with a well thickness of 4.3nm. Similarly, Sample C was grown at 830°C and has a well thickness of 4.55nm. Each sample was cut into four pieces and Ag/Au/Al metal films were deposited.

Table 1: Sample Classification

Sample Name	QW Energy (eV)	QW Thickness	Growth Temperature	Metal Deposited
Sample A-No Metal	2.53	4.05nm	830°C	None
Sample A-Silver	2.53	4.05nm	830°C	Silver
Sample A-Gold	2.53	4.05nm	830°C	Gold
Sample A-Aluminum	2.53	4.05nm	830°C	Aluminum
Sample B-No Metal	2.25	4.3nm	800°C	None
Sample B-Silver	2.25	4.3nm	800°C	Silver
Sample B-Gold	2.25	4.3nm	800°C	Gold
Sample B-Aluminum	2.25	4.3nm	800°C	Aluminum
Sample C-No Metal	2.1	4.55nm	780°C	None
Sample C-Silver	2.1	4.55nm	780°C	Silver
Sample C-Gold	2.1	4.55nm	780°C	Gold
Sample C-Aluminum	2.1	4.55nm	780°C	Aluminum

Results and Discussion

a) Surface Characterization

Scanning Electron Microscopy did not show significant quantitative roughness. Hence, AFM characterization was carried out on uncoated and metal-coated samples to determine the surface roughness. A scan size of 6 μ m x 6 μ m and a scan rate of 5.0Hz were used to scan the samples. The GaN domains of 1 μ m x 1 μ m (approximately) were observed on Sample A-No Metal, which are not periodic and, an average roughness of ~ 1nm was observed over a range of 6 μ m x 6 μ m of the scanned area. Due to the existence of domains on the GaN surface, some domains were observed on the silver-coated surface. These domains contribute to the roughness in the silver-coated sample. For gold-coated samples, a sample roughness of ~2.5nm was observed. Cluster formation was observed on both the gold and aluminum-coated samples of Sample A. From the images of AFM on Sample A, it was observed that the samples have an average roughness of approximately 1 to 2nm and do not have any periodic roughness.

An AFM characterization on Sample B was carried out on both the uncoated and metal-coated samples in order to determine the surface roughness. Based on the study of AFM images, it was observed that the samples had an average

roughness of approximately 1 to 2nm and did not have any periodic roughness. Cluster formation was observed on gold- and aluminum-coated samples. From the images of AFM on Sample C, it was observed that the samples had an average roughness of approximately 2 to 3nm and did not have any periodic roughness.

b) Photoluminescence Characterization

In the front incidence and front collection geometry as discussed earlier, photoluminescence (PL) characterization on the samples was conducted using an excitation of a 325 nm line of the He-Cd laser, operated at < 22.5mW, and detected using a charge-coupled device (CCD) array. Figure 2 shows the PL spectrum of Sample A at room temperature (300K). The peak at 360 nm corresponds to the emission peak, mostly from the GaN cap layer and partially from the GaN buffer layer. The peak at 495 nm corresponds to the quantum-well emission at room temperature. The small broad peaks from 400 to 475 nm are identified as optically-deep-level transition peaks from GaN cap/buffer layers. An increase in the intensity of emission from both quantum-well and GaN (cap/buffer) layers was observed from the spectrum at low temperatures.

Figure 3 shows the PL spectrum of Sample B at room temperature (300K). The peak at 360nm corresponds to the emission peak, mostly from the GaN cap layer and partially from the GaN buffer layer. The peak at 544nm corresponds to the quantum-well emission at room temperature. An increase in the intensity of emission from both quantum-well and GaN (cap/buffer) layers was observed from the spectrum at low temperatures. The PL intensity peak was observed at a wavelength of 550 nm.

Figure 4 shows the PL spectrum of Sample C at room temperature (300K). The peak at 360nm corresponds to the emission peak, mostly from the GaN cap layer and partially from the GaN buffer layer. The peak at ~585nm corresponds to the quantum-well emission at room temperature. An increase in the intensity of emission from both QW and GaN (cap/buffer) layers was observed from the spectrum at low temperatures. At low temperatures, the intensity peak was observed at 595 nm.

Non-radiative recombination of the electron-hole pairs in the light emitters dominates at room temperature due to phonons being produced instead of photons. Hence, the intensity

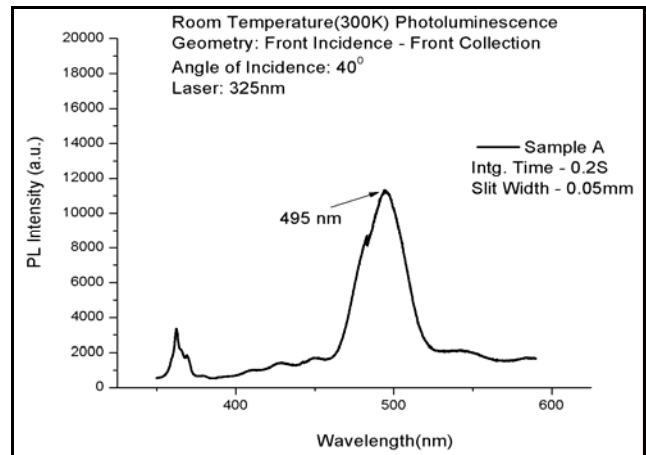


Figure 2: Room Temperature PL of Sample A

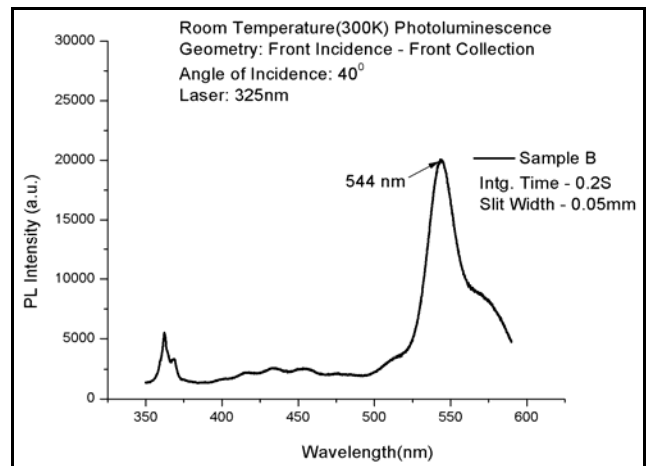


Figure 3: Room Temperature PL of Sample B

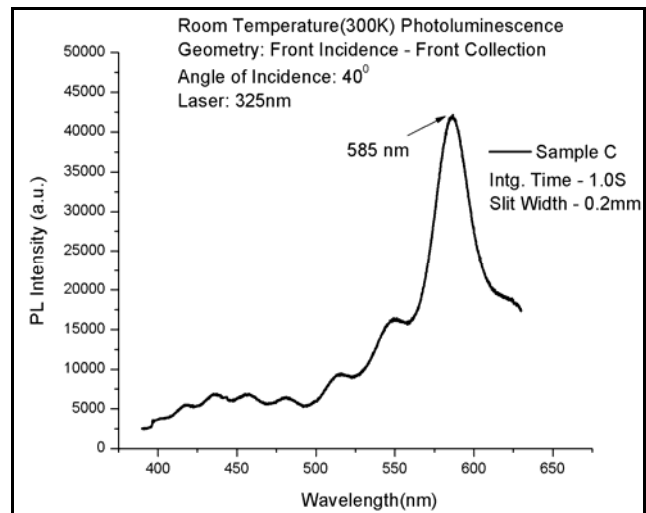


Figure 4: Room Temperature PL of Sample C

drops. At low temperatures, the electrons recombine with holes in a radiative recombination process releasing more photons, resulting in higher intensity.

c) Angle-Resolved PL Spectroscopy in the Backscattered Geometries

The metal-coated samples were photo-excited at 35°, 40°, 45°, 50°, and 55° angle of incidence and PL was measured from the back of the unpolished sapphire substrate. Reflection from the metal films on the front side of the sample restricts the use of front-incidence, front-collection geometry. When exciting the quantum well from the backside of the sample, the 325nm (~3.8eV) He-Cd laser cannot be used since the laser light is absorbed mostly by the bulk GaN buffer layer (emission energy ~3.4eV). Thus, not enough photons reach the quantum-well layer to excite the electron-hole recombination. Therefore, a 405nm (~2.8eV) diode laser was used in the back-incidence, back-collection geometry. In this geometry, GaN is transparent to the incident light and, hence, maximum light reaches the quantum well. Scattering was observed on the uncoated gold- and aluminum-coated samples of Sample A. A peak at 490 nm was observed only on silver-coated samples (Sample A-Silver) at all angles of incidence. A statistical analysis using a T-test was carried out to decide whether there is a significant change in the PL intensities from polished and unpolished samples.

With μ_p being the mean of peak PL intensities from polished Sample A-silver and μ_{up} being the mean of peak PL intensities from unpolished Sample A-silver, the null and alternate hypothesis can be stated as follows:

Null Hypothesis H_0 : There is no significant change in peak PL intensity from unpolished and polished samples at all angles of incidence.

$$H_0: \mu_p = \mu_{up}$$

Research Hypothesis (Alternate Hypothesis) H_1 : There is a significant change in peak PL intensity from unpolished and polished samples at all angles of incidence.

$$H_1: \mu_p \neq \mu_{up}$$

Test Statistic: The statistical T-test of “Paired Two Sample for Means” created using Microsoft Excel is shown in Table 2 [16]. This test was conducted on the data with a confidence coefficient (α) of 0.05 to test the equality of means of peak PL intensities from polished and unpolished samples.

Since $|T_{stat}| > T_{critical\ two\ tail}$, the decision rule is to reject the null hypothesis and, hence, accept the Alternate Hypothesis

(H_1). This implies that there is a significant difference (significance level, $\alpha = 0.05$) in the mean peak PL intensities between unpolished and polished samples. Thus, it can be inferred that polishing is required to avoid scattering and enhance the light emission from quantum wells.

d) PL Spectroscopy

The variation of peak photoluminescence intensity with angle of incidence for sample A is shown in Figure 5. No enhancement was observed in the gold-coated sample. Similar plots for sample B and sample C are shown in Figure 6 and Figure 7, respectively.

Table 2: T-Test on Peak PL Intensity from Polished and Unpolished Samples

T-Test: Paired Two Sample for Means		
	Unpolished Sample A-Silver	Polished Sample A-Silver
Mean	14588.88588	47523.21135
Variance	1970594.689	50934464.45
Observations		5
Pearson Correlation	-0.986459103	
Hypothesized Mean Difference		0
Df		3
T Stat	-7.726783237	
P(T<=t) two-tail	0.004507007	
T Critical two-tail	3.182449291	

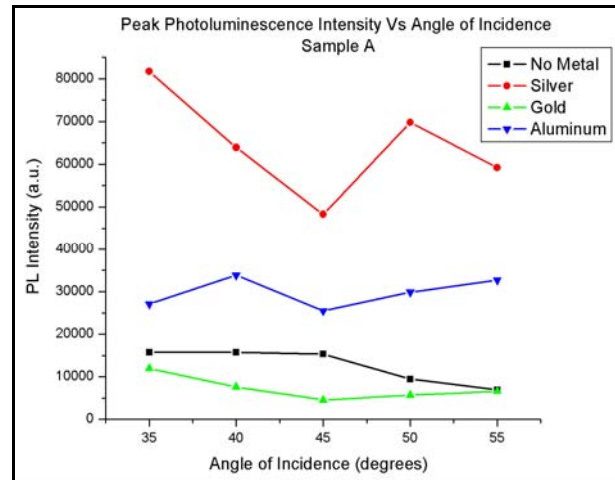


Figure 5: Peak PL intensity of Sample A versus Angle of Incidence

The PL enhancement after coating the samples (Sample A, Sample B with different metals) is attributed to the strong interaction with surface plasmons. Electron hole pairs excited in the quantum well couple to the surface plasmons at the GaN/Metal interface when the energies of the electron-hole pairs in InGaN ($\hbar\omega_{InGaN}$) and of metal surface plasmons

($\hbar\omega_{SP}$) are similar. Then, electron-hole recombination produces surface plasmons instead of photons and this new recombination path increases the spontaneous recombination rate. According to the condition for surface-plasmon coupling:

$$\hbar\omega_{SP} \geq \hbar\omega_{InGaN}$$

For silver, $\hbar\omega_{SP} > \hbar\omega_{InGaN}$, hence the electron-hole pairs excited in Sample-A and Sample-B couple to the

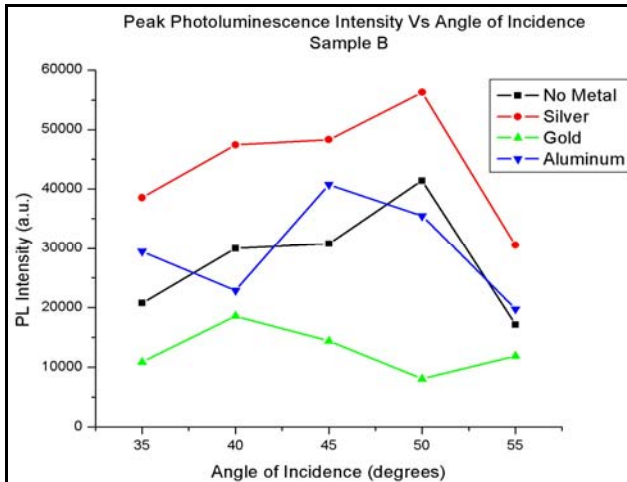


Figure 6: Peak PL intensity of Sample B versus Angle of Incidence

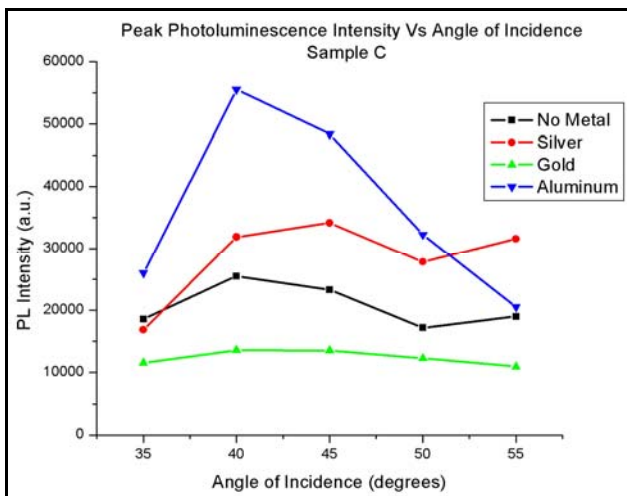


Figure 7: Peak PL intensity of Sample C versus Angle of Incidence

surface plasmons at the GaN/Ag interface. Surface plasmons increase the density of states and, in turn, increase the spontaneous-emission recombination rate. Hence, more electrons recombine with holes to produce more photons. The resulting enhancement was observed in the silver-coated samples. In the case of aluminum-coated samples of both Sample-A and Sample-B, $\hbar\omega_{SP} \gg \hbar\omega_{InGaN}$, hence the electron-hole

pairs couple to the surface plasmons at the GaN/Al interface. The real part of the dielectric constant of aluminum is negative over a wide wavelength region for visible light. Thus, an increase in PL intensity was observed on the aluminum-coated samples. For the gold-coated samples, $\hbar\omega_{SP} < \hbar\omega_{InGaN}$. This does not satisfy the condition for surface-plasmon coupling. Therefore, no enhancement was observed in the gold-coated samples.

Tuning the angle of incidence or polarization of excitation light can effectively excite surface plasmons. In general, surface plasmons cannot be excited on flat metallic film by electromagnetic radiation with optical frequencies since light does not have enough momentum (k_{ph}) to excite a surface plasmon with momentum k_{sp} . The photons can obtain additional momentum ($k_{roughness}$) via the roughness or defects on the sample surface. Hence:

$$k_{SP} = k_{ph} + k_{roughness} = \frac{\omega}{c} \times \sin \theta + k_{roughness}$$

where ω is the excitation photon frequency in s^{-1} ,
 θ is the angle from the surface normal to the incoming photon direction (angle of incidence) in degrees, and
 c is speed of light in nm/s^2

Surface plasmons can be excited only when momentum conservation is fulfilled. With ω and c being constant, momentum conservation can be achieved by rotating either the sample with respect to the excitation beam or by introducing periodic roughness, i.e., by fabricating periodic corrugations. In the present set up, the excitation beam was rotated with respect to the stationary sample. In Sample A, an increase in the PL peak intensity was observed from the silver-coated sample when compared to the uncoated sample at all incident angles. The drop in the peak PL intensity in the silver-coated sample at a 45° angle of incidence can be attributed to the roughness and non-uniformity of the sample surface. An enhancement in the peak PL intensity from the aluminum-coated sample was observed at all angles of incidence when compared to the uncoated sample and no enhancement was observed in the gold-coated samples. For Sample B, an increase in the PL peak intensity from 35° to 50° angles of incidence was observed in both silver-coated and uncoated samples. No particular trend was observed in the aluminum-coated sample. A drop in PL intensity was observed from the gold-coated samples at all angles of incidence.

Compared to Samples A and B, the enhancement in the peak PL intensity observed in the silver-coated Sample C was not as high. Also, a drop in the peak PL intensity was observed in the gold-coated samples (Sample C-Gold). The reduction in the PL enhancement ratio could be due to the higher plasmon energy of silver compared to the quantum-

well energy, which leads to a mismatch in the energies. Inefficient resonant plasmon coupling occurs due to the energy mismatch, which leads to a reduced spontaneous emission rate. The PL enhancement after coating the quantum-well samples of Sample C with different metals is attributed to the strong interaction with surface plasmons.

According to the condition for surface-plasmon coupling:

$$\hbar\omega_{SP} \geq \hbar\omega_{InGaN}$$

For silver, $\hbar\omega_{SP} > \hbar\omega_{InGaN}$, hence the electron-hole pairs excited in Sample C should couple to the surface plasmons at the GaN/Ag interface. The quantum-well energy is much smaller than the plasmon energy resulting in weak coupling and, in turn, lower enhancement was observed. Part of the enhancement in the PL can also be attributed to the reflection of pump light at the silver/GaN interface. In the case of the aluminum-coated samples, $\hbar\omega_{SP} \gg \hbar\omega_{InGaN}$, hence the electron-hole pairs couple to the surface plasmons at the GaN/Al interface. Also, the sub-wavelength roughness on the sample surface helps to effectively excite the surface plasmons. Some enhancement in the PL intensity can be attributed to the reflection of pump light at the GaN/Al interface back through the quantum well. Thus, an increase in PL intensity was observed on the aluminum-coated samples. In the case of the gold-coated samples, even though $\hbar\omega_{SP} > \hbar\omega_{InGaN}$, the high absorption of gold in the visible region is responsible for no enhancement. The pump light and the light emitted by the light emitter are absorbed by the gold film, which leads to quenching of the quantum-well peak.

e) Statistical Analysis

An analysis of Variance (ANOVA) was performed to determine the effect of different metals at different angles of incidence on each sample. In the ANOVA, a comparison was made between three or more population means to determine whether they could be equal [16]. With μ_{metal} being the mean of the peak PL intensities from different metal-coated and uncoated samples, and μ_{angle} being the angle of incidence, the null and alternate hypotheses can be stated as follows:

Null Hypothesis (H_n): There are two variables (Columns and Rows) based on which hypothesis written and ANOVA analysis is performed.

Rows: There is no significant variation in the mean peak PL intensities due to different angles of incidence.

Columns: There is a no significant variation in the mean peak PL intensities due to different metal coatings on samples.

$$H_{n1}: \mu_{35} = \mu_{40} = \mu_{45} = \mu_{50} = \mu_{55}$$

$$H_{n2}: \mu_{Ag} = \mu_{Au} = \mu_{Al} = \mu_{uncoated}$$

Alternate Hypothesis (H_a):

Rows: There is a significant variation in the mean peak PL intensities due to different angles of incidence.

Columns: There is a significant variation in the mean peak PL intensities due to different metal coatings on sample.

H_{a1} : At least two of μ_{35} , μ_{40} , μ_{45} , μ_{50} and μ_{55} , differ.

H_{a2} : At least two of μ_{Ag} , μ_{Au} , μ_{Al} and $\mu_{uncoated}$ differ.

ANOVA on Sample A:

The peak PL intensities at all angles of incidence from uncoated and metal-coated samples of Sample A were tabulated for statistical analysis. Using Microsoft Excel, a "Two-Way ANOVA Without replication" was performed to either accept or reject the null hypothesis. The results of the ANOVA analysis are shown in Table 3.

Since $|F_{Calculated}|$ (Rows) $< F_{critical}$ (Rows), the decision rule is that we fail to reject the null hypothesis (H_{n1}) and, hence, accept the null hypothesis (H_{n1}). This implies that there is no significant difference (significance level, $\alpha = 0.05$) in the mean peak PL intensities due to a change in the angle of incidence in Sample A.

Since $|F_{Calculated}|$ (Columns) $> F_{critical}$ (Columns), the decision rule is to reject the null hypothesis (H_{n2}) and, hence, accept the alternate hypothesis (H_{a2}). This implies that there is a significant difference (significance level, $\alpha = 0.05$) in the mean peak PL intensities due to different metal coatings on Sample A.

Table 3: ANOVA of Sample A

Source of Variation	SS	Degree of Freedom	MS	F	F _{crit}
Rows	261244655.5	4	65311163.88	1.540945367	3.259160053
Columns	10042560323	3	3347520108	78.98106991	3.490299605
Error	508605939.9	12	42383828.32		
Total	10812410919	19			

ANOVA on Sample B:

The peak PL intensities at all angles of incidence from the uncoated and metal-coated samples of Sample B were tabulated for the ANOVA analysis. Using Microsoft Excel, a "Two-Way ANOVA (without replication)" was performed to either accept or reject the null hypothesis. The results of ANOVA analysis are shown in Table 4.

Since $|F_{\text{Calculated}}| (\text{Rows}) < F_{\text{critical}} (\text{Rows})$, the decision rule is that we fail to reject the null hypothesis (H_{n1}) and, hence, accept the null hypothesis (H_{n1}). This implies that there is no significant difference (significance level, $\alpha = 0.05$) in the mean peak PL intensities due to change in the angle of incidence in Sample B.

Since $|F_{\text{Calculated}}| (\text{Columns}) > F_{\text{critical}} (\text{Columns})$, the decision rule is to reject the null hypothesis (H_{n2}) and, hence, accept the alternate hypothesis (H_{a2}). This implies that there is a significant difference (significance level, $\alpha = 0.05$) in the mean peak PL intensities due to different metal coatings on Sample B.

Table 3: ANOVA of Sample B

Source of Variation	SS	Degree of Freedom	MS	F	F crit
Rows	556641588	4	139160396.9	2.997535964	3.259160053
Columns	1606538106	3	535512702.1	11.53502447	3.490299605
Error	557099159	12	46424929.88		
Total	2720278853	19			

ANOVA on Sample C:

A similar statistical analysis was conducted on readings obtained for Sample C. The results of the ANOVA analysis are shown in Table 5.

Since $|F_{\text{Calculated}}| (\text{Rows}) > F_{\text{critical}} (\text{Rows})$, the decision rule is that we reject the null hypothesis (H_{n1}) and, hence, to accept the alternate hypothesis (H_{a1}). This implies that there is a significant difference (significance level, $\alpha = 0.05$) in the mean peak PL intensities due to change in the angle of incidence in Sample C.

Since $|F_{\text{Calculated}}| (\text{Columns}) > F_{\text{critical}} (\text{Columns})$, the decision rule is to reject the null hypothesis (H_{n2}) and, hence, accept the alternate hypothesis (H_{a2}). This implies that there is a significant difference (significance level, $\alpha = 0.05$) in the mean peak PL intensities due to different metal coatings on Sample C.

Table 3: ANOVA of Sample C

Source of Variation	SS	Degree of Freedom	MS	F	F crit
Rows	596880200.7	4	149220050.2	3.379185273	3.259160053
Columns	2480818808	3	826939602.5	18.72658616	3.490299605
Error	529903055.8	12	44158587.98		
Total	3607602064	19			

Conclusions

The SEM characterization carried out on all the samples did not show significant roughness. The AFM characterization performed on the samples showed surface features at atomic resolutions. Cluster formation was observed on gold- and aluminum-coated samples and a Z-scale roughness on the order of $\sim 2\text{nm}$ was observed on all the samples. It can be concluded that surface plasmons can be effectively excited by introducing roughness in the sample. Since the roughness in all the samples was not uniform, the angle of resonant surface-plasmon enhancement in each sample could not be determined. A better enhancement can be observed if uniform periodic corrugations are fabricated on the sample instead of random roughness. A statistical analysis revealed a significant difference in the mean peak PL intensities due to different metal coatings. Except for sample C, changing the incidence angle did not play a significant role in inducing a significant change in mean peak PL intensity. Photons from the light emitter couple more to the surface plasmons if the bandgap of the former is close to the surface-plasmon resonant energy of a particular metal.

Acknowledgments

The authors are grateful to the editors of IJERI for their support in the development of this paper.

References

- [1] James D. Meindl, Qiang Chen, Jeffrey A. Davis, *Limits of Silicon Nanoelectronics for Terascale Integration*, Science, Vol 293, pp. 2044-2049, Sep 14, 2001.
- [2] Gordon E. Moore, *Cramming More Components onto Integrated Circuits*, Electronics, Volume 38, Number 8, April 19, 1965.
- [3] 1999- International Technology Roadmap for Semiconductors Edition.
- [4] Anatoly V. Zayats and Igor Ismolyaninov, *Near-field Photonics: Surface Plasmon Polaritons and Localized Surface Plasmons*, Journal of Optics A: Pure and Applied Optics 5(2003), pp. S16-S50, IOP Publishing Ltd, 2003.
- [5] Motoichi Ohtsu, Kiyoshi Kobayashi, Tadashi Kawazoe, Suguru Sangu, Takashi Yatsui, *Nanophotonics: Design, Fabrication, and Operation of Nanometric Devices using Optical Near Fields*, IEEE Journal of Selected Topics in Quantum Electronics, Vol. 8, No. 4, pp. 839-851, July / August 2002.
- [6] Stephen Wedge, and W.L.Barnes, *Surface Plasmon-Polariton Mediated Light Emission Through Thin*

-
- Metal Films*, Optics Express, Vol 12, No. 16, pp. 3673-3685, August, 2004.
- [7] William L. Barnes, Alain Dereux, and Thomas W. Ebbesen, *Surface Plasmon Subwavelength Optics*, Nature, Vol. 24, pp. 824-830, Nature Publishing Group, 2003.
- [8] Ohtsu M (Ed), *Nanotechnology and Nano/atom Photonics by Optical Near Fields*, Proc. SPIE- Int. Soc. Opt. Engg., Vol 4416, pp. 1-13, 2001.
- [9] M. Boroditsky, R. Vrijen, T. F. Krauss, R. Coccioli, R. Bhat, and E. Yablanovitch, *Spontaneous Emission Extraction and Purcell Enhancement from Thin-Film 2-D Photonic Crystals*, Journal of Lightwave technology, Vol. 17, pp. 2096-2112, 1999.
- [10] Koichi Okamoto, Isamu Niki, Alexander Shvarster, Yukio Narukawa, Takashi Mukai, and Axel Scherer, *Surface-Plasmon-Enhanced Light Emitting Based on InGaN Quantum Wells*, NATURE, Vol 3, pp. 601-605, September 2004, Nature Publishing Group, 2004.
- [11] T. W. Ebbesen, H. J. Lezec, H. F. Ghaemi, T. Thio, and P. A. Wolff, *Extraordinary Optical Transmission Through Sub-wavelength Hole Arrays*, Nature, Vol. 391, pp. 667, Nature Publishing Group, 1998.
- [12] Mark A. Emanuel, *Metalorganic Chemical Vapor Deposition for the Heterostructure Hot Electron Diode*, Noyes Publications, NY, April 1, 1989.
- [13] Donald M. Mattox, *Handbook of Physical Vapor Deposition (PVD) Processing- Film Formation, Adhesion, Surface Preparation and Contamination Control*, Noyes Publications, NJ, 1998.
- [14] John D. Cutnell, Kenneth W. Johnson, *Physics*, Fifth Edition, John Wiley & Sons Publications, NY, 2001.
- [15] Rhianna A. Riebau, *Photoluminescence Spectroscopy of Strained InGaAs/GaAs Structures*, Thesis dissertation, University of Maryland at Baltimore County, 2002.
- [16] Lyman Ott, *An Introduction to Statistical Methods and Data Analysis*, 3rd edition, PWS-Kent Publishing Company, Boston, 1988.

VIJAY VAIDYANATHAN is Associate Dean for Undergraduate Studies in the College of Engineering at the University of North Texas. He earned his B.S. degrees in Physics (1985) and Electronics Engineering Technology (1988) from the University of Mumbai, India. He earned his M.S. and Ph.D. degrees in Biomedical Engineering from Texas A&M University, College Station, Texas.

ARUP NEOGI is Professor of Physics at the University of North Texas. He received his M.S. degree (1988) in Applied Physics from R.D. University in India. He earned his Ph.D. degree (1992) in Physics from Vikram University in India. He obtained a Doctor of Engineering degree (1999) from Yamagata University in Japan.

Biographies

PADMAREKHA VEMURI graduated from the Electronics Engineering Technology program at the University of North Texas with a Master's degree. Her M.S thesis was a study of surface plasmons and the factors influencing their efficiency.

INSTRUCTIONS FOR AUTHORS

MANUSCRIPT REQUIREMENTS

THE INTERNATIONAL JOURNAL OF ENGINEERING RESEARCH AND INNOVATION is an online and print publication, specifically for the Engineering, Engineering Technology, and Industrial Technology professionals. Submissions to this journal, such as an article submission, peer-review of submitted documents, requested editing changes, notification of acceptance or rejection, and final publication of the accepted manuscript will be handled electronically.

All manuscripts must be submitted electronically. Manuscripts submitted to the International Journal of Engineering Research and Innovation must be prepared in Microsoft Word 98 or higher (.doc) with all pictures, jpg's, gif's, pdf's included in the body of the paper. All communications must be conducted via e-mail as described on journal web site: www.ijeri.org.

The editorial staff of the International Journal of Engineering Research and Innovation reserves the right to format any submitted word document in order to present submissions in an acceptance PDF format for the print journal. All submitted work content will not be changed without express written consent from the author(s).

1. Word Document Page Setup: Top = 1", Bottom = 1", Left=1.25", and Right = 1.25". This is the default setting for Microsoft Word. Do Not Use Headers or Footers
2. Text Justification: Submit all text as "LEFT JUSTIFIED" with No Paragraph Indentation.
3. Page Breaks: No page breaks are to be inserted in your document.
4. Font Style: Use 11-point Times New Roman throughout the paper except where indicated otherwise.
5. Image Resolution: Images should 96 dpi, and not larger than 460 X 345 Pixels.
6. Images: All images should be included in the body of the paper. (.jpg or .gif format preferred)
7. Paper Title: Center at the top with 18-point Times New Roman (Bold).
8. Author and Affiliation: Use 12-point Times New Roman. Leave one blank line between the Title and the "Author and Affiliation" section. List on consecutive lines: the Author's name and the Author's Affiliation. If there are two authors follow the above guidelines by adding one space below the first listed author and repeat the process. If there are more than two authors, add on line below the last listed author and repeat the same procedure. Do not create a table or text box and place the "Author and Affiliation" information horizontally.
9. Body of the Paper: Use 11-point Times New Roman. Leave one blank line between the "Author's Affiliation" section and the body of the paper. Use a one-column format with left justification. Please do not use space between paragraphs and use 0.5 indentation as break between paragraphs.
10. Abstracts: Abstracts are required. Use 11-point Times New Roman Italic. Limit abstracts to 250 words or less.
11. Headings: Headings are not required but can be included. Use 11-point Times New Roman (ALL CAPS AND BOLD). Leave one blank line between the heading and body of the paper.
12. Page Numbering: The pages should not be numbered.
13. Bibliographical Information: Leave one blank line between the body of the paper and the bibliographical information. The referencing preference is to list and number each reference when referring to them in the text (e.g. [2]), type the corresponding reference number inside of bracket [1]. Consider each citation as a separate paragraph, using a standard paragraph break between each citation. Do not use the End-Page Reference utility in Microsoft Word. You must manually place references in the body of the text. Use font size 11 Times New Roman.
14. Tables and Figures: Center all tables with the caption placed one space above the table and centered. Center all figures with the caption placed one space below the figure and centered.
15. Page limit: Submitted article should not be more than 15 pages.

College of Engineering, Technology, and Architecture

University of Hartford



For more information please visit us at
www.hartford.edu/ceta

For more information on undergraduate programs please contact Kelly Cofiell at cetainfo@hartford.edu.

For more information on Graduate programs please contact Laurie Grandstrand at grandstran@hartford.edu.

Toll Free: 1-800-766-4024
Fax: 1-800-768-5073



DEGREES OFFERED :

ENGINEERING UNDERGRADUATE

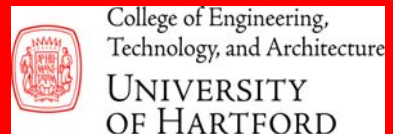
Acoustical Engineering and Music (B.S.E)
Biomedical Engineering (B.S.E)
Civil Engineering (B.S.C.E)
-Environmental Engineering Concentration
Environment Engineering (B.S.E)
Computer Engineering (B.S.Comp.E.)
Electrical Engineering (B.S.E.E.)
Mechanical Engineering (B.S.M.E.)
- Concentrations in Acoustics and
- Concentrations in Manufacturing

TECHNOLOGY UNDERGRADUATE

Architectural Engineering Technology (B.S.)
Audio Engineering Technology (B.S.)
Computer Engineering Technology (B.S.)
Electronic Engineering Technology (B.S.)
-Concentrations in Networking/
Communications and Mechatronics
Mechanical Engineering Technology (B.S.)

GRADUATE

Master of Architecture (M.Arch)
Master of Engineering (M.Eng)
• Civil Engineering
• Electrical Engineering
• Environmental Engineering
• Mechanical Engineering
- Manufacturing Engineering
- Turbomachinery
3+2 Program (Bachelor of Science and
Master of Engineering Degrees)
E²M Program (Master of Engineering and
Master of Business Administration)



The International Journal of Engineering Research & Innovation (IJERI) is one of the three official journals of the International Association of Journals and Conferences (IAJC). IJERI is a highly-selective, peer-reviewed print journal which publishes top-level work from all areas of engineering research, innovation and entrepreneurship.



IJERI Contact Information

General questions or inquiries about sponsorship of the journal should be directed to:

Mark Rajai, Ph.D.

Editor-In-Chief

Office: (818) 677-5003

Email: editor@ijeri.org

Department of Manufacturing Systems Engineering & Management

California State University-Northridge

18111 Nordhoff St.

Room: JD3317

Northridge, CA 91330